

**3-D Characterization of the Plume of a  
Lithium Lorentz Force Accelerator (LiLFA)**

**Diplomarbeit von**

**cand. aer. Thomas Krämer**

**IRS-03-S-03**

**Februar 2003**

Institut für Raumfahrtsysteme  
Universität Stuttgart  
Pfaffenwaldring 31, D-70550 Stuttgart, Germany  
Tel ++49-(0)711/685-2375  
Fax ++49-(0)711/685-3596  
<http://www.irs.uni-stuttgart.de/>

# Abstract

Mass flux measurements were performed in the plume of a Lithium Lorenz Force Accelerator to determine the contamination issues that come with this thruster. A Condensing Mass Flux Probe system utilizing a Quartz Crystal Microbalance Method was developed and used to achieve a repeatable mass flux measurement in the high-temperature, corrosive lithium plume environment. It was found that with this approach mass flux measurements in the plume of an electric propulsion device are possible. In a survey of possible methods for mass flux measurements the Quartz Crystal Microbalance Method was found as the most promising technique to perform mass flux measurements. A rough estimation of the conditions in the plume led to the conclusion that the measurement technique has to be shielded and cooled by a surrounding Condensing Mass Flux Probe that includes a shutter system. Tests were performed to determine the influence of temperature and pressure changes as well as vibrations on the measurements. It was found that a sharp increase in the temperature could be an issue. The method was tested using an Ablative Z-Pinch Pulsed Plasma Thruster with Teflon as propellant. It was found that measurements are repeatable if the Quartz Crystal Microbalance Method is used with the Condensing Mass Flux Probe. The mass deposition rate measured using the pulsed plasma thruster was found to decrease significantly with the number of shots and reached steady-state conditions at a low level when compared with the initial amount. A rough characterization of the mass flux in the plume was performed using the method without the Condensing Mass Flux Probe. It was found that the mass flux decreases significantly with an increasing horizontal angle to the thruster axis. Mass flux measurements were performed in the plume of the Lithium Lorentz Force Accelerator. The mass flux increased with time during a firing sequence. The signal was found to be very noisy. The surrounding shielding and cooling technique including the shutter system succeeded in keeping the temperature of the probe constant which allowed the probe to function without problems during the experiment. With a total mass flow rate of 10 mg/s, a discharge current of 300 A and an applied field strength of 0.07 T, the measured mass flux on the thruster axis in the plume at a distance of 148 cm from the cathode tip was between  $2.0 \pm 1.25 \mu\text{g}/(\text{cm}^2 \text{ s})$  and  $6.0 \pm 1.25 \mu\text{g}/(\text{cm}^2 \text{ s})$ .

## Acknowledgments

First I want to thank my advisor Prof. Dr. Monika Auweter-Kurtz at the Universität Stuttgart, Germany. Without her contacting top international researchers in the field of electric propulsion it would never have been possible for me to perform research at Princeton. I am very fortunate to have been advised by an expert in the field, Prof. Edgar Choueiri, director of the Electric Propulsion and Plasma Dynamics Laboratory at Princeton University. He has taught me much about electric propulsion, basic research and performing experiments in general. A very special thank goes to Bob Sorenson. He is an universal expert in solving unforeseen problems especially in the field of electronics and mechanics. I want to thank Kurt Polzin for his help during the performance of the experiments with the Ablative Z-Pinched Pulsed Plasma Thruster. Andrea Kodys and Lenny Cassady taught me much about performing experiments with the Lithium Lorentz Force Accelerator. Without their help I would not have been able to perform my measurements with the LiLFA. Apart from that I got a lot of help from everyone in the lab. I cannot say how thankful I am for all the good advice and suggestions I received from you guys during my time here in Princeton!

This diploma thesis carries the designation IRS-03-S-03 in the records of the Institut für Raumfahrtsysteme at the Universität Stuttgart, Germany. All research was performed at the Electric Propulsion and Plasma Dynamics Laboratory, Mechanical and Aerospace Engineering Department, Princeton University, Princeton, NJ, USA.

# Contents

|  |           |
|--|-----------|
| Abstract . . . . .   | i         |
| Acknowledgments . . . . .  | ii        |
| Nomenclature . . . . .   | 1         |
| <b>1 Introduction</b>  | <b>3</b>  |
| <b>2 The Lithium Lorentz Force Accelerator</b>                               | <b>5</b>  |
| 2.1 Basic design and thrust generating process . . . . .                     | 5         |
| 2.2 Lithium as propellant . . . . .  | 7         |
| 2.2.1 The lithium feeding system . . . . .                                   | 7         |
| 2.2.2 Technical issues associated with the use of lithium . . . . .          | 8         |
| 2.2.3 Human safety . . . . .   | 9         |
| 2.3 Results of previous experiments . . . . .                                | 9         |
| <b>3 The Quartz Crystal Microbalance Method</b>                              | <b>11</b> |
| 3.1 Comparison of different Mass Deposition Measurement Techniques . . . . . | 11        |
| 3.1.1 Ellipsometry . . . . .   | 11        |
| 3.1.2 Langmuir probes . . . . .  | 13        |
| 3.1.3 Quartz Crystal Microbalance Method . . . . .                           | 14        |
| 3.1.4 Other ideas . . . . .  | 15        |
| 3.2 The QCM-Theory . . . . .   | 17        |
| 3.2.1 Basics . . . . .   | 17        |
| 3.2.2 History in the use for Thruster Contamination . . . . .                | 19        |
| 3.3 The Equipment . . . . .  | 22        |
| 3.3.1 Hardware . . . . .   | 22        |
| 3.3.2 Basic specifications and free parameters . . . . .                     | 24        |
| <b>4 Design of a Condensing Mass Flux Probe (CMFP)</b>                       | <b>25</b> |
| 4.1 Expected Mass Flux . . . . .   | 25        |
| 4.2 Requirements . . . . .   | 27        |
| 4.2.1 High Temperature Environment . . . . .                                 | 27        |
| 4.2.2 Interaction between the plume and a bluff body . . . . .               | 29        |
| 4.2.3 Other requirements . . . . .   | 30        |
| 4.3 The Shutter System . . . . .   | 32        |
| 4.3.1 Basic layout . . . . .   | 32        |
| 4.3.2 Choice and test of a proper actuator . . . . .                         | 32        |
| 4.3.3 Kinematics and geometrical aspects . . . . .                           | 33        |
| 4.4 Drawings and description of the design . . . . .                         | 34        |
| 4.4.1 drawings . . . . .   | 34        |
| 4.4.2 Description of the design . . . . .                                    | 38        |

|   |           |
|---|-----------|
| <b>5 Conceptual design of a positioner system</b>                                 | <b>41</b> |
| 5.1 Basic description . . . . .   | 41        |
| 5.2 Kinematics and geometrical limits . . . . .                                   | 41        |
| 5.3 Description of the conceptual design . . . . .                                | 43        |
| <b>6 Precursor tests with the Ablative Z-Pinch Pulsed Plasma Thruster (AZPPT)</b> | <b>46</b> |
| 6.1 The Ablative Z-Pinch Pulsed Plasma Thruster . . . . .                         | 46        |
| 6.1.1 Basic design and acceleration process . . . . .                             | 47        |
| 6.1.2 The AZPPT plume compared with the LiLFA plume . . . . .                     | 47        |
| 6.2 Motivation of precursor tests with the QCM-probe and the AZPPT . . . . .      | 48        |
| 6.3 Experimental setup . . . . .  | 49        |
| 6.3.1 Positioning and supply of the probe . . . . .                               | 49        |
| 6.3.2 Avoiding an arc between the thruster and the sensor head . . . . .          | 51        |
| 6.3.3 Safety requirements . . . . .   | 52        |
| <b>7 Experiments with the LiLFA</b>   | <b>53</b> |
| 7.1 Experimental setup . . . . .  | 53        |
| 7.1.1 Mounting of the CMFP and feedthroughs . . . . .                             | 55        |
| 7.1.2 Water and gas supply . . . . .  | 56        |
| 7.1.3 Critical cable length . . . . .   | 56        |
| 7.1.4 Other issues . . . . .  | 57        |
| 7.2 Precursor tests . . . . .   | 58        |
| 7.2.1 Thermal calibration . . . . .   | 58        |
| 7.2.2 Pressure calibration . . . . .  | 61        |
| 7.2.3 Influences of the shutter system . . . . .                                  | 62        |
| 7.3 Methodology . . . . .   | 62        |
| <b>8 Results and Analysis</b>   | <b>65</b> |
| 8.1 AZPPT Experiments . . . . .   | 65        |
| 8.1.1 Results of the AZPPT experiments . . . . .                                  | 65        |
| 8.1.2 Analysis of the AZPPT experiments . . . . .                                 | 71        |
| 8.2 LiLFA Experiments . . . . .   | 73        |
| 8.2.1 Results of the LiLFA experiments . . . . .                                  | 74        |
| 8.2.2 Analysis of the LiLFA experiments . . . . .                                 | 76        |
| <b>9 Conclusions</b>  | <b>78</b> |
| <b>A Complete AZPPT Results</b>   | <b>81</b> |
| <b>B CMFP Detailed Photos</b>   | <b>84</b> |
| <b>Bibliography</b>   | <b>87</b> |

# Nomenclature

|                  |  |
|------------------|--|
| $A_{expose}$     | Area of the quartz crystal that is exposed to the environment                              |
| $A_{Plume}$      | Estimated surface area of the plume  |
| $A_{QCM}$        | Area of one side of the entire quartz crystal  |
| $B$              | Magnetic field strength of the applied field of the LiLFA                                  |
| $d$              | Distance between the cathode tip and the mass flux measurement                             |
| $d_A$            | Diameter of the aperture in the CMFP   |
| $d_{AZPPT}$      | Distance between the center of the orifice of the AZPPT and the mass flux measurement      |
| $d_{mt}$         | Horizontal distance between the mounting tracks in the LiLFA tank                          |
| $d_{sb}$         | Horizontal distance between the supporting bars of the positioner system in the LiLFA tank |
| $e$              | Elementary charge  |
| $E_p, E_s$       | Finite field components  |
| $F$              | Lorentz force  |
| $f_c$            | Frequency of the coated quartz crystal   |
| $F_{A-QCM}$      | Radiation shape factor LiLFA anode-quartz crystal  |
| $F_{C-QCM}$      | Radiation shape factor LiLFA cathode-quartz crystal  |
| $f_q$            | Frequency of the uncoated quartz crystal   |
| $\Delta f$       | Change of frequency of the quartz crystal  |
| $I$              | Discharge current of the LiLFA   |
| $I_{ion}$        | Ion saturation current   |
| $I_{sp}$         | Specific Impulse bit   |
| $j$              | Current density  |
| $k$              | Boltzmann constant   |
| $Kn$             | Knudsen number   |
| $L$              | Length of the actuator arm of the shutter  |
| $L_C$            | Characteristic length of a body  |
| $\dot{M}$        | Total mass flow  |
| $M_f$            | Mass of the coated quartz crystal  |
| $\dot{m}$        | Mass flux  |
| $m_{bit}$        | Mass bit   |
| $m_{Li}$         | Atomic mass of lithium   |
| $\Delta M_{max}$ | Mass deposition at which the quartz crystal saturates                                      |
| $M_q$            | Mass of the uncoated quartz crystal  |
| $\Delta M$       | Change in mass of the quartz crystal   |
| $n_e$            | Plasma number density  |
| $n_{Li}$         | Plasma number density of the lithium in the LiLFA plume                                    |

|                           |  |
|---------------------------|--|
| $n_{Air}$                 | Number density of the neutral remaining air in the LiLFA tank    |
| $p_B$                     | Background pressure in the LiLFA tank                            |
| $P_{kinetic}$             | Kinetic energy flux to the quartz crystal                        |
| $P_{radiation(crystal)}$  | Radiation energy flux from the quartz crystal                    |
| $P_{radiation(thruster)}$ | Radiation energy flux to the quartz crystal                      |
| $P_{recombination}$       | Recombination energy flux to the quartz crystal                  |
| $r_A$                     | Radius of the anode exit of the LiLFA                            |
| $r_C$                     | Radius of the cathode tip of the LiLFA                           |
| $r_{Li}$                  | Radius of the lithium atom                                       |
| $R_p, R_s$                | Fresnel reflection coefficients                                  |
| $r_S$                     | Radius of a sphere   |
| $T$                       | Thrust force   |
| $T_B$                     | Background temperature in the LiLFA tank                         |
| $T_e$                     | Electron temperature of the plasma                               |
| $t_{sat}$                 | Time until the quartz crystal saturates                          |
| $T_T$                     | Thruster temperature   |
| $v$                       | Velocity of the flow   |
| $W_{ion}$                 | Ionization energy of lithium                                     |
| $x$                       | Distance between the cathode tip and the anode exit of the LiLFA |
| $\Delta y$                | Maximum extension of the plunger of the air cylinder             |
| $Z_q$                     | Acoustic impedance of the quartz crystal                         |
| $\alpha$                  | Rotation angle of the shutter                                    |
| $\alpha_{QCM}$            | Absorptivity of the quartz crystal                               |
| $\epsilon_{QCM}$          | Emissivity of the quartz crystal                                 |
| $\epsilon_T$              | Emissivity of the thruster                                       |
| $\eta$                    | Thrust efficiency  |
| $\lambda$                 | Mean free path of a molecule                                     |
| $\Psi, \Delta$            | Ellipsometric angles   |
| $\sigma$                  | Stefan-boltzmann constant  |
| $\Theta$                  | Estimated opening angle of the LiLFA plume                       |
| $\varphi$                 | Angle off the thrust centerline of the CMFP                      |

# Chapter 1

## Introduction

High-power electric propulsion systems especially magnetoplasmadynamic thrusters (MPDT's) have long been recognized as among the most promising options for heavy-payload orbit raising and piloted planetary missions as well as for nearer term orbit raising missions. However, they have lagged behind their lower-power counterparts in laboratory testing. With the renewed interest in the development of nuclear power systems for spacecraft, the steady-state spacecraft power necessary for the practical application of MPDT's may soon be available. Due to that, an increased interest in developing and testing MPDT's can be observed. One of the main issues with this kind of thruster is its high cathode erosion rate. The cathode erosion rate has slowed significantly the evolution of steady-state MPDT's toward flight application. In experiments it was found that an increased lifetime of the cathode could be achieved by using an alkali metal as propellant instead of an inert gas [1]. The alkali metal lithium was found as a good option to increase the lifetime through lowering significantly the effective work function of the cathode. In combination with a multi channel cathode lower erosion rates have been observed. Due to that, the development of a MPDT that uses lithium as propellant seemed to be promising. This led to the development of the Lithium Lorentz Force Accelerator (LiLFA) in Russia and in the USA. The LiLFA is a version of the steady state MPDT using a hollow channel cathode and lithium as propellant. Recent work performed at the Moscow Aviation Institute (MAI) under NASA-JPL contract concentrated on LiLFA's on power levels between 30 KW and 500 KW. NASA-JPL's research program on LiLFA's is concentrated primarily on demonstrating engine performance in a 500 KW-class thruster and proving the feasibility of long-lived, high current cathodes. Fortunately, many of the fundamental processes controlling the efficiency and lifetime of the LiLFA can be studied at relatively low power. Due to that the program includes the construction and fabrication of a 30 KW class LiLFA at the Moscow Aviation Institute (MAI) and the testing and advancement of this thruster by Princeton University's Electric Propulsion and Plasma Dynamics Laboratory (EPPDyL).

The goal of a three-year research program at EPPDyL is to address the fundamentals underlying the critical issues related to the development of a new class of high efficiency steady-state LiLFA's. One significant issue for using the LiLFA on actual spacecraft is the contamination issue. Lithium is highly reactive and could coat the surfaces and subsystems of a future spacecraft. Due to that one main focus of the LiLFA program at EPPDyL is the determination of the contamination issue.

Although designs of spacecraft using LiLFA's would have the main propulsion system mounted on a boom away from the vehicle the issues that come with the lithium contamination are not negligible. Lithium can deposit on the surface of a spacecraft and coat

lenses and cameras and also other technical equipment due to its metal character. Another fact that comes with lithium is its high reactivity. Depositing lithium could destroy sensitive electronic parts by reacting with the surface and also by causing short circuits due to its high electrical conductivity.

It is planned to study the contamination issue by a measured characterization of the mass flux distribution in the plume of the LiLFA and its scaling with power, discharge current, applied field strength and total mass flow rate. The mentioned approach will lead to a better practical spacecraft contamination evaluation. It will be crucial for the formulating of design guidelines for a spacecraft which will be affected by the contamination issue. In previous studies a heating of the surfaces of a spacecraft was considered to get rid of the contamination problem. A measurement of the mass flux distribution in the plume will help to validate devise schemes to combat the adverse effects of such contamination. Apart from a determination of the contamination of a spacecraft there are a few other reasons for mass flux distribution measurements in the plume. This kind of measurements will lead to a better understanding of the thruster operation in general. Mass flux measurements would also support the validation of plume codes intended to numerically simulate the plume. Plume codes for the LiLFA plume are currently being developed at the EPPDyL.

To measure mass flux in the plume a Quartz Crystal Microbalance Method (QCM) will be used. The QCM is a device that translates deposited mass on the surface of a quartz crystal to a measured mass flux. This thesis will show that using a QCM can provide plume mass flux measurements even in the harsh conditions presented by lithium. However, care must be taken to properly protect the instrument from the hot lithium environment.

This thesis describes the choice, testing and implementation of a suitable contamination measurement technique including the design of the required supplementary technique. In chapter 2, the technical background of the LiLFA is described including a determination and summary of the issues that come with lithium as propellant and the required feeding system. In chapter 3, the choice and the technical background of a suitable mass deposition measurement technique is explained and discussed. In chapter 4, the advancement of this technique to a Condensing Mass Flux Probe is explained including an explanation of the requirements and the accomplishment of the design. In chapter 5, the design of a necessary positioner system for the Condensing Mass Flux Probe is introduced with a summary of the issues that come with an implementation of this system. Chapter 6 shows the testing and validating of the chosen measurement technique and the Condensing Mass Flux Probe by using an Ablative Z-Pinch Pulsed Plasma Thruster (AZPPT) as precursor test to the LiLFA experiment. The experimental setup of the LiLFA experiment and further precursor tests are explained and discussed in chapter 7. In chapter 8, the results of the contamination measurements with the AZPPT and the LiLFA are shown, summarized and discussed. Finally, the conclusions arising from the results of the measurements and the experience in the contamination studies in general are addressed in chapter 9, including recommendations for further studies.

# Chapter 2

## The Lithium Lorentz Force Accelerator

The 30 kW Lithium Lorentz Force Accelerator (LiLFA) fabricated at the Moscow Aviation Institute (MAI) under NASA- JPL contract has been at Princeton University's EP-PDyL since 1998. After necessary calibrations, a lithium safety review and the development of a lithium feeding system the first successful firing took place in March 2000. Soon it was clear that performing measurements with the alkali metal propellant is challenging. At the beginning of this chapter the technological background of the LiLFA is described including an explanation of the thrust generating process. After that, the requirements and issues that come with lithium as propellant are summarized. The most important results of previous experiments with the LiLFA conclude the chapter.

### 2.1 Basic design and thrust generating process

As mentioned in the introduction, the LiLFA is basically a magnetoplasmadynamic thruster. The basic design and the acceleration process do not differ significantly from the design and the acceleration process of gas-fed magnetoplasmadynamic thrusters. Figure 2.1 shows the basic schematic of the 30 kW MAI LiLFA.

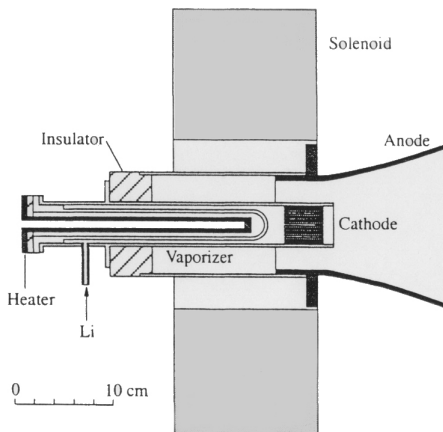


Figure 2.1: A schematic of the 30 kW MAI thruster (from Ref. [2]).

The stainless steel tube of a feed system that provides liquid lithium is connected to the propellant inlet of the LiLFA [4]. The inlet leads to the inside of the hollow cathode of the LiLFA. The cathode is basically composed of a hollow tungsten tube with an outside diameter of 24 mm. At its front the inside of the cathode is filled with axially ordered 2

mm diameter solid tungsten rods that provide a more uniform distribution of the electric field and due to that a better ionization of the propellant, which flows between the rods. It is suspected that this leads to a lower erosion rate of the cathode. As shown in figure 2.1 a heater is integrated into the center of the hollow cathode. Its function is to heat the inside of the cathode by radiation allowing for the vaporizing of the liquid lithium provided by the feed system. The heater requires a 1.5 kW power supply. It is made of graphite that allows a temperature of more than 1300 deg. C. A spiral channel is cut on the inside of the cathode for the lithium to flow through thus lengthening the time that it is heated. That helps to ensure that the propellant is vaporized. The cathode is insulated from the anode by a cylinder shaped piece of aluminum boron nitride that encircles the cathode. Aluminum boron nitride is a ceramic material that is able to survive the high temperatures of the cathode during the firing of the thruster. The tungsten anode has an exit diameter of 70 mm. Its profiled surface corresponds to the flux lines of the applied magnetic field. Such a profile provides for a uniform current attachment with a lower erosion of the anode. The mostly axial applied magnetic field is produced by a water-cooled solenoid that surrounds the anode. At  $I = 100$  A the coil of the solenoid produces a magnetic field strength of  $B = 0.032$  T at the anode tip that leads to a greater acceleration of the plasma [2].

For the experiment, the LiLFA is mounted on a thrust stand. The electrical power for the thruster, cathode heater, and solenoid is brought to the thrust stand by copper wires. Flexures carry the power to the top of the stand where it is distributed to the thruster and the subsystems. Table 2.1 shows the operation range of the 30 kW MAI LiLFA.

Table 2.1: Operation parameters of the LiLFA

| <b>Total mass flow [<math>\dot{M}</math>]</b> | <b>Discharge current [<math>I</math>]</b> | <b>Applied magnetic field [<math>B</math>]</b> |
|---|---|--|
| 10-20 mg/s                                    | 400-700 A                                 | 0-0.1 T  |

About 30 minutes before an experiment with the LiLFA the cathode has to be pre-heated to about 1300 C to provide a small amount of vaporized lithium between the anode and the cathode. For the starting process the applied magnetic field has to be switched off because it would retard the transport of electrons from the cathode to the anode. For starting the thrust generating process a voltage is applied between the anode and the cathode. Usually a voltage of 80 volts is enough to initiate a breakdown and to produce an arc due to the low ionization potential of lithium. Once an arc is established the current, mass flow rate and the applied magnetic field are set to the desired values. When the arc is stabilized and its current is high enough, its self-induced azimuthal magnetic field produces the desired Lorentz force  $F = j \times B$  on the lithium flow that has an axial and a radial component. Figure 2.2 shows the circumstances in the LiLFA.

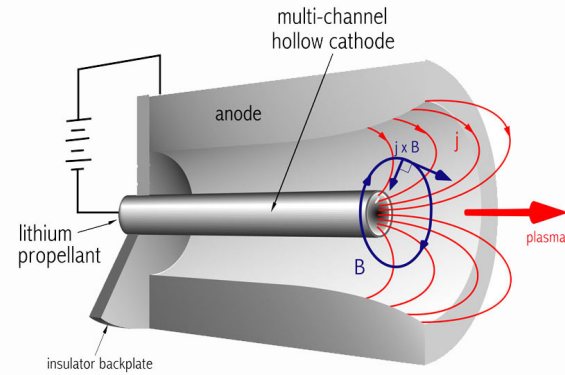


Figure 2.2: The acceleration process in the LiLFA.

The axial component acts to expel the lithium from the thruster. The radial component compresses the propellant flow towards the centerline producing a very hot and dense plasma on the axis just in front of the cathode tip. The applied field enforces this so called pinch effect due to its more axial directed magnetic field. The expansion of the compressed plasma along with the axial component of the produced Lorentz force leads to a very high exhaust velocity  $v$ .

## 2.2 Lithium as propellant

The main difference between the LiLFA and gas-fed magnetoplasmadynamic thrusters is its alkali metal propellant. That leads to requirements and issues that are unknown for gas-fed thrusters. First a sophisticated feed system is needed which is showed and explained. The technical problems and the human safety issues are also discussed.

### 2.2.1 The lithium feeding system

The mechanically driven lithium feeding system supplies liquid lithium to the explained vaporizer cathode in the thruster. A schematic is shown in figure 2.3 with arrows indicating the path of lithium flow through the system.

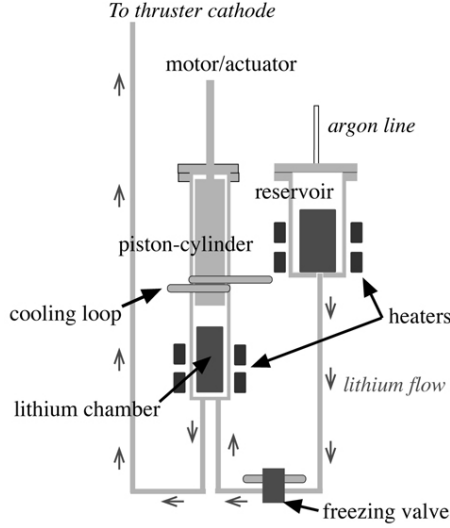


Figure 2.3: The liquid lithium feeding system (from Ref. [2]).

The lithium is loaded in solid condition into a leak-tight reservoir under argon atmosphere. This avoids a reaction of the propellant with air. Under vacuum, the lithium is melted by heaters surrounding the reservoir and fed into a lithium chamber below the piston-cylinder. A freezing valve located between the reservoir and the lithium chamber fed by chilled water solidifies the lithium and prevents back-flow of the propellant to the reservoir during thruster operation by forming a plug of solid lithium. Heaters surrounding the lithium chamber provide liquid lithium temperatures between 200 deg. C and 300 deg. C during operation. The motor and controller that drive the piston allow for a continuous mass flow to the thruster and also for a feedback of speed and position during the firing. Leakage around the piston during the firing process is avoided by a chilled-water loop above the lithium chamber that freezes the lithium.

With this system, mass flow rates of  $\dot{M} = 10\text{-}120 \text{ mg/s}$  are achievable with an error of 1 % due to a calibration of the system. The system was not calibrated for lower mass flow rates than  $\dot{M} = 10 \text{ mg/s}$  because a stable operation of the thruster is not expected under such conditions.

### 2.2.2 Technical issues associated with the use of lithium

The use of lithium as propellant causes a few requirements and problems during the experiment. The main issue comes with the start of the firing process in general. As mentioned in section 2.1 the lithium provided by the feed system is vaporized in the hollow cathode. Unfortunately the entire vaporization cannot be ensured during the start of the firing. Earlier tests showed that liquid lithium escaped the cathode if the mass flow was chosen too high at the begin of the firing. Also the existence of solid parts in the plume during the start of the firing was discovered. This is caused by solid parts of lithium on the cathode tip that lasted on the cathode as a result of the previous firing. When the cathode is heated this solid parts can melt away. The existence of liquid and solid parts of lithium is a non-negligible danger for sensitive measurement technique in the plume. When the cathode heats up during the start of the firing, caused mainly by added heat of the arc, the vaporization rate increases and the vaporization point moves upstream inside the cathode until it stabilizes. Due to that, a measurement under steady-state conditions is not possible until 6-10 minutes after the ignition. This necessary time period is hard to reach because

the lithium in the plume condenses on surfaces in the tank and causes an undesirable arc due to the high electric conductivity of this alkali metal. Such arcing causes damage and ends the firing of the thruster.

The high reactivity of lithium requires an elaborate coverage of sensitive parts such as cables by several layers of aluminum foil. For simplifying the clean up after the experiment the inside of the tank also has to be covered by aluminum foil to capture the lithium as it condenses on the wall. The diffusion pump has to be saved from direct lithium flow by a set of aluminum baffles at the end of the chamber.

### 2.2.3 Human safety

If lithium gets in contact with air it reacts quickly releasing a lot of energy and hydrogen. That could cause a fire or an explosion if the lithium is not converted to another material by a chemical reaction before the tank is vented. For that a small amount of water is bled into the tank at the end of the experiment after the pumps are switched off. The water reacts the lithium in lithium hydroxide ( $\text{LiOH}$ ). After a few hours the roughing pump and the roots blower are switched on to pump out hydrogen gas. When the tank is finally opened the  $\text{LiOH}$  reacts with air to form lithium carbonate  $\text{LiCO}_3$ . The two resulting lithium compounds are both toxic [3]. They may cause serious kidney or central nervous system damage if inhaled or swallowed. Apart from that, they cause skin or eye irritation. Due to that gasmasks, several layers of gloves, and an entire body protective clothing must be worn during the cleaning of the tank. The tank has to be cleaned with water and paper towels. The parts of the feed system have to be put in a provided glove box for a later cleaning. Even after a cleaning of the tank the use of gloves and protective clothes is necessary for performing work in the tank.

## 2.3 Results of previous experiments

The first experiments with the 30 kW LiLFA were performed at the Moscow Aviation Institute (MAI) after the finished fabrication in 1996 [4]. The task was mainly studying cathode erosion rates on different operation modes but also thrust measurements were taken. Experiments were performed with lithium as propellants or a mixture of barium and lithium. In the test using just lithium it was found that it takes about 6-15 minutes to reach steady-state conditions because of the uncontrollable moving of the vaporization point in the cathode as mentioned in section 2.2.2. The experiments often had to be stopped before running out of propellant due to unforeseen and undesired arcs. Cathode erosion experiments took place with a total mass flow of  $\dot{M} = 20 \text{ mg/s}$ , an applied field strength of  $B = 0.1 \text{ T}$  and a discharge current of  $I = 600 \text{ A}$ . After running 17 tests with a total time of 50 hours and 54 minutes using the same cathode a cathode specific erosion was found to about  $K_m = 10^{-12} \text{ g/Coul}$ . This figure was estimated by using an instrumental microscope to estimate the size of a pore formed as a result of a discharge. A more useful result concerning tests at the EPPDyL is a thrust measurement test that was undertaken with a mass flow rate of  $\dot{M} = 13.5 \text{ mg/s}$  lithium, applied magnetic field strength  $B = 0.1 \text{ T}$  and a discharge current of  $I = 500 \text{ A}$ . These specifications correspond with planned tests at the EPPDyL. A thrust was measured of  $T = 0.504 \text{ N}$  which leads to a thrust efficiency of  $\eta = 32.5 \%$ . Taking into account the total mass flux a speed at the anode exit of  $v = 37300 \text{ m/s}$  can be calculated. This can be used as a good estimation of the speed in the plume for the contamination measurements.

Since the first successful firing of the LiLFA at EPPDyL in March 2000, just four firings of the thruster could be performed due to its sophisticated technology and the handling problem of the propellant. These tests were mainly performed to learn the handling of the lithium and to determine a successful firing procedure for the 30 kW MAI LiLFA. The longest firing period was limited to about 10 minutes due to the appearance of undesirable arcs that stopped the firing. Steady-state conditions are not yet repeatably reached. At a total mass flow of  $\dot{M} = 9.5$  mg/s, a discharge current of  $I = 518$  A and an applied field strength of  $B = 0.07$  T, it was possible to measure one thrust measurement point [2]. The measured thrust was  $T = 265 \pm 58$  mN by a thrust efficiency of  $\eta = 20 \pm 8\%$ . The data was not obtained under ideal conditions due to an arc that was attaching to the thrust stand and leaded to an early termination of the test. The large uncertainty is due to a not entirely steady-state process.

# **Chapter 3**

## **The Quartz Crystal Microbalance Method**

For the reasons mentioned in chapter 1 an experimental determination of the mass flux is needed. The next step was the choosing of a capable method for the designated task. For that reason a few measurement techniques were compared and analysed in consideration of applicability in high vacuum, extreme thermal environment and lithium contamination. The accuracy and the costs of the determined techniques and probes were also not irrelevant. In addition the most applicable technique was analysed in a deeper matter. This includes physical basics, history in using for thruster contamination and the associated equipment of the probe.

### **3.1 Comparison of different Mass Deposition Measurement Techniques**

In that case the extreme thermal environment but also other factors put a probe to a hard test. With these challenges in mind three established plasma measurement techniques could be identified and are explained in this section. Apart from that also a few unconventional possibilities are introduced.

#### **3.1.1 Ellipsometry**

The first measurement method that was investigated concerning mass deposition measurements was ellipsometry. The idea with this technique is to allow the lithium to collect on a small surface in the plume. Ellipsometry in its general form studies the change of the polarization state of light due to interaction with a sample. It is a non-intrusive optical technique, which deals with the measurement and interpretation of changes of the polarization state of polarized light undergoing oblique reflection from a sample surface.

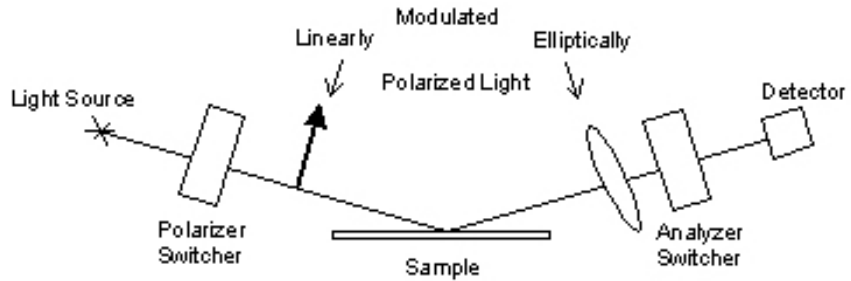


Figure 3.1: Setup of an ellipsometry experiment.

A typical setup of an ellipsometry experiment is sketched in 3.1. The incident light is linearly polarized with finite field components  $E_p$  and  $E_s$  in the directions parallel and perpendicular to the plane of incidence of the light. Upon reflection, the s- and p-components experience a different attenuation and phase shift according to the Fresnel equations. The reflected light therefore is elliptically polarized giving the technique its name. The ellipse of polarization of the reflected light is then measured with a second polarizer. The figures which characterize the ellipse of polarization are the ellipsometric angles  $\Psi$  and  $\Delta$  which stand for the differential changes in amplitude and phase. They are related to the complex ratio of the Fresnel reflection coefficients  $R_p$  and  $R_s$  for light polarized parallel (p) and perpendicular (s) to the plane of incidence such as

$$\rho = \frac{R_p}{R_s} = \tan \Psi e^{i\Delta} \quad (3.1)$$

The effect of the sample surface on the polarization state of a probing beam is described by two coefficients,  $R_p$  and  $R_s$ . These complex reflectances describe the action of the sample on the electric field components parallel (p) and perpendicular (s) to the plane of incidence. This reflection coefficients are determined by the optical properties and composition of the substrate and overlayers, by the surface roughness and morphology but also by the thickness. Because of that the thickness of a deposition is a function of these factors and the ellipsometric angles and can be obtained from the ellipticity of the reflected light by an inversion of the Fresnel-equations. The Fresnel-equations are derived from Maxwell's equations of electrodynamics. The problem of the inversion of these equations is solved by numerical models. Due to the use of mathematical models no calibration is needed.

There are many advantages of ellipsometry. One of the advantages of this method is the fact that the measurements can be made ex-situ which saves the whole equipment from the extreme thermal and lithium contaminated environment in the plume. In this case the light is beamed into the tank through one of the tank windows. The reflected beam is also beamed through one of the windows. This method would help to avoid risks concerning a damaging of the equipment. Another advantage is the high accuracy of this technique. Because no moving mechanical parts are needed it can measure deposition layers of only a few angstroms thick, which is more than adequate for the designated application. Ellipsometry requires no calibration, and no extrapolation of the reflectivity towards zero and infinite energy. That makes it much more accurate than other reflection techniques.

But this method comes with a set of problems. Discussions with a vendor showed that the required hardware and the associated software cost at least ten times more than

comparable other measurement techniques. The immense costs are not within the limits of the budget provided for contamination studies of the LiLFA. And also the assumption of a really high accuracy is not correct in our case. The determination of the thickness depends on many other factors like those mentioned above. For lithium it is difficult to measure those properties due to its health risk and ease of contamination. Due to this the accuracy of the measurement is restricted. Another problem is the limited positioning of the deposition surface. The light beam must be reflected off the sample at a particular angle. The beam must be shone perpendicular to the windows. This greatly limits the range of possible positions in the vacuum tank.

### 3.1.2 Langmuir probes

The second possibility that was discussed was the use of a langmuir probe. A langmuir probe is a piece of wire which is held in the plasma. If a voltage is applied, a current flows from the wire to the plasma. The loop is closed by the chamber or in that case the tank that is grounded.

With this kind of probe the ion saturation current  $I_{ion}$  and the electron temperature  $T_e$  of the plasma can be measured. With the help of these figures it is possible to calculate the plasma number density  $n_e$ . If we assume the velocity  $v$  at a specific position in the plasma we can calculate the mass flux with the help of the measured number density  $n_e$  and the atomic mass of lithium  $m_{Li}$ .

$$\dot{m} = n_e v m_{Li} \quad (3.2)$$

The advantages of that technique are obvious. The easy design and the fact that the probe can be build in the lab lead to low costs and a lower financial risk. The probe can easily be replaced by another one if the test fails or for any other reason. No water cooling or other additional equipment is needed. Due to that the design of a mounting and the fixing of the probe in the tank would be negligible problems. Another advantage is that langmuir probes have a documented history of use in various other electric thrusters which leads to a good support concerning experts and literature.

But on the other hand the technique using a langmuir probe contains various sources for measurement errors and inaccuracies. First of all it is really difficult to assume or calculate the velocity at a specific position in the plasma. For such a task sophisticated numerical models are needed to get a reasonably estimation of the velocity field. Such models and the associated computer simulations are not yet available. Also especially at the beginning of the firing the thruster is not steady-state. So it is absolutely impossible to get accurate measurements during the first few minutes. The second problem is the lithium contamination of the probe during the test. If lithium deposits on the probe the surface characteristics change and the measurement is not accurate anymore. Another reason why langmuir probes are not the best solution for this application is the extreme thermal environment. On one hand the use of a tungsten wire could prevent a melting of the probe. On the other hand a hot environment leads to sputtering which causes an erosion of the probe. If the area of the wire changes due to the erosion the measured electron density which depends on the amount of the area also changes. Because of the preponderant negative attributes concerning an application with the lithium thruster the use of a langmuir probe was abandoned.

### 3.1.3 Quartz Crystal Microbalance Method

Another possibility apart from ellipsometry to measure mass deposition is the quartz crystal microbalance method or QCM. It takes advantage of the condensation of a material inside the vacuum tank by measuring mass deposition on an exposed Quartz Crystal in the plume. When an alternating voltage is applied across the faces of a properly shaped piezoelectric crystal, the crystal vibrates and changes shape in proportion to the applied voltage. At certain discrete frequencies of applied voltage, a condition of very sharp electro-mechanical resonance is encountered. The QCM utilizes this piezoelectric sensitivity of the mentioned quartz crystals resonance to added mass. When mass is added to the face of a resonating quartz crystal, the frequencies of these resonances are reduced. This change in frequency is very repeatable and is precisely understood for specific oscillating modes of quartz. The system works by oscillating the crystal and monitoring its resonance frequency. The change in frequency,  $\Delta f = f_q - f_c$ , of a quartz crystal with coated (or composite) and uncoated frequencies,  $f_c$  and  $f_q$  respectively, is basically related to the change in mass from the added material,  $M_f$ , as follows:

$$\frac{M_f}{M_q} = \frac{\Delta f}{f_q} \quad (3.3)$$

$M_q$  is the mass of the uncoated quartz crystal [5]. It is obvious that the deposited mass is inferred from the precise measurement of the crystals frequency shift. Figure 3.2 shows the basic schematic of the crystal and its associated layers:

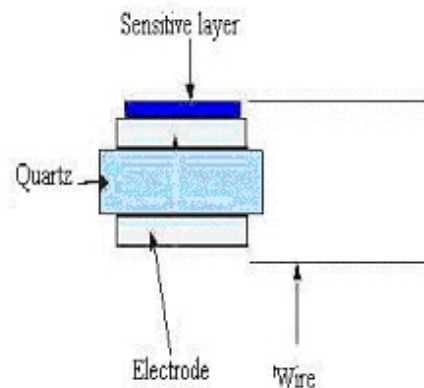


Figure 3.2: Schematic of a QCM.

A quartz crystal is sandwiched between two electrodes. The crystal is excited by a variable frequency oscillator. The mass is deposited on one of the electrodes (sensitive layer).

This method comes with its own set of advantages as well as problems. As with ellipsometry the QCM-Method takes advantage of the condensation of lithium by measuring mass deposition. That means that in contrast to the use of langmuir probes the measurement is not disturbed by this condensation. Most of the vending companies offer their sensors with a housing made of stainless steel. Stainless steel is one of the materials that have a really low reactivity in terms of lithium. Because of that a damaging of the probe by a reaction with lithium is minimized. The interaction between the lithium and other materials will be discussed in a following chapter. One of the most important advantages of the QCM method is the really good accuracy of less than one angstroem, providing far

more sensitivity than even ellipsometry. A sensitivity of less than one angstroem deposition means a sensitivity in a change of mass in terms of a lithium deposition of less than 2 ng/cm<sup>2</sup>. That means that this Method could be used also for plume measurements of low energy thrusters like the Ablative Z- Pinched Pulsed Plasma Thruster (AZPPT) that is also developed and determined in the lab. Discussions with vendors showed that in spite of this good accuracy the costs for the probe and the associated equipment is in the limits of the budget for contamination studies of the LiLFA. Another advantage is the unrestricted positioning with this system. It is easy to install and allows a scan of the whole plume. Also the fact that the QCM method has a history of use in thruster contamination studies is not negligible.

The fact that this probe has to be put directly in the plume presents a problem. On one hand the circumstances mentioned above save the probe from damage by lithium. On the other hand the extreme thermal environment caused by the lithium contains a big risk of measurement inaccuracies and in the worst case damage to and failure of the crystal. The crystal can be used up to at least 130 C and is directly cooled by its own water cooling system. But an expert at the vendor admitted that the QCM is really sensitive concerning temperature changes. A thermal drift can appear even with a few degrees of temperature change. Another problem is the saturation and failing of the replaceable crystal. The film introduces stress onto the crystal that limits the useable range depending on the material. An expert at a competing company assured us that at least 6 mg of lithium can be deposited on the crystal before it fails. Rough estimations of the very diverging plume showed that at a low distance from the thruster the deposition and its rate can be measured for just a few minutes until the crystal fails. The calculations will be discussed in more depth in the following sections.

### 3.1.4 Other ideas

Due to the disadvantages of the three mentioned conventional measurement systems two other unconventional ideas were considered. First, other methods were considered which take advantage of the condensation of lithium inside the vacuum tank. Since lithium is easily condensable, it was planned to construct a specialized mass flux condenser (MFC) to measure the steady-state mass flux distribution in the plume [6]. The concept is showed in figure 3.3 and consists of a water-cooled condenser copper back plate (panel a) on which a set of flat copper control strips (panel b) are attached in a wheel spoke configuration (panel c). The MFC assembly can be moved axially in front of the thruster and used to intercept and condense the plume. Under steady-state conditions the mass flux distribution can be calculated by removing the control strips and measuring the thickness of the condensed lithium with a micrometer. The use of control strips instead of a large flat plate allows easy access for the micrometer.

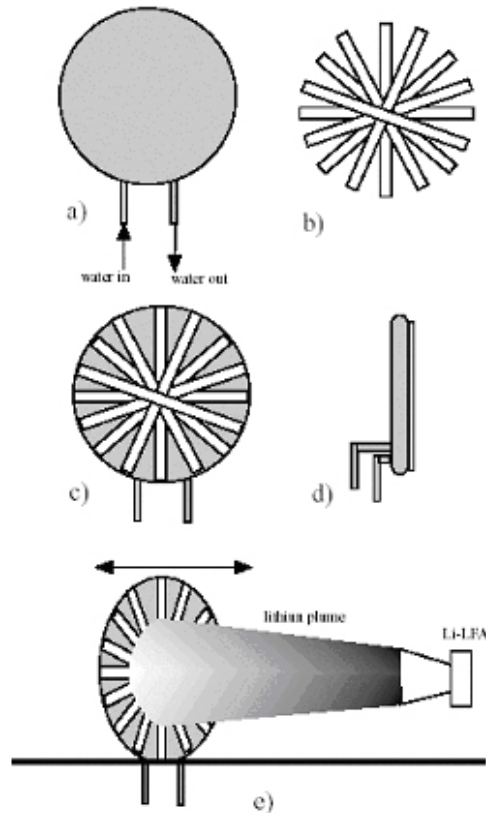


Figure 3.3: Schematics of the MFC. a) water-cooled condenser copper back plate b) copper control strips c) Front view of condenser assembly d) Side view of condenser assembly e) Li-LFA plume impinging on the MFC which can be displaced axially. [6]

A careful mapping of the thickness of the condensed plume profiles (and a knowledge of the velocity field) can be used to construct a 3-D picture of the mass flux inside the plume. A big advantage of that system is that it takes advantage of the condensing of the lithium. That leads to a lower risk of inaccuracies and failures. Also the fact that the whole plume is measurable during one firing of the thruster is an advantage. It distinguishes that method from the others in a positive way. The most significant problem is the required knowledge of the velocity field. It leads to the same disadvantage that langmuir probes have. The second disadvantage is the safety risk in handling the lithium. The lithium contaminated strips have to be moved out of the tank and measured carefully. Because of that the researcher has to be exposed to the lithium for a long time.

Finally the Quartz Crystal Microbalance Method was found as the most promising method for mass flux measurements in the plume of the LiLFA.

Another possibility was the use of a force transducer. The idea is based on a very small metal plate exposed directly to the plume. If lithium deposits on that plate its increasing weight can be measured with a force transducer. This idea was abolished because the amount of lithium is to small to measure with such a measurement device. Another way to use a force transducer would be to measure the force perpendicular to the plate that would also lead to a measurement of the thrust. But this possibility also requires a knowledge of the velocity field which should be avoided.

### 3.2 The QCM-Theory

When a measurement device is used for a specific task it is always useful to know the principles that make it work. In this case, the extreme environment necessitates careful calibration of the system, and an understanding of its theory of operation will make this task easier. It will also help prevent mistakes. The QCM has been used successfully in thruster contamination studies and knowledge gleaned from these is also beneficial and will be described in a subsequent section.

### 3.2.1 Basics

The sensor is a quartz crystal that can be modeled as a mechanical spring-mass-damper system that is driven by a sinusoid. Because of the piezo-electric properties of quartz, the mechanical vibrations manifest as an electrical signal. The measurement of the deposited mass is based on the sensitivity of the quartz crystals resonance to the added mass. No matter how sophisticated the electronics surrounding it, the heart of the deposition monitor is the quartz crystal. The quartz crystal has a frequency response spectrum that is schematically shown in figure 3.4. The ordinate shows the relative response, which is represented by the current flow through the crystal at the specified frequency.

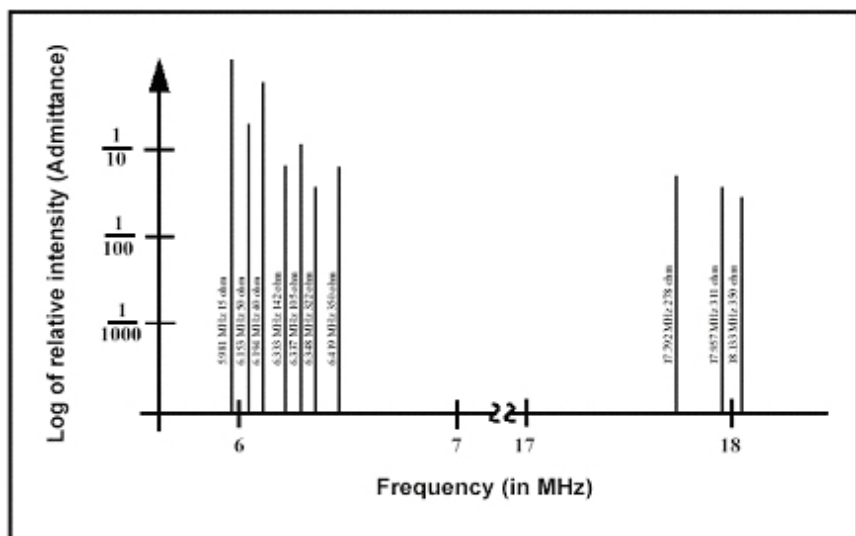


Figure 3.4: Frequency response spectrum. [7]

There are two different modes of distortion of the crystal. They are called thickness shear mode and thickness twist mode. The lowest frequency response showed in figure 3.4 represents the so-called fundamental that is a pure thickness shear mode. The fundamental is the only mode used for the measurements. The responses located slightly higher in frequency are called anharmonics [7]. They are a combination of both modes and should be avoided. To avoid unwanted anharmonic modes and any other undesirable effects, a few approaches were considered in the design of the crystal and its electrodes. First, it was decided to use circular crystals which reduces the number of allowed vibrational modes. The second approach was to contour one face of the crystal to dissipate the energy of the traveling wave before it reaches the edge of the crystal. The energy is not reflected back to the center where it can interfere with other waves and create measurement errors. The wave-free edges are used to clamp the crystal to the holder.

A synthesizer that is connected to the QCM sensor through a diplexer applies a sine wave of a known but variable frequency. When the synthesizer is switched on it has to find the desired lowest resonant frequency that corresponds to the minimum impedance. It finds this lowest frequency by an iterative process [8]. The search for the correct direction is basically a trial-and-error process. The frequency  $f_q$  finally found is saved as the reference. At resonance the phase between voltage and current at the crystal should be zero degrees. However, the capacitance of the cable connecting the crystal to the diplexer is still not known and must be compensated for. This is done with a variable- capacitance diode (varactor). The controller adjusts the capacitance of the varactor diode until the phase is zero and this capacitance is saved. With this the diplexer is balanced and ready to make measurements.

As mass is added to the crystal, the spring mass-damper-system is getting more massive and its electrical characteristics change. Because of the added mass the resonant frequency is lower. The task of the equipment is to measure the exact frequency shift from of the saved start frequency  $f_q$ . It does that by looking for the frequency at which the phase between voltage and current is exactly zero. A micro-controller is employed for controllably varying the frequency of the drive signal and then monitoring the frequency at which the phase detector signal indicates zero [8]. Near resonance the phase changes much more rapidly than the impedance and is a much better indicator of the resonant frequency. The impedance response also becomes broader as mass is deposited making its value harder to determine. The determination of the resonance frequency by detecting zero phase also offers the ability to measure heavily loaded crystals and avoids a mode hopping to the nearest anharmonic. This mode hopping could cause a false reading for the deposited mass. Figure 3.5 Shows the crystal frequency near the series resonance point and also the direction of change of impedance and phase as the crystal is loaded.

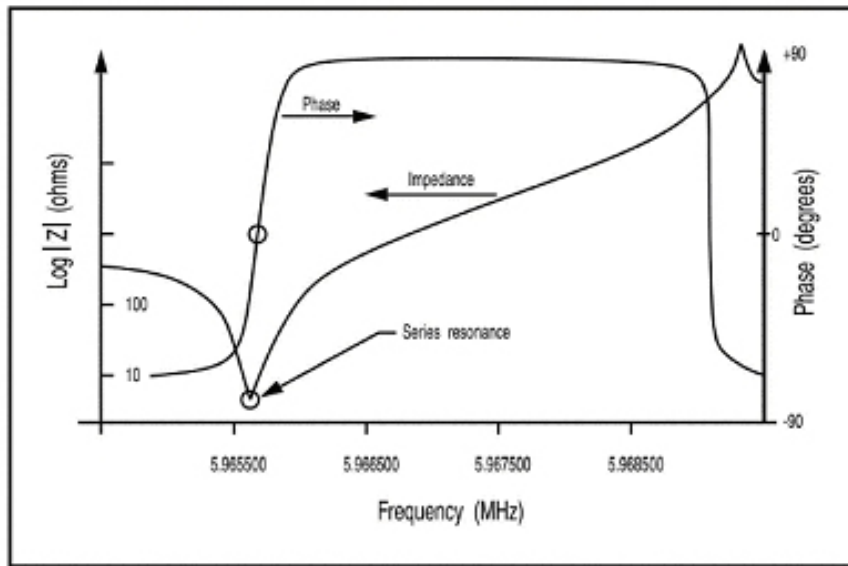


Figure 3.5: Crystal frequency near series resonance point. [7]

The calculation of the amount of the added mass  $\Delta M$  is accomplished using a formula that takes into account the acoustic impedance  $Z_q$  of the quartz crystal [5].

$$\Delta M = \frac{Z_q}{2} * \left( \frac{1}{f_c} - \frac{1}{f_q} \right) \quad (3.4)$$

This equation is a sophisticated version of formula 3.4. The acoustic impedance of quartz crystal is  $Z_q = 8.77 * 10^{-6}$  kg /( $m^2$  s). If the thickness of the deposited film is to be measured, the more complicate z-match equation is needed which takes into account the acoustic properties of the deposited film, the density of the added material and the shear modulus of the quartz. This equation is solved numerically in real-time during the experiment. The physical background of this formula is very complicated and will not be discussed further because our task is limited to mass deposition measurements. The amount of deposition however is limited. In practice, the useable range of the crystal is limited depending on the material and the process conditions. Further details will be discussed in section 3.3.2. Whenever the measurement system is unable to effectively identify and drive a monitor crystal, a special set of sweep and find instructions are executed. This sequence takes up to five seconds as it is repeated a number of times. If the measurement system is unable to recover the measurement will stop.

### 3.2.2 History in the use for Thruster Contamination

The contamination of a space vehicle and its associated equipment by the plumes of electric propulsion thrusters is not a new issue. Because of this, the development of new thrusters is often accompanied by contamination measurements and the improvement of the associated techniques. One successful and common used method is QCM. Due to that the search for former research projects was focused on QCM based measurements. The brief overview of several methods important for the future measurements with the LiLFA will be listed in historical order. A detailed discussion of the projects and a summary of the results is not attempted.

The first project, in historical order, worth mentioning is a research work carried out 1979 by the Jet Propulsion Laboratory at the California Institute of Technology [9]. The task was to determine Pulsed Plasma Thruster Backflow Characteristics. The exhaust plume of a millipound pulsed plasma thruster which uses Teflon as propellant has been investigated using a unique vacuum facility with cryogenically cooled low backscatter chamber walls. Measurements of the plume material scattered from the cooled chamber walls were used with articulated collimator-quartz crystal microbalance measurements of the total flux to estimate the upstream flux originating in the plume. The motivation for that test came from a previous test. That previous test showed that accurate results of a plume measurement are masked by the backscattered flux of particles reflected and eroded from the test facility vacuum chamber. Local measurements of the PPT plume wall backscatter were made using several QCMs mounted in molecular skimmers tied to the cryogenically cooled low backscatter chamber wall. These skimmers were designed to isolate a small portion of the PPT plume and to examine the backscatter from this portion as it impinged on the cooled wall. Figure 3.6 shows a very rough sketch of the experimental setup.

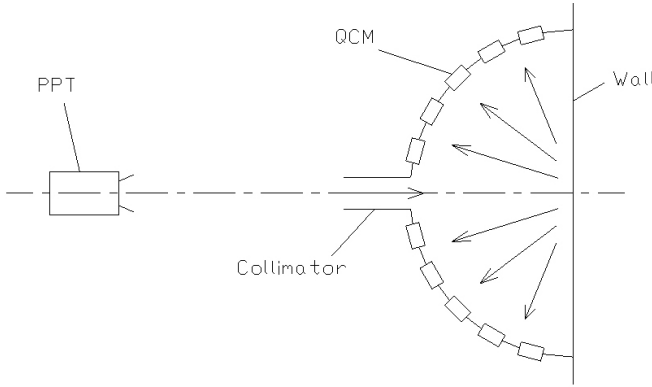


Figure 3.6: Experimental setup of the backscatter test.

The backscattered mass flux was measured by doublet temperature compensated quartz crystal microbalances mounted inside the hemispherical portions of the skimmers. To insure that the PPT plume mass flux that impinges on the QCM is actually deposited on the QCM electrode, the entire QCM was cooled to LN<sub>2</sub> temperature. Due to this temperature requirement and to insure the QCMs would survive in the electromagnetically noisy PPT discharge environment, these QCMs were designed and built at JPL.

There are mainly three results and conclusions of that project which should be considered in the planned tests of the LiLFA. First of all the mentioned tests showed that the backscattering by the walls of a tank is not negligible. Even with the cryogenically cooled wall a detection of a backscattering was possible. Former experiments with the LiLFA showed that the aluminum foil used for covering the inside of the tank got hot and therefore is a large source for backscattering. Another problem is the QCM itself. All vending companies selling QCM equipment sell it with a water cooling system. That means that the QCM-Crystal is warm compared with the LN<sub>2</sub> cooled crystal in the PPT test. This is a source of measurement errors and it cannot be guaranteed that all the material deposits on the QCM. A design of an own QCM system is not possible because of the limited budget. Also the effects of electromagnetically noise should not be neglected.

The next experiment worth mentioning is a test carried out 1995 at the Aerospace Corporation in California [10]. The task was to determine surface modifications in an Ion Thruster plume. The motivation for this test was to investigate the influences of the plume to the surfaces of a future spacecraft. Especially to determine the quantitative effects on optical, thermal and other properties of several materials and paints not known until then. Measurements were made on unexposed control materials to indicate variations within the batch of each material. Control plates were stationed along an arc at about 54 cm distance downstream from the decelerator center. In addition to that mass deposition rates measured as a function of plume coordinate, ion beam current, vacuum chamber background pressure, and extraction grid voltages were accomplished with the use of a quartz crystal microbalance. To reduce the negative effects of material sputtering from vacuum chamber walls an aluminum collimator designed for the 54-cm radial distance, was lined with tantalum foil and attached to the QCM. The single-aperture collimator was designed using ray tracing to view an area slightly larger than the grids at 90 degrees. The QCM was mounted rotatable on a boom to measure the mass flux at the same angle as the control plates with the materials.

The results shall not be discussed in detail but two basic findings are crucial. First, the

repeated mention of backscattering from the chamber walls as source for measurement errors approves the need of a shielding sanction. Second, the thermal influences are not negligible. Trial runs prior to the main test showed that the QCM signal was clearly dependent on the thermal characteristics of the object in view. With grid voltages off, the equilibrium beat frequency varied substantially for many minutes after the main discharge or neutralizer was switched off. As a result, the extreme thermal environment of the LiLFA will require careful thermal calibration of the QCM. During the same test run it was found that a 15-min time interval was necessary for the QCM to reach stability after being moved. That shows the necessity of prior tests to block out regions of the data file where mass flux measurements were likely to be affected by a change in settings. Enjoyable is the fact that the influences of vacuum chamber pressure on the QCM were found negligible. Another point is interesting for the LiLFA contamination studies in general. While a number of the samples on the control plates acted as simple sputter monitors, the behavior of the paints was complex, showing strong dependence of surface deposition layer on paint chemistry.

The last test examined in this section is a flight experiment accomplished 1999 [11]. The Electric Propulsion Space Experiment (ESEX) was launched and operated in early 1999 to demonstrate the compatibility and readiness of a 30-kW class ammonia arcjet for satellite propulsion applications. A major goal of ESEX was to measure the surface contamination affects due to the 30-kW class arcjet in flight. An array of sensors was positioned at strategic locations of the ESEX package to assess the contamination effects. As part of this onboard sensor array, four thermoelectric quartz crystal microbalances were used to measure material deposition at selected locations on the spacecraft surface. The sensors were held at a temperature that would allow them to condense metallic materials eroded from the electrodes, but that were insensitive to possible deposition of the propellant gas. In preflight thermal analysis a 210-K temperature was found to be maintainable through the solar cycle. This temperature was achieved by thermoelectrical cooling, giving the sensor its name. The first result worth mentioning is the fact that significant deposition was observed near the arcjet nozzle but just during the first firing. This anomalous deposition is attributed to contaminants within the arcjet body, collected during handling and storage, which were ejected during the first firing. That shows that it is not advisable to trust the first measurements, referring to time, during the firing of a thruster. Also a temperature gradient across the crystal diameter influenced the measurement. During the test it was found that an exposure of the TQCM sensor crystal to radiation from the sun or the arcjet firing affected the oscillation frequency by creating such a gradient. Just the solar flux for instance causes an oscillation amplitude of about 200 Hz. It also showed that the measured frequency decreases with increasing temperature, causing an increase in the measured mass deposition. Although the sensor crystal returned to the original frequency when the radiation source was removed, it confirms the need for a thermal calibration.

In conclusion it can be said that the mass deposition measured by the QCM can be a result of several physical processes including condensation, vaporization, absorption, chemical reaction into more or less volatile molecules, energy deposition releasing previously collected material, sputtering, etc. All these effects must be taken into account if an exact mass flux in a plume shall be measured. Also the effects of temperature, electromagnetical noise and repositioning are not negligible.

### 3.3 The Equipment

After understanding the basic background of the QCM it is important to know how the hardware and its associated software works. This is necessary to understand the possibilities and limits of this measurement device and to know which factors and problems must be considered in the experimental setup. For that the probe itself and the monitoring unit are discussed in more detail. After that, the basic specifications will be listed to understand the possibilities and limits mentioned above. The limits of this technique and a few adjustable parameters important for the LiLFA test will be explained.

#### 3.3.1 Hardware

The most critical part of the equipment is definitely the probe since it will be exposed to the extreme environment of the lithium plume. For a better understanding of the following explanation, figure 3.7 shows the complete sensor head as it will be used in the tests. Figure 3.8 shows the internal structure of the probe and the crystals.

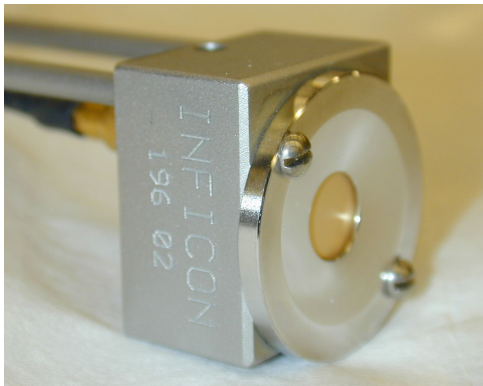


Figure 3.7: The compact sensor head housing.



Figure 3.8: Internal details and crystals.

The probe itself is a QCM compact sensor and consists of a housing made of stainless steel [7]. This material has a big advantage in the system because of its very low reactivity with lithium. It also has very low thermal conductivity. This helps to keep the heat on the outside of the probe. The circular standard crystal holder in front of the housing can be detached to replace the crystals. Two holes were added to the crystal holder to secure it to the front of the housing using machine screws. That will be discussed in more detail in chapter 4. The water cooling of the inside of the housing is realized by two water tubes. These tubes are also made of stainless steel and have an outside diameter of 3.2 mm (1/8 in.). Two tapped holes are provided on the back of the sensor body for attaching the probe to the system. The inside of the housing shown in figure 3.8 is the place where the measurement itself takes place. The circular finger spring contact system provides contact to the front side of the crystal; This side of the crystal will be contaminated during the test. The three leaf springs mounted on the crystal retainer in the center of the housing provide contact to the backside of the crystal. Springs and other electrical contacts are made of gold plated Beryllium-Copper. The crystal retainer is the most critical part of the probe and is made of Teflon. The melting point of Teflon limits the temperature range of the sensor head. Both spring systems are wired to the Microdot connector on the back of the sensor head. It consists of Teflon and glass insulated stainless steel. The supplied wire is a 50 Ohm Teflon insulated coaxial cable.

The crystals used are circular and have a diameter of 14 mm and a thickness of 0.25 mm. The front side of the quartz crystal is covered by a layer of gold. This layer is one of the electrodes. Gold was favored instead of silver because of its lesser reactivity with lithium. The backside of the crystal is covered by an electrode made of another metal. This is the exciting electrode. Its size is reduced compared to the crystal to dissipate the energy of the travelling acoustic wave before it reaches the edge of the crystal. During the measurement just the center part of the crystal is exposed. The outer part is used to clamp the crystal to the crystal holder. The diameter of the exposed part is 7.9 mm.

The largest part of the whole measurement device is the monitor unit and its associated cable system. The task of the monitor is to supply a signal to resonate the crystal and to maintain a constant phase as explained in section 3.2.1. It is also a device to display the data and to provide connections to a computer. For an understanding of that hardware device, just the parts and features of the monitor concerning our experiments will be shown. A detailed listing and explanation can be found in the users manual of the monitor [7]. Figure 3.9 shows the monitor with its liquid-crystal display.



Figure 3.9: The monitor unit.

The liquid-crystal display shows the deposited mass and its rate of deposition. It can also be used to show the thickness or the frequency. The modes and the unit of the mass deposition can be changed with switches on the back of the monitor. Switching between modes during the test is not possible. Apart from other data, the display shows the time since zeroing the device and highlights a warning if the crystal fails. The keypad can be used to show the used lifetime of the crystal during the test and for zeroing the device. Apart from the "Prog" button the shutter keypad is not used because the probe was ordered without a shutter system to save costs and to prevent problems during the design. With the help of the "Prog" mode a few parameters like the density can be adjusted. Apart from the power supply, the rear of the monitor contains connectors for the communication with other devices. A high density 15-pin female "D" connector provides the connection to the sensor head. To wire this connector with the feed through a 4.58 m long multi conductor cable with coax is used. At the end of this cable there is a RF diplexer, cable capacitance compensation and an amplitude and phase detector. At the rear of the monitor there are also three different connectors to obtain an output from the monitor. One is a BNC connector that supplies an analog voltage proportional to rate or mass deposition. The second one is a RS232 connector and the third one is an optional GPIB-connector. Because a software interface was planned, the GPIB-connector was ordered to connect the monitor to the computer.

### 3.3.2 Basic specifications and free parameters

For a later analysis of the results and for preventing failures and errors during the measurement it is important to know the basic specifications of the QCM probe and its associated equipment. For this mainly four factors are important. The accuracy of the quartz crystal and its limits concerning the maximum amount of mass the crystal can take before it fails. This limit is important for a subsequent estimation of the saturation time of the device. Also needed is the resolution of the values provided by the QCM monitor. They are needed for a later analysis of the results, especially for the estimation of error bars. The sampling rate of the device is needed to prevent a loss of data in the computer setup.

The measurement usually starts with an uncoated crystal which vibrates at a frequency of  $f_q = 6 \text{ MHz}$  [7]. When mass is deposited the frequency decreases as explained in section 3.2.1. According to the vendor, the lower limit of the measured crystal frequency is  $f_c = 5 \text{ MHz}$ . That means the maximum frequency shift is  $\Delta f = 1 \text{ MHz}$ . According to section 3.2.1 the maximum mass can be calculated:

$$\Delta M = \frac{Z_q}{2} * \left( \frac{1}{f_c} - \frac{1}{f_q} \right) = 14.6 \text{ mg/cm}^2 \quad (3.5)$$

If we take into account the exposed area of the crystal which is  $A_{expose} = 0.49 \text{ cm}^2$  the crystal will saturate if the amount of deposited mass is higher than  $\Delta M_{max} = 7.1 \text{ mg}$ . The same calculation can be done for estimating the accuracy of the quartz crystal. The accuracy of the frequency shift is  $\Delta f = \pm 0.1 \text{ Hz}$ . With this and the exposed area of the crystal we get an accuracy of  $\Delta M = \pm 0.5 \text{ ng}$ . An engineer from the vendor confirmed these theoretical assumptions [5]. In practice, the deposited film introduces stress to the crystal which limits the useable range depending on the ductility of the material. Apart from that the impedance of the lithium itself was neglected in equation 3.5. Unfortunately data concerning lithium was not available. Due to that, the maximum amount of lithium which can be deposited on the crystal is a bit lower and was estimated to  $M_{max} = 5 \text{ mg}$  for further calculations. This corresponds with the experience of the vendor with similar materials. The calculated amounts and the figures provided by the vendor are listed in table 3.1.

Table 3.1: Basic specifications

|                                |                      |
|--------------------------------|----------------------|
| <b>Accuracy</b>                | $\pm 0.5 \text{ ng}$ |
| <b>Resolution</b>              | $\pm 1.0 \text{ ng}$ |
| <b>Sampling rate</b>           | 4 Hz                 |
| <b>Maximum mass deposition</b> | $\sim 5 \text{ mg}$  |

Apart from the basic specifications it is important to know which are the free parameters of the device and which ones are important concerning mass deposition measurement. The QCM was originally developed to measure the thickness of the film of a deposited material on the crystal. For this the density is needed which allows a conversion of the mass information into thickness. It is obvious that this parameter does not influence the measurements in our case. That applies also to the Z-Ratio that is a parameter that corrects the frequency change to thickness transfer function for the effects of acoustic impedance mismatch between the crystal and the coated material. Due to the fact that neither of the free parameters is important concerning mass deposition measurements it obvious that these parameters need not to be considered in our case because they do not influence the measurements [5].

# Chapter 4

## Design of a Condensing Mass Flux Probe (CMFP)

After the comparison of the different mass deposition measurement techniques and the analysis of the advantages and disadvantages of the quartz crystal microbalance probe it was determined that a shielding of the sensor head was necessary. The extreme environment of the lithium plume and the risk of early saturation of the QCM required the design of a Condensing Mass Flux Probe (CMFP) in which the QCM sensor head can be integrated. The chapter starts with a rough estimation of the expected mass flux, followed by an analysis of the requirements of the CMFP. Next the necessity and the technical problems concerning a shutter system are discussed. The design and the fabrication of the CMFP are explained.

### 4.1 Expected Mass Flux

For the calculation and analysis of the thermal environment and the estimation of the time until the saturation of the QCM an estimation of the expected mass flux is needed. The range of the total mass flux of the LiLFA thruster is  $\dot{M} = 10\text{-}20 \text{ mg/s}$ . The amount of lithium that deposits on the QCM obviously depends also on the distance  $d$  between the thruster and the CMFP. This could lead to saturation and heat flux problems, especially if the total mass flux is increased and the mentioned distance is small. Therefore, the estimated mass flux was calculated as a function of the total mass flux  $\dot{M}$  and the distance  $d$  between the thruster and the CMFP. It shall be mentioned that the following calculation is a very rough estimation using very liberal approximation.

First of all it is necessary to determine how the thruster basically works and how the applied magnetic field and the geometry of the thruster influences the plume in general. In chapter 2 it was mentioned that the exit of the anode has a radius of  $r_A = 3.5 \text{ cm}$ . Its shape was designed to follow the magnetic field lines of the external solenoid coil. These field lines generate a magnetic nozzle that goes of the thruster, limiting plume divergence. The cathode tip is the source of the total mass flux. The shape of the plume was modeled like a section of a sphere. This section of a sphere is touching the outside of the tip of the cathode and the inside of the end of the anode. A rough sketch of the explained approach is showed in figure 4.1.

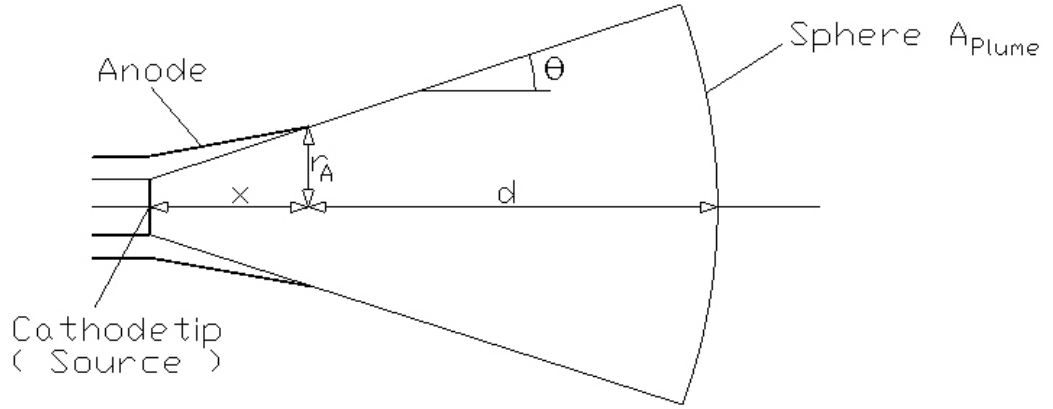


Figure 4.1: Plume modelling.

According to drawings the distance between the cathode tip and the exit of the anode is  $x = 7$  cm. The radius of the cathode is  $r_C = 1.2$  cm. From this the half angle  $\Theta$  is calculated by:

$$\Theta = \arctan \frac{r_A - r_C}{x} = 18.19 \text{ deg.} \quad (4.1)$$

In the following calculation of the radius of the sphere it was assumed that the cathode tip is infinitesimal. With this the radius  $r_S$  of the sphere is  $r_S = x + d$ . The total mass flux is assumed to cover the part of the sphere uniformly. The surface area of the part of the sphere  $A_{Plume}$  can be calculated as a function of the half angle  $\Theta$ , the radius at the anode exit  $r_A$  and the distance  $d$ :

$$A_{Plume} = \int \int dA_{Plume} = r_s^2 \int_0^{2\pi} \int_0^\theta \sin\theta \, d\theta \, d\phi = 2\pi(1 - \cos\theta)(x + d)^2 \quad (4.2)$$

Finally the mass flux  $\dot{m}$  as a function of the total mass flux  $\dot{M}$  can be estimated:

$$\dot{m} = \frac{\dot{M}}{A_{Plume}} = \frac{\dot{M}}{2\pi(1 - \cos\theta)(x + d)^2} \quad (4.3)$$

The LiLFA is operating between  $\dot{M} = 10$  mg/s and  $\dot{M} = 20$  mg/s total mass flux. However the most tests will be with a total mass flow of  $\dot{M}=10$  mg/s. In addition the minimum distance  $d$  to the thruster is limited to  $d = 40$  cm. Due to the applied field of the LiLFA and the resulting magnetic nozzle the acceleration of the plume continues after the lithium leaves the anode. But measurements should be taken just in the fully developed plume. The baffles at the end of the tank are marking the maximum distance  $d = 160$  cm. Table 4.1 shows the expected mass flux dependent on the total mass flux  $\dot{M}$  and the distance  $d$ .

Table 4.1: Expected mass flux  $\dot{m}$

|                   | $d=40$ cm                                  | 60 cm | 80 cm | 100 cm | 120 cm | 140 cm | 160 cm |
|-------------------|--|-------|-------|--------|--------|--------|--------|
| $\dot{M}=10$ mg/s | $14.4 \mu\text{g}/(\text{s } \text{cm}^2)$ | 7.1   | 4.2   | 2.8    | 2.0    | 1.5    | 1.1    |
| $\dot{M}=20$ mg/s | 28.8                                       | 14.2  | 8.4   | 5.6    | 4.0    | 3.0    | 2.3    |

In a real test the magnetic field lines are diverging with increasing distance. Former tests also showed that lithium contamination took place even upstream of the anode. That confirms that the magnetic field does not keep the plasma directed. Especially at large distances  $d$ . Because of that the amounts of table 4.1 are the upper limits of the expected mass flux for measurements off the thruster axis. Just in a really small distance and also in the axis of the thruster the amounts can be higher because the assumption of an infinitesimal cathode tip is not valid anymore.

## 4.2 Requirements

For a determination of the design requirements of the CMFP a determination of the plume environment is essential. The problems that come with this environment have to be analysed and estimated previous to the start of the design. For this, the thermal environment and the interaction between a body and the hypersonic flow are discussed in a deeper manner. The saturation problem, the interaction between lithium and other materials and the sputtering from the tank walls are also not negligible factors.

### 4.2.1 High Temperature Environment

The most critical issue is doubtless the high temperature environment. The vendor specified the maximum temperature of the QCM probe to 130 degrees Celsius [7]. This limit is based on the melting temperature of the teflon parts behind the crystal inside the probe. An exposure of the whole sensor head to the plume is not necessary. Just the crystal has to be directly in the plume to ensure a correct measurement. Due to this and the fact that the most sensitive parts are directly behind the crystal the crystal shall be considered isolated from the rest of the probe in the following calculations. In a real test the probe is water cooled to keep the temperature far below the maximum temperature and to ensure the accuracy of the highly temperature sensitive quartz crystal. During the test an emergency shut down of the water cooling could be necessary because of leaks or other unforeseen incidents. It shall be determined if the probe will be destroyed in that case. Because of this the following calculations do not consider an active cooling of the crystal. To calculate the temperature of the crystal exposed to the plume an estimation of the energy flux to and from the crystal is necessary. The energy flux to the crystal consists mainly of three parts. First, there is the radiation by the thruster and the plume. The anode and the cathode have an average temperature of about 2500 K and are a significant source of radiation. Also not negligible is the radiation of the plume itself due to its large surface. Also the lithium itself is an energy source. The incoming lithium ions are decelerated and condensed on the crystal and transfer their high kinetic energy to its surface. Also a large source of energy is the recombination of the lithium ions on the surface of the crystal. With this the ions give off all their energy they got during the ionization process. On the other hand the crystal radiates energy especially if the temperature increases. The crystal lays free on its front side. On its backside it lays just on three thin leaf springs which provide contact to the probe. Due to that it can be assumed that the crystal radiates to both sides. The energy accumulation by the crystal is negligible because of its low mass compared to the big surface. The conduction between the crystal and the rest of the probe was also neglected. There are just very small contact points between the crystal and other parts of the probe which have a really bad conductivity. A neglect of the conductivity gives us the maximum temperature the crystal and thus the other parts can get. With all

these assumptions the power balance of the crystal is basically

$$P_{kinetic} + P_{radiation(thruster)} + P_{recombination} = P_{radiation(crystal)}. \quad (4.4)$$

This leads to the more detailed equation.

$$\begin{aligned} 0.5 & A_{expose} \dot{m} v^2 + (F_{A-QCM} + F_{C-QCM}) A_{expose} \epsilon_T \alpha_{QCM} \sigma T_T^4 + A_{expose} \frac{\dot{m}}{m_{Li}} W_{ion} e \\ &= 2A_{QCM} \epsilon_{QCM} \sigma (T_{QCM}^4 - T_B^4) \end{aligned} \quad (4.5)$$

Table 4.2 shows the figures and amounts used in equation 4.5 [12],[13]. The speed  $v$  of the incoming lithium ions is calculated with the help of former tests with the LiLFA at the Moscow Aviation Institute [4]. With a total mass flow of  $\dot{M} = 13.5$  mg/s a thrust of  $T = 0.504$  N was measured. This leads to a speed of about  $v = 37000$  m/s.

Table 4.2: Basic specifications

|                              |                  |                            |
|------------------------------|------------------|----------------------------|
| Atomic weight of lithium     | $m_{Li}$         | $1.152 \times 10^{-26}$ kg |
| Emissivity of the QCM        | $\epsilon_{QCM}$ | 0.1                        |
| Ionization energy of lithium | $W_{ion}$        | 5.392 eV                   |
| Emissivity of the Thruster   | $\epsilon_T$     | 0.29                       |
| Cathode radius               | $r_C$            | 1.2 cm                     |
| Absorptivity of the QCM      | $\alpha_{QCM}$   | 1.0                        |
| Anode radius                 | $r_A$            | 3.5 cm                     |
| Thruster Temperature         | $T_T$            | 2500 K                     |
| Area of the entire crystal   | $A_{QCM}$        | 1.54 cm <sup>2</sup>       |
| Flow speed                   | $v$              | 37000 m/s                  |

Equation 4.5 shows, that a rough estimation of the mass flux in the plume is needed for the assumption of the kinetic energy flux and the recombination effects. The mass flux in the plume as a function of the distance  $d$  can be estimated with the help of the calculations in section 4.1. The term for the radiation and the energy storage of the plume is missing. Because of the very complicated physics of the plume a satisfying mathematical model for its radiation could not be found. Due to that all other factors were chosen to be a worst case scenario. The anode and the cathode are modeled as two plates normal to the thruster axis. The radiation shape factors  $F_{C-QCM}$  and  $F_{A-QCM}$  can be calculated as a function of the distance  $d$  with the help of equations in literature about heat transfer that shall not be discussed in a deeper matter [12]. A more significant problem is caused by the factors concerning lithium. The emissivity  $\epsilon$  of similar shiny materials like gold which covers the crystal is around  $\epsilon_{QCM} = 0.1$ . An amount for the absorptivity  $\alpha$  could not be found and was set to  $\alpha_{QCM} = 1.0$  for a "worst case" scenario. For an estimation of the radiation of the quartz crystal the geometry of the probe has to be considered. Just a part of the crystal is exposed to the plume while the outer parts of the front side and the whole backside is covered by the circular front part of the sensor head without a significant contact area. The assumption of the same emissivity  $\epsilon_{QCM}$  for the lithium covered exposed part and the gold covered rest of the crystal simplifies the calculations. The background temperature was assumed to be  $T_B = 80$  degrees Celsius ( 353.1 K) which is approximately the temperature of the inside of the tank during the test. A separate calculation of the three different kinds of incoming energy flow showed, that the kinetic energy flux is the main part. It contributes about 90 % of the total energy flux even in positions close to the thruster while

recombination counts less than 10 % and the radiation of the entire thruster is negligible with less than 1 %. Table 4.3 shows the expected energy flux to a body facing the thruster as a function of total mass flow  $\dot{M}$  and distance  $d$ .

Table 4.3: Expected energy flux

|                   | $d=40$ cm              | 60 cm | 80 cm | 100 cm | 120 cm | 140 cm | 160 cm |
|-------------------|------------------------|-------|-------|--------|--------|--------|--------|
| $\dot{M}=10$ mg/s | 11.6 W/cm <sup>2</sup> | 5.7   | 3.4   | 2.2    | 1.6    | 1.2    | 0.9    |
| $\dot{M}=20$ mg/s | 23.1                   | 11.4  | 6.7   | 4.5    | 3.2    | 2.4    | 1.8    |

According to calculations with equation 4.5, tab. 4.4 shows the resulting temperature of the crystal dependent on the distance  $d$  and the total mass flow  $\dot{M}$ .

Table 4.4: Expected crystal temperature

|                   | $d=40$ cm | 60 cm  | 80 cm | 100 cm | 120 cm | 140 cm | 160 cm |
|-------------------|-----------|--------|-------|--------|--------|--------|--------|
| $\dot{M}=10$ mg/s | 1080 C    | 860 C  | 720 C | 630 C  | 560 C  | 500 C  | 450 C  |
| $\dot{M}=20$ mg/s | 1330 C    | 1070 C | 910 C | 790 C  | 710 C  | 640 C  | 590 C  |

The figures show that the resulting temperatures are much higher than the maximum temperature of 130 degrees C. The probe will be destroyed if the whole exposed area of the crystal or even the whole front side of the sensor head is covered by lithium. Due to that it was thought about reducing the exposed area of the crystal by an aperture in a future CMFP in front of the crystal not too far away from it.

Discussions with the vendor of the QCM probe resulted that the exposed area can be reduced without effecting the measurement negatively if the remaining area is circular and in the middle of the crystal. Further calculations using equation 4.5 considering a reducing of the exposed crystal area by a aperture resulted in the fact that the temperatures are still much too high without a water cooling. Even if the largest distance  $d = 160$  cm and the lowest total mass flux  $\dot{M} = 10$  mg/s is assumed the required diameter of a aperture is less than 1 mm. Such a small aperture is not possible because the influence of other negative effects like a blockage of the aperture by lithium contamination is not acceptable. Concluding it can be said that the QCM probe will be destroyed if its own water cooling fails even if the exposed area is limited. Though a slight reducing of this area could be useful to provide an exacter measurement of the temperature sensitive crystal. Due to not destroy the QCM and the fact that the energy flux is high in general a water cooling of the surrounding CMFP is necessary for using it as a second heat sink for the QCM probe. Apart from that a shutter system would be convenient to save the probe from the energy flux of the plume in times were no measurement is taken and in case of an emergency shut down of the water cooling.

#### 4.2.2 Interaction between the plume and a bluff body

A very important issue for the design of a CMFP is an analysis of its expected influence on the measurements. Basically is has to be determined if the interaction between the plume and the body is like a gas continuum flow or if it has to be modeled as a molecular flow. In a continuum flow effects like shock fronts or shock waves have to be considered because they are affecting the measurement. If the flow can be seen as a molecular flow

these effects are not important and the shape and size of the CMFP should not affect the measurements. This depends on the Knudsen number  $\text{Kn}$  which is the ratio of the mean free path  $\lambda$  of a molecule and the characteristic length of a body  $L_c$ . This characteristic length  $L_c$  is in this case the diameter of the front side of the CMFP. Different values of the Knudsen number  $\text{Kn}$  imply different flow regimes [14]:

Table 4.5: Flow regimes

|                       |                  |
|-----------------------|------------------|
| $\text{Kn} > 1$       | → Molecular flow |
| $1 > \text{Kn} > 0.3$ | → Slip flow      |
| $\text{Kn} < 0.3$     | → Continuum flow |

If we take into account the necessity of a shutter system and a water cooling of the CMFP this device will be much bigger than the QCM itself. Its characteristic length can be assumed to be  $L_c = 10 \text{ cm}$ . The mean free path  $\lambda$  can be calculated as

$$\lambda = \frac{1}{\sqrt{2\pi n_{Pl} r_{Li}^2}} \quad (4.6)$$

Where  $r_{Li} = 1.52 \times 10^{10} \text{ m}$  is the radius of the lithium atom and  $n_{Pl}$  is the number density in the plume [13]. The necessary number density inside the plume  $n_{Pl}$  consists of two parts, the number density of the lithium  $n_{Li}$  and the number density of the remaining air in the tank  $n_{air}$ . With this the number density  $n_{Pl}$  can be calculated.

$$n_{Pl} = n_{Li} + n_{Air} \quad (4.7)$$

The number density  $n_{Li}$  can be calculated with the liberal estimated mass flux of lithium in section 4.1, the speed  $v$  and the atomic mass  $m_{Li}$ .

$$n_{Li} = \frac{\dot{m}}{vm_{Li}}. \quad (4.8)$$

In addition we can calculate the number density  $n_{air}$  with the familiar thermodynamic equation

$$n_{Air} = \frac{p_B}{kT_B}. \quad (4.9)$$

Where  $p_B = 6.67 \times 10^{-3} \text{ Pa}$  is the pressure inside the tank. Considering  $d = 40 \text{ cm}$  and  $\dot{M} = 20 \text{ mg/s}$  for a worst case scenario we obtain a mean free path of  $L_c = 4.75 \text{ m}$  and a Knudsen number of  $\text{Kn} \sim 40$ . This shows that the aerodynamic properties of the CMFP and its size play a negligible role. Even if we assume a one hundred times higher mass flux than the estimated mass flux of section 4.1 the flow can still be modeled like a molecular flow. However, the sputtering and reflection of material from parts located upstream of the QCM in such cases would probably not be negligible. This has to be considered for instance for a design of a shutter system.

### 4.2.3 Other requirements

The most important issue apart from the requirements concerning high temperature environment and flow interaction with the CMFP is doubtless the saturation problem of the crystal. According to section 3.3.2 the maximum amount of mass that can be deposited on the crystal before it fails is 5 mg.

The maximum load of the feeding system of the LiLFA is about 300 g of lithium. Experience from former tests has shown that about 50% of the propellant is wasted due to losses in the feed system. That means that the maximum time of the experiment is between 250 minutes and 125 minutes depending on the limits of the total mass flow  $\dot{M}$  that were mentioned in section 4.1. The following calculations are accomplished with a total mass flux of  $\dot{M} = 10 \text{ mg/s}$  and the resulting maximum time of 250 minutes. It is important that at the minimum distance  $d = 40 \text{ cm}$  to the thruster the saturation time  $t_{sat}$  of the crystal is in this time limit for using the entire firing time for a scan of the plume. Calculations of the saturation time  $t_{sat}$  using the results of section 4.1 leaded to a saturation time of about  $t_{sat} = 12 \text{ minutes}$  if the whole open area of the crystal is exposed to the plume. It is obvious that such a small saturation time is unacceptable. The estimation shows the necessity of a limitation of the exposed area  $A_{expose}$  by a aperture and/or the use of a shutter system which intercepts the mass flow to the crystal after a data set is completed. The shutter should allow a reopening during the test after the thruster parameters are changed. Table 4.6 shows the estimated saturation time  $t_{sat}$  dependent on the diameter  $d_A$  of a future aperture. The use of a shutter is not considered.

Table 4.6: Saturation time  $t_{sat}$  of the crystal in a distance  $d=40 \text{ cm}$

|           | $d_A=6 \text{ mm}$ | 5 mm    | 4 mm    | 3 mm    | 2 mm     | 1.7 mm   | 1 mm     |
|-----------|--------------------|---------|---------|---------|----------|----------|----------|
| $t_{sat}$ | 21 min.            | 30 min. | 46 min. | 82 min. | 184 min. | 254 min. | 736 min. |

The results show that a aperture diameter of about  $d_A = 1.7 \text{ mm}$  is needed to confirm a use of the QCM probe for the entire time of the measurement if a shutter system is not considered. It was mentioned in section 4.2.1 that such a small diameter  $d_A$  could lead to a blockage of the aperture by lithium contamination. Due to that a larger diameter  $d_A$  in combination with a shutter system is needed. Finally, a diameter of

$$d_A = 3.18 \text{ mm (1/8in.)} \quad (4.10)$$

was seen as a good compromise. In combination with a shutter system it allows measurements during 1/3 of the maximum possible time of an experiment and avoids a blockage of the aperture in all likelihood. Apart from avoiding a possible saturation of the QCM there is another reason for a shutter system. At the beginning of the test the plume will consist not just of vaporized and charged lithium but also of liquid lithium. If liquid particles hit the QCM-probe the measurement will be destroyed. In the worst case even the whole probe. Apart from that measurements shall be taken just under steady state conditions that takes about 6 to 8 minutes. Due to that the probe has to be covered during the start of the firing.

Another issue that should be considered in the design of a CMFP is the interaction of lithium with other materials. For budget reasons the CMFP will mainly consist of the four materials steel, aluminum, copper and stainless steel. The parts of the CMFP that are directly exposed to the plume should consist of stainless steel because this material has the lowest thermal conductivity and the best resistivity to lithium of the mentioned materials. Also the high melting point avoids a damage of the probe. The low conductivity will save the inside of the CMFP from the hot plume environment. Due to the fact that the inside of the CMFP and with that the QCM shall be actively cooled the high conductive materials copper and aluminum should be used in the inside of the probe. The backside of the QCM probe should be kept open for the integration of a thermocouple. Due to an

expected sputtering of material from the tank walls a gap is needed between the aperture and the QCM. The sputtered material is considered to enter the aperture in a very high angle to the normal axis of the aperture plane. Because of the gap this material hits the surface of the circular front part of the QCM sensor head and not the crystal. Due to that this material will not be measured.

## 4.3 The Shutter System

Before the design of the Condensing Mass Flux Probe (CMFP) was started, thought was given to the basic layout and integration of a shutter system. As mentioned in the requirements for the CMFP, a shutter system is needed for several reasons. The basic layout of the shutter system is described below and the selection and testing of a proper actuator and its basic kinematics, including geometry, is described.

### 4.3.1 Basic layout

Basically the shutter was designed as a thin plate made of stainless steel due to the fact that the plate is directly exposed to the plume. It should be parallel to the crystal leaving a small gap between these two devices. It should also move parallel to the surface of the crystal. Layouts with a tilting plate were rejected because of expected opening effects. It is fixed on one of its ends to a turning actuator shaft. The shutter plate should expose the Quartz Crystal in the open position and shield it in the closed position.

### 4.3.2 Choice and test of a proper actuator

At the start of the design it was thought about a proper actuator for the movement of the future shutter. A few requirements were identified. First, the actuator should be strong enough to move the shutter and it should work reliably. It must not be allowed to disturb the plume in any case. If necessary, this had to be proven in preliminary tests. In addition to this the actuator must be able to survive the hostile environment; at least if it is not directly exposed to the plume. Finally it should be small and not too expensive. At first an electromotor was considered. The advantages are obvious. On one hand an electromotor would drive the axis of the shutter directly without the need for a transmission or any other kind of complicate kinematics. On the other hand small and light electro motors are available and are not too expensive. The problems of such an actuator can be found in the plume environment. Nearly all of the available small electro motors come with a housing made of plastic or at least parts of plastic. Earlier tests with the LiLFA showed that plastic parts melted even if they were cooled or not directly exposed to the plume. Another problem comes with the inherent magnetic field of such a device. Even if the motor is powered only during the movement of the shutter a residual magnetic field remains that can possibly disturb the highly charged plume. Because of these disadvantages the use of an electro motor was abandoned. A solenoid that could move an actuator arm with the help of a magnetic field was abandoned for the same reasons. A solenoid would be more likely to survive the plume but it has an even stronger magnetic field. After the rejection of electric devices, it was thought about actuating the system with an air cylinder that uses pressurized gas to extend and retract a little plunger. The advantages are on one hand no disturbance of the plume by a magnetic field and on the other hand the material of the actuator. Most of the actuators were made of stainless steel that has a very high melting point, low thermal conductivity and low reactivity with lithium. These facts help

it to survive the hostile environment. Another advantage is the low cost of such a device. But the device comes with a few disadvantages. Most of the actuators are large and that makes it difficult to integrate into the CMFP. Such an air cylinder has no rotating parts but a plunger that moves forward and backwards. This dictates the layout of the kinematics that moves the shutter. Another disadvantage is the fact that small leaks could disturb the plume perhaps as much as the magnetic field of a solenoid.

The smallest available air cylinder was chosen. It was decided that the required kinematics is doable and that the cylinder can be mounted on the backside of a plate that shields it from the lithium environment. Also it can be determined in a preliminary test if the cylinder leaks.



Figure 4.2: Air cylinder with gas connectors.

The cylinder can be seen in figure 4.2. On the very right side is the plunger in the extended position. Including the extended bar, the air cylinder has a length of about 11.5 cm. In the retracted position the bar emerges about 1 cm out of the cylinder body. The maximum extension is  $\Delta y = 2.54$  cm. The plunger can be retracted by pressurizing the right 0.32 cm outside diameter gas connector and extended by pressurizing the left connector. The upper limit for pressurization is  $1.72 \times 10^6$  Pa providing a force of about 70 N. A hole located on the very left side is provided to attach the cylinder to another device. The mentioned leak test was implemented in a small bell jar that is used in the lab. With the use of a mechanical and a diffusion pump, a pressure of  $p = 6.67 \times 10^{-2}$  Pa could be reached in the bell jar. This is enough analogous to the LiLFA tests which were accomplished with a pressure of  $p = 6.67 \times 10^{-3}$  Pa. Pressurized gas was provided by a bottle of nitrogen at a maximum pressure of  $6.2 \times 10^5$  Pa. The gas was sent to the cylinder by plastic tubes connected to the nitrogen gas bottle, the feedthrough of the bell jar and two 0.32 mm outside diameter copper tubes inside the bell jar that served as mounts for the cylinder. The plunger of the cylinder was moved about 25 times by alternately pressurizing the tubes. The monitor of the discharge vacuum gauge used a resolution of  $\Delta p = 6.67 \times 10^{-4}$  Pa. During the test no increase of the pressure inside the bell jar was detected. This validated the air cylinder for the use as a shutter actuator in the LiLFA test.

### 4.3.3 Kinematics and geometrical aspects

After the leak test was accomplished successfully and the use of the air cylinder as an actuator of the shutter system was sure it was thought about the kinematics. The extension and retraction of the plunger of the air cylinder had to be formed into a rotation of the axis of the shaft connected to the shutter plate. Because the plunger of the air cylinder is linear a solution with two fixed and one moving pivot points was chosen. Figure 4.3 shows the basic kinematics. The air cylinder was drawn shorter compared to the other parts to highlight the more important movement of the plunger and the actuator arm.

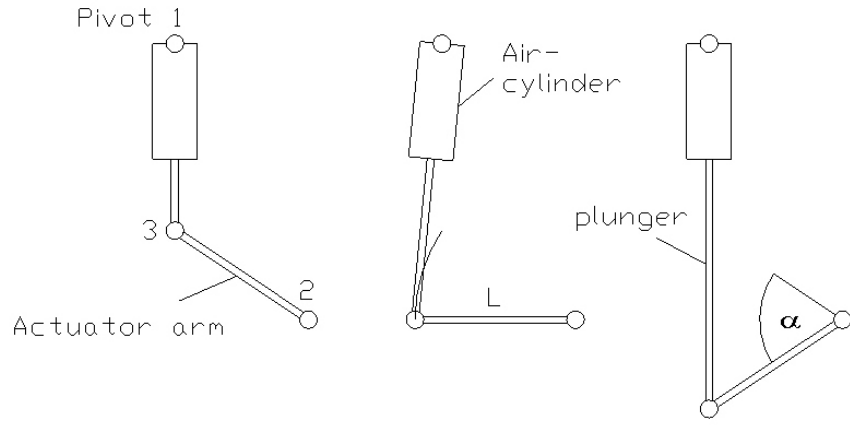


Figure 4.3: Kinematics of the shutter system.

To simplify the design, it was decided to mount the air cylinder vertical on the back plate of the CMFP with the tip of the plunger pointing toward the floor. The air cylinder is mounted to the plate with the hole that is located on the end of the cylinder as seen at the left side of figure 4.2. It is able to rotate around the axis of pivot point one. The maximum extension is  $\Delta y = 2.54$  cm as mentioned before. The tip of the plunger is connected to the end of a small actuator arm corresponding with the moveable pivot point three. The other end of the actuator arm is connected to the shaft that turns the shutter plate. The axis of the shaft corresponds with the fixed pivot point two. During the extension of the bar that moves the actuator arm, the air cylinder pivots around pivot point one. After moving the actuator arm the air cylinder is in the same vertical position as at the beginning of the process. According to figure 4.3 the necessary length  $L$  of the actuator arm can be calculated as a function of the required angle of rotation  $\alpha$ .

$$L = \frac{\Delta y}{2\sin(\frac{\alpha}{2})}. \quad (4.11)$$

For a rotation of the shaft of  $\alpha=90$  deg., for instance, the required length  $L$  of the actuator arm is approximately  $L \sim 1.8\text{cm}$  that is short compared with the length of the air cylinder. When the pivoting of the air cylinder is taken into account the minimum required area on the back plate of the CMFP for the entire actuator system is  $11.5 \times 3.5$  cm. This is important for a later integration of the shutter system with the CMFP.

## 4.4 Drawings and description of the design

After the requirements of the CMFP were determined and the shutter system was basically dimensioned, a design that includes all the features named in the description of the requirements, including the integration of the shutter system, was formulated. In this section the drawings of the design are presented. After that a detailed description of the design, issues such as ensuring the basic function of the CMFP, its fabrication and mounting are presented.

### 4.4.1 drawings

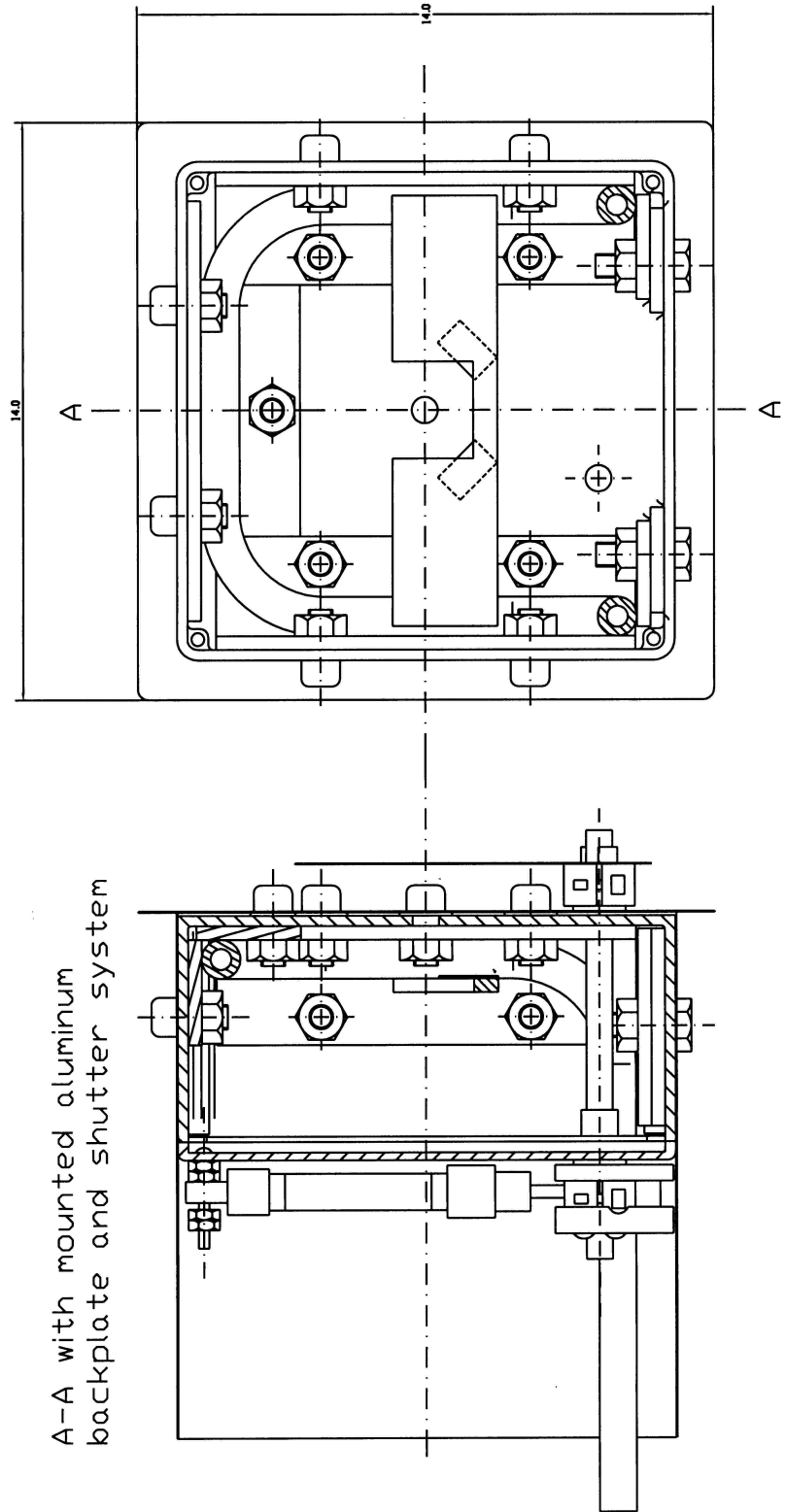


Figure 4.4: CMFP rear view and internal details.

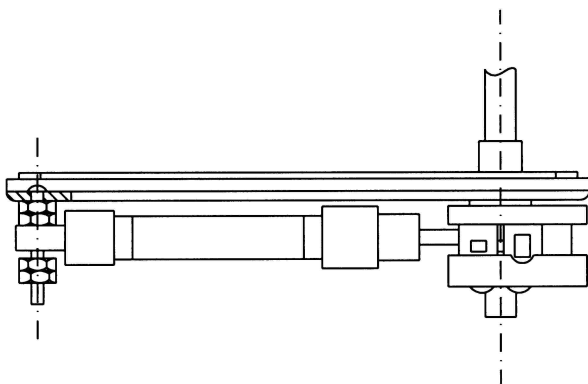
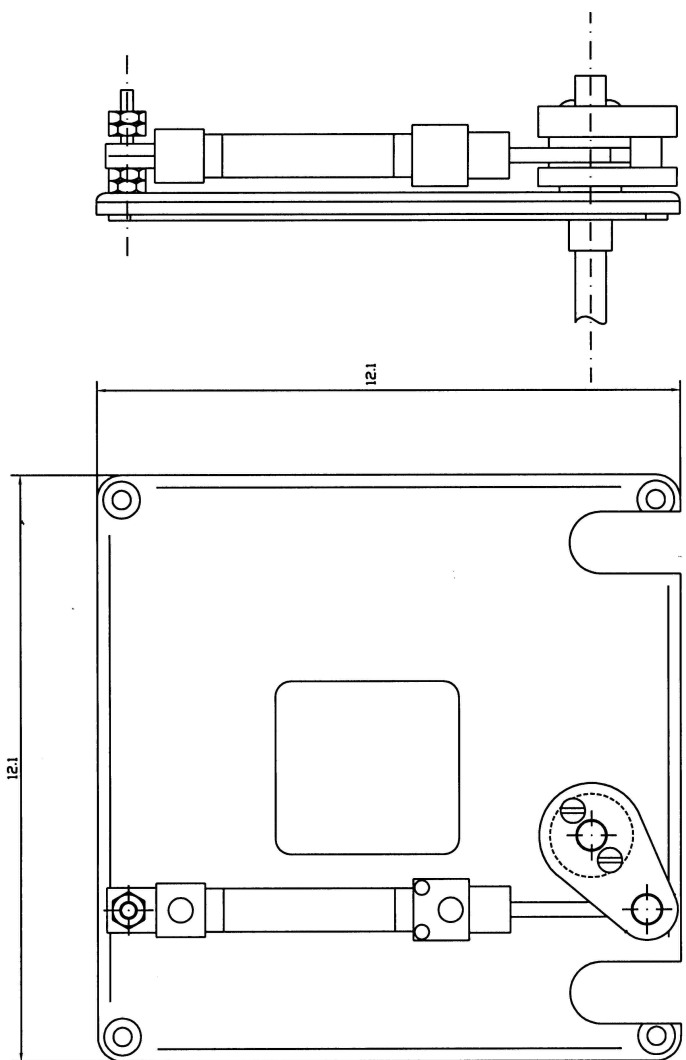


Figure 4.5: Aluminum backplate with integrated shutter system.

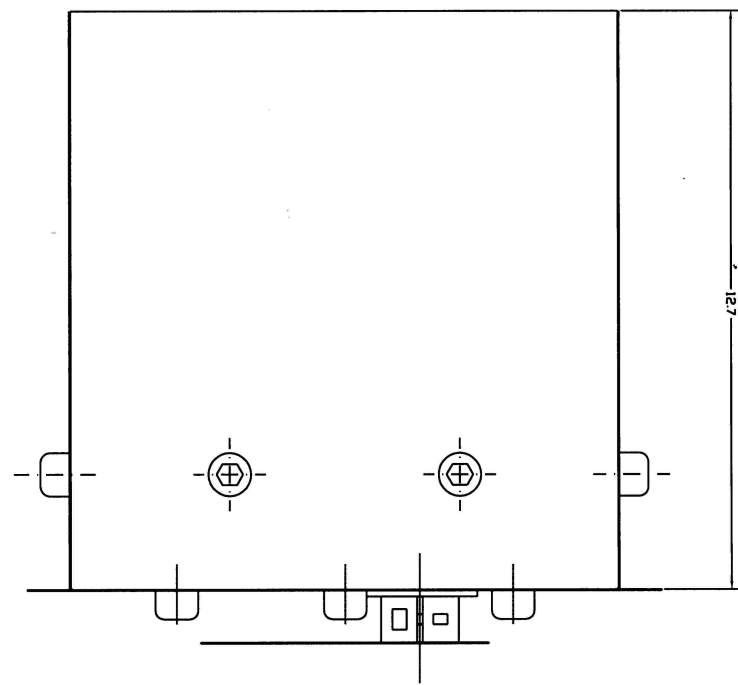
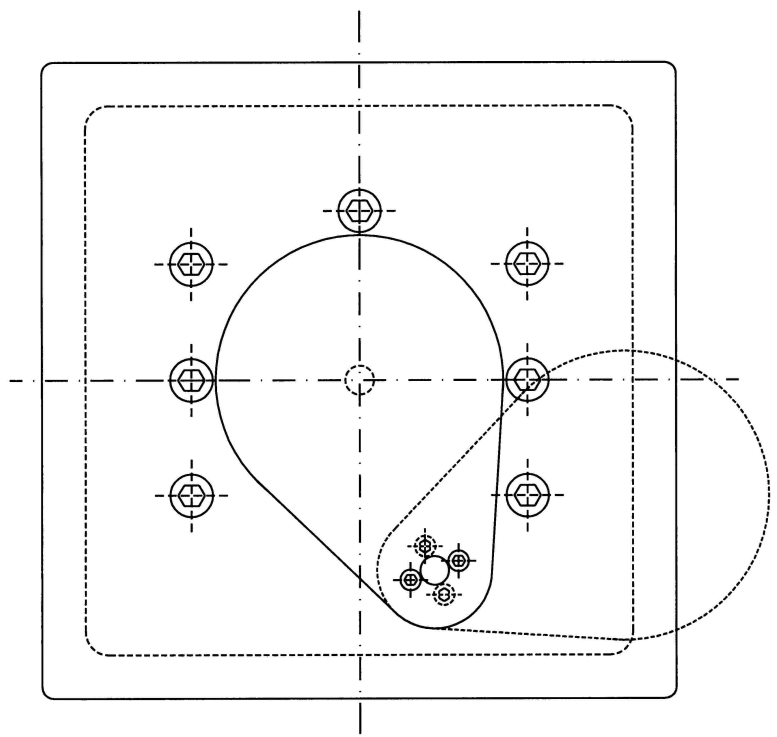


Figure 4.6: CMFP front- and topview

#### 4.4.2 Description of the design

The basic idea of the design of the CMFP was to put the sensitive QCM sensor head in a box to shield it from the extreme environment of the lithium plume. Just the part of the crystal calculated in section 4.2.3 should be exposed directly to the plume by a aperture in the mentioned box. In section 4.2.1 it was determined that the environment is so extreme that the box has to be actively cooled to prevent it from melting and to save the QCM probe from damage. This requires the integration of a metal tube in the box. It would be an advantage if the active cooling of the box could be used as a second cooling source of the QCM probe apart from its own cooling system. The integration of the shutter system with its large actuator is also not a negligible issue. Due to that facts it was clear that the required box would be much larger than the QCM probe itself. Fortunately the size and form of the box is not an issue as proved in section 4.2.2. The main motivation of contamination studies was to determine the lithium deposition on a future spacecraft. The surfaces of such a vehicle can be modeled more like a blunt body with a flat surface than like an aerodynamic body. Due to all the mentioned problems and facts the CMFP was designed like a big, blunt body in the lithium plume.

At first a 12 cm x 12 cm x 5 cm aluminum box with a mountable aluminum back plate was bought from a vending company. The size and the available back plate of the box were seen as optimal to integrate the large actuator of the shutter system. The material offers low weight and a good thermal conductivity that is important for the active cooling. The large 12 cm x 12 cm front side of the box is facing the thruster. This provides enough room for the QCM probe. Active cooling of the box is provided by a 1 cm diameter copper tube. The tube is attached to the inside of the box mainly at the front wall that is the most charged part. It enters and escapes the box at its bottom and runs along the edges of the front wall to provide also a cooling of the remaining walls and to leave enough space for a mounting of the QCM sensor head in the middle of the box. Unfortunately the aluminum box offers now possibilities to attach copper tubes by soldering. Due to that rectangular copper plates were attached to every wall of the box touching the edges. These plates have the advantage of an even higher thermal conductivity than aluminum and their large surface offers a good contact with the box. The copper plates were attached to the box by screw-nut connections which were placed as far as possible away from the edges of the box providing enough space for the tube. Because of the lack of space the use of washers was abandoned. Two layers of crinkled copper foil were placed between the plates and the box to provide a good contact between these parts. Due to the danger of outgassing the use of heat flux paste was rejected. The copper tube was soldered to the plates by the use of high temperature soldering to avoid a melting of the connection during the soldering of other parts.

The attachment of the QCM probe to the box was a larger challenge. From the beginning of the planning of the LiLFA test it was clear that the temperature of the QCM probe has to be controlled during the test to avoid a malfunction or damaging of the probe. Due to that it was planned to fix the tip of a thermocouple in one of the holes on the back-side of the QCM probe that were originally provided to attach the QCM to other devices. Apart from that the backside of the QCM should kept free of any other parts because connections like the coaxial connection or the wire of the mentioned thermocouple have to be accessible. The probe should be fixed in a way that it has no possibilities to tilt or shift. Especially if a positioner system is used this is a not negligible problem. Due to the permit of a screwed connection it was thought about taking advantage of the fact that the diameter of the circular front of the probe is larger than the diameter of the cubic housing.

For this a deep U-shaped notch was milled in the symmetry axis of the broader side of a rectangular copper plate. This notch has the same diameter as the cubic housing of the QCM-probe. The cubic part of the QCM-housing can be deployed in the notch. The circular front of the housing stays in front of the plate and avoids a backwards shifting and a tilting of the probe. A shifting to the front side is avoided by two little thin copper plates which were soldered on the front side in a 45 deg. angle across the bottom edges of the notch. Figure 4.7 shows the integration of the QCM sensor head.

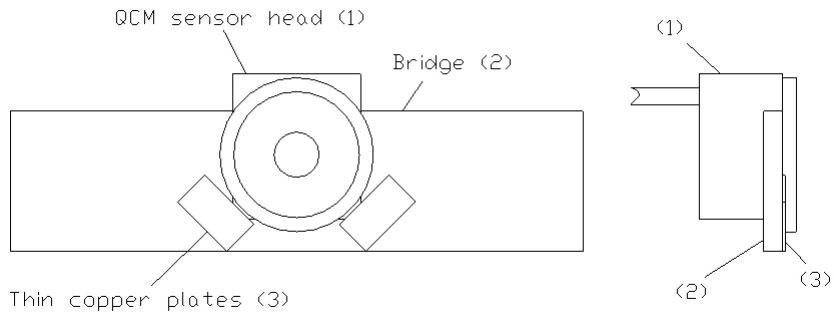


Figure 4.7: Integration of the QCM sensor head.

The notched copper plate is soldered like a "bridge" on the copper tube inside the box like showed in the drawings. It was ensured that this "bridge" has contact just to the tube and not to the walls of the box for an optimal cooling of the QCM housing. Due to inaccuracies of the soldering process of the bridge the aperture in the box for the incoming lithium was not drilled before this point of time. It has to be ensured that the lithium deposition takes place exactly in the center of the crystal to avoid measurement errors. According to thermal flux and saturation calculations the diameter of the aperture is  $d_A=3.18$  mm.

A disadvantage of the aluminum box however is its low melting temperature and its high reactivity with lithium. Due to that, every wall of the box was covered by thin stainless steel plates with the help of the same connections like the attached copper plates. Stainless steel has a high melting temperature and a low reactivity with lithium. The heat flux to the box was reduced by thin stainless steel washers mounted between the stainless steel plate and the box providing a little gap between these two parts. The plate that faces the thruster was designed with a larger diameter than the front side of the box to save connections in the back of the box from lithium. The thin plates that cover the sidewalls were designed much longer than the sidewalls to avoid a lithium contamination of the shutter actuator that will be mounted on the mentioned aluminum back plate of the box. This aluminum back plate needed a few cuts before it could be attached to the box. First of all the water tube of the box needs two escapes which requires two milled notches on the bottom of the aluminum plate. A large piece in the middle of the aluminum-plate is milled out to ensure that the tubes and wires of the QCM are able to escape the box. The diameter of this rectangular hole is chosen much larger than the diameter of the QCM-housing for a possible mounting of the probe after a mounting of the aluminum- back plate and the shutter system. This ensures an easier mounting of the entire CMFP and with this more safety for the sensitive QCM probe and its connectors during the mounting.

The shutter actuator has to be attached on the far left side of the aluminum-back plate vertically like explained in the kinematic description. A mounting crossing the center

of the aluminum-plate is not possible because of the QCM support. Its gas connectors should point away from the aluminum back plate. The mounting of the shutter actuator on the al- back plate needed a hole on the left top of the aluminum plate for the fixing of the actuator. The center of this hole is the first fixed pivot point of the shutter system explained in section 4.3.3. Another fixed pivot point is the shaft of the shutter plate. It requires a hole in the box and a hole in the aluminum back plate providing a pass for the turning shaft that moves the shutter plate. The actuator arm transmitting the movement of the bar in a turn of the shutter shaft is  $L = 1.8$  cm long which gives a rotation angle of the shutter shaft of  $\alpha = 90$  deg. This defined the location of the holes. They were drilled together with the mounted aluminum back plate on the box to ensure alignment. Low friction in the holes is ensured by a running fit. The actuator is mounted rotatable on the first pivot point to the aluminum back plate with the help of a little screw and two nuts which were screwed up against each other. A third nut is attached between the actuator and the back plate to keep the actuator away from the plate and to ensure that friction between the back plate and the actuator does not lead to a failure of the mechanism. The actuator arm consists of two little metal plates formed like a cam. These two parts are screwed to either side of a shaft collar, sandwiching it. The shaft collar itself is clamped to the rotating shaft of the shutter with the help of a little screw that adjusts the perimeter of the collar by reducing a gap in the collar ring. On the side of the CMFP facing the thruster the thin shutter plate is attached to the same kind of shaft collar. The connection between the shaft collar and the shaft is like described before. The shutter plate is designed like a cam. In the closed shutter position the center of the broader circular part is aligned with the center of the crystal. A diameter of 6.35 cm was determined as large enough for a secure shielding of the crystal during the closed shutter period. This diameter is small enough to provide sufficient space between the plate and the aperture if an angle  $\alpha = 90$  deg. is assumed in the shutter open position. This space is important for a disturbance free measurement. Finally a connection between the plunger of the actuator and the actuator arm at pivot point three is provided by a thread at the end of the bar that is screwed and locked to a little shaft. This little shaft is rotatable and oriented perpendicular between the two plates of the actuator arm. The axis of this little shaft corresponds to pivot point number three.

On the very back of the CMFP a thin plate of stainless steel is attached to shield the backside of the QCM and especially the shutter actuator from lithium. This plate has basically the same cuts than the aluminum back plate apart from two holes which ensure the escape of the gas tubes of the shutter actuator. These tubes are shifting slightly because of the mentioned pivoting of the shutter actuator during a movement of the shutter. Because of that the diameter of these holes is much larger than the diameter of the gas tubes. The attachment of the stainless steel plates to the CMFP and the closing of the remaining gaps were ensured by stainless steel tape that was successfully used before in tests with the LiLFA.

Photographs of the CMFP are shown in appendix B.

# Chapter 5

## Conceptual design of a positioner system

For a three dimensional characterization of the mass flux in the plume of the LiLFA during one firing sequence, a positioner system for the CMFP is needed. If we assume an axi-symmetric plume, at least a repositioning of the CMFP in the horizontal plane that includes the thruster axis should be performed.

In this chapter, the basic concept of a positioner system for the planned LiLFA experiments is introduced, including a description of the kinematics and geometry. After that, three dimensional drawings of the system are shown and described. A detailed discussion of the design is not attempted.

### 5.1 Basic description

The CMFP should always face the thruster. To ensure this, the CMFP will be suspended from a trolley riding on a horizontal boom, one end of which pivots about a point located directly above the tip of the cathode of the LiLFA. The other end of the boom is free to slide on a horizontal support bar near the far end of the boom. The trolley is moved along the boom by a lead screw driven by a motor attached to the far end of the boom, thereby changing the distance  $d$  of the CMFP to the thruster. The horizontal boom angle is changed by a second lead-screw-driven nut attached near the first motor and driven by a second motor mounted near the side wall of the tank. Both the second motor and the lead screw nut must be free to pivot as the boom angle is changed.

### 5.2 Kinematics and geometrical limits

The kinematics of the positioner system consists of two fixed and one moving pivot point. The distance between the moving pivot point 2 at one end of the boom and the pivot point 3 located close to the tank wall causes the angle between the thruster axis and the CMFP to change. Figure 5.1 shows the basic geometry of the system and the directions of motion of the main parts. The figure is not to scale.

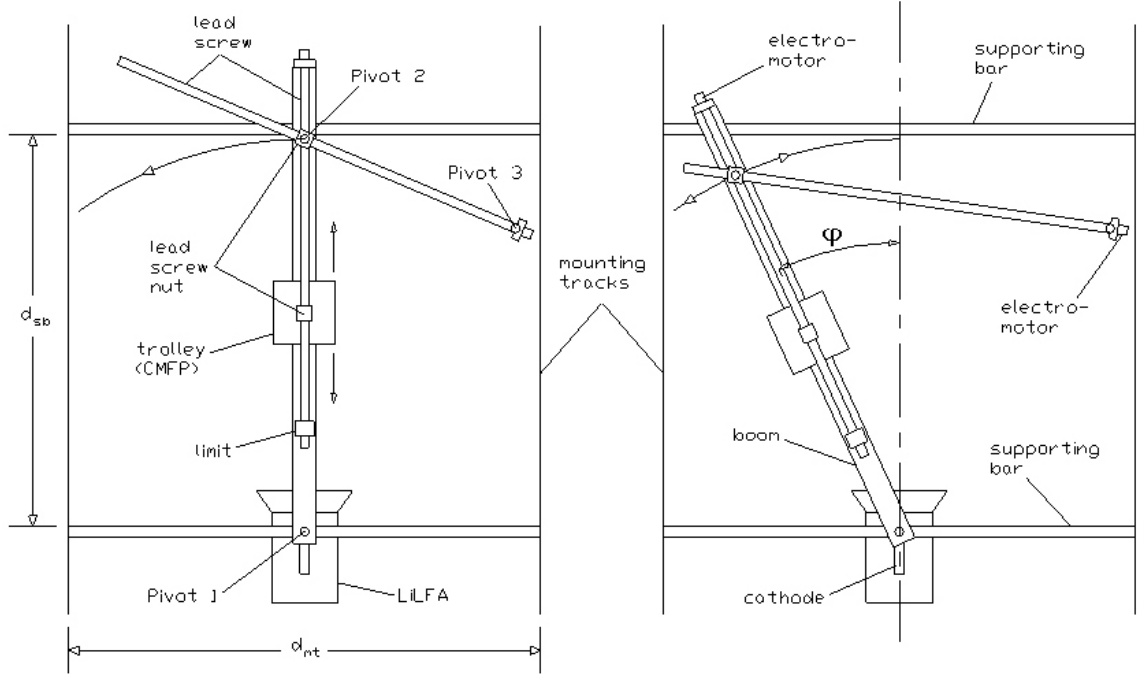


Figure 5.1: Kinematics and geometry of the positioner system.

First, the maximum angle  $\varphi_{max}$  and distance  $d$  between the CMFP and the thruster have to be determined. The distance between the mounting tracks that the positioner system support frame is mounted to in the tank is about  $d_{mt}=107$  cm (42 in.). We assume that the maximum angle is reached when the boom extended by the electro-motor contacts the left mounting track. It is obvious that this maximum angle decreases with an increasing length of the boom. For estimating the length of the boom it has to be considered that it has to glide on the second supporting bar which is located downstream toward the far end of the tank. The largest distance to the thruster at which this supporting bar can be mounted is about  $d_{sb}=160$  cm from the cathode tip. One end of the boom has to be located above the cathode tip to ensure a pivoting of the entire system around the cathode tip; this ensures the CMFP will always point directly at the thruster. The electro-motor attached at the downstream end of the boom has to stay behind the second supporting bar and cannot touch it. The required space for the electro motor is about 7 cm x 7 cm. With this we can estimate the maximum angle we can get.

$$\varphi_{max} = \arctan \frac{d_{mt}}{2(d_{sb} + 7\text{cm})} \approx 17.5\text{deg.} \quad (5.1)$$

With this we get a length of the boom without the electro motor of about 168 cm. There is basically no reason why we should not move the lead screw nut at pivot point 2 close to the end of the boom. If we assume this, the maximum distance between the thruster and the trolley is limited by the supporting bar at the end of the tank. If we also assume that the trolley has about the same length than the CMFP (about 13 cm) the maximum distance  $d_{max}$  between the cathode tip and the aperture of the CMFP is about

$$d_{max} = d_{sb} - 13\text{cm} \approx 147\text{cm.} \quad (5.2)$$

This distance can be extended if the measurements are taken off the thruster axis.

## 5.3 Description of the conceptual design

After the limits of the system were determined, a more detailed design was developed using 3-dimensional ray tracing software. Figure 5.2 shows a side view of the positioner system in the tank of the LiLFA looking from a horizontal plane containing the thruster cathode axis. The tank is drawn semi-transparent to show the relationship of the positioner to the mounting rails welded to the walls of the tank. The figure is to scale, but is a perspective view which distorts dimensions.

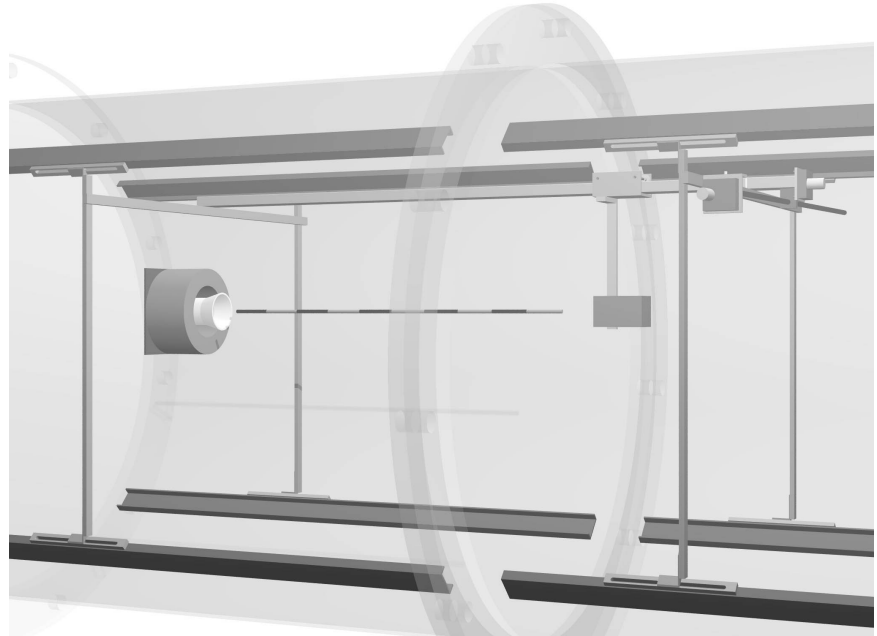


Figure 5.2: Side-view of the implementation of the positioner system.

The rod in front of the cathode is one meter long and each segment is ten centimeters. The CMFP is hanging from the trolley near the right end of the rod. The horizontal support bars that carry the entire system are mounted on a vertical frame which is mounted to the dark U-shaped tracks on the walls of the tank. The supporting bars are vertically located 42 cm above the center line of the tank; the thruster center line is 11.5 cm above this same center line. If the system is located too high, the maximum angle  $\varphi_{max}$  is more limited due to possible contact with the supports. If the system is vertically located too close to the thruster axis reflection and sputtering of lithium could disturb the measurement significantly. A vertical distance of 42 cm was seen as a good compromise. The lead screw and its nut which changes the angle  $\varphi$  was put under the boom downstream of the supporting bar so that a shield (not shown) could be attached to the supporting bar to reduce the amount of Lithium that could condense on the drive mechanism. Figure 5.3 shows a top-view on the entire system. The figure is to scale and is an orthographic view.

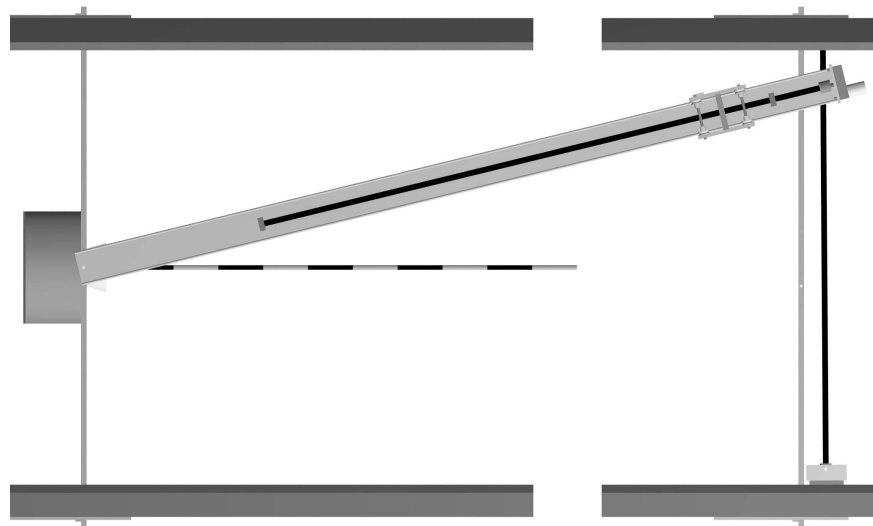


Figure 5.3: Top-view of the implementation of the positioner system.

The rod is implemented as explained for figure 5.2. The lead screw which changes the angle  $\varphi$  is mounted behind the supporting bar and as close to it as possible for better protection from the lithium plume and to maximize the travel of the boom. Installation of a long vertical shield on the boom to increase this protection is recommended; this shield would be much more complex if the drive mechanism is in front of the support. The shape of the boom and the trolley can be seen in figure 5.4. The figure is to scale but is also a perspective view.

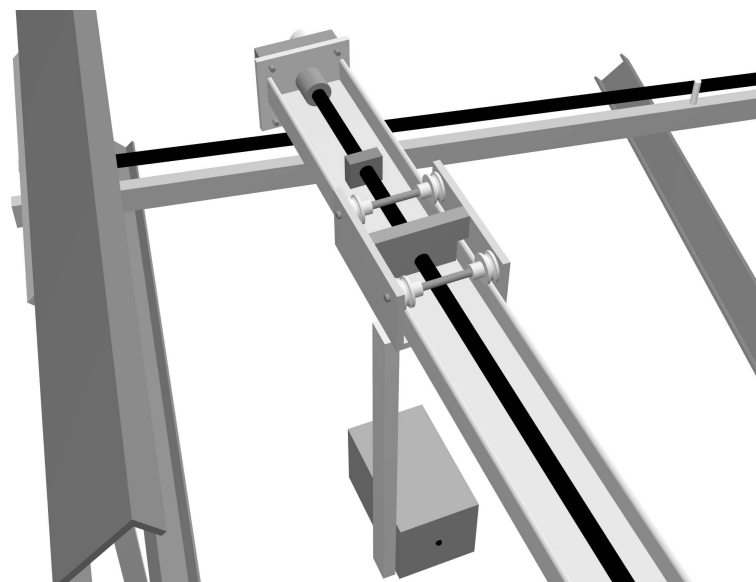


Figure 5.4: Conceptual layout of the boom and the trolley.

The boom is basically a long U-shaped piece of aluminum which carries the trolley. A layer of Teflon between the boom and its support may help reduce friction, but may also deteriorate rapidly in the hostile environment. The trolley encircles the boom without

touching it and rolls on four wheels on the tracks of the boom. The lead screw nut is attached to a plate which is perpendicular to the boom and attached to the trolley. The only part of the trolley that touches the boom is the four wheels, making it free to move along its length. The CMFP is attached to the plate on the bottom of the trolley with a long vertical bar and an L-bracket.

This conceptual positioner system allows for radial and angular motion of the CMFP without a significant disturbance of the plume. In further work a detailed design of the connections, a better shielding of the critical parts, like the lead screws and the electro motors, and also a concept for an exact actuation of the system needs to be determined.

# **Chapter 6**

## **Precursor tests with the Ablative Z-Pinch Pulsed Plasma Thruster (AZPPT)**

As mentioned in chapter 2 the LiLFA is a very complicated thruster. The fixing of newly discovered problems, such as unexpected arcs and damages in general, after each test require a lot of time. The initial testing of the QCM probe and the CMFP was accomplished using the simpler, more reliable Ablative Z-Pinch Pulsed Plasma Thruster (AZPPT). This thrusters design and performance is described in Markusic et. al. [15]. The AZPPT is comparatively easier to handle than the LiLFA.

At the beginning of this chapter the basic background of the AZPPT and its characteristics are explained and compared with the LiLFA. After that the motivation for performing experiments with the QCM probe and AZPPT is mentioned followed by a description of the experimental setup. The description contains the mounting and supply of water to the QCM probe and explains how the possibility of an arc between the thruster and the sensor head is an issue. This issue presents a safety problem which will be explained.

### **6.1 The Ablative Z-Pinch Pulsed Plasma Thruster**

There is presently a strong renewed interest in using pulsed plasma thrusters especially ablative PPT, for such tasks as attitude control of a satellite. PPts especially those with higher thrust to power ratios, can accomplish such tasks at greatly reduced mass and costs compared to other thrusters. This motivated the development of a new kind of ablative PPT. Four generations of these thrusters were constructed with the goal to create a thruster with a higher thrust-to-power ratio than its rectangular geometry counterparts. For that the Z-pinch configuration which was originally conceived as a method for producing hot, dense plasmas for nuclear fusion research was adapted for an ablative Z- pinch pulsed plasma thruster (AZPPT).

Initially the basic design and the acceleration process will be explained including basic specifications of the AZPPT. A very detailed explanation and a comparison with other PPTs will not be attempted. Finally, it will be compared and contrasted with the LiLFA.

### 6.1.1 Basic design and acceleration process

The discharge chamber of the AZPPT consists of a solid inner electrode (anode) and a hollow outer electrode (cathode) with an orifice at the top. The space between the electrodes is occupied by a solid hollow cylindrical bar of Polytetraflouoroethylene (PTFE) propellant. A  $38.3 \mu\text{F}$  Maxwell capacitor can be charged to a desired voltage. Four ignitors at the orifice end of the thruster allow current to start flowing from the capacitor. Figure 6.1 shows the schematic of the ablative Z- pinch thruster geometry.

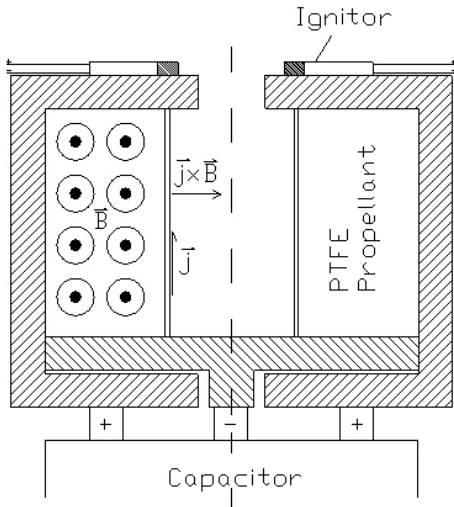


Figure 6.1: The Z-pinch thruster geometry.

The thruster operation begins with a charging of the capacitor to a high voltage. After this the ignitor is pulsed and creates a small spark which provides enough charge carriers to start the discharge between the anode and the cathode. Due to the fact that the propellant face is the point of the lowest initial inductance the discharge starts on the exposed surface of the solid PTFE propellant. The current which flows in the AZPPT circuit creates a magnetic field which is azimuthal. This flowing current on the propellant surface interacts with the magnetic field creating a Lorentz-Force  $F = j \times B$ . At approximately the same time material is ablated from the surface of the propellant because of heat from the discharge. This heat melts, vaporizes and ionizes propellant on the surface. The mentioned pinch effect produced by the Lorentz force squeezes the ablated material radially. Because of squeezing the material radially the pressure on the axis of the thruster increases. Finally the pressure gradient between the discharge chamber and the vacuum in the tank accelerates the ablated material through the orifice in the axial direction, generating thrust. The mentioned acceleration process provides a maximum specific impulse bit of  $I_{sp} = 800\text{s}$  with mass bits in the order of  $m_{bit} = 100 \mu\text{g}/\text{shot}$  and a maximum thrust to power ration of  $T/P = 45 \text{ mN/W}$  [15].

### 6.1.2 The AZPPT plume compared with the LiLFA plume

To determine the possibilities and applicability of the AZPPT as a device for precursor tests of the LiLFA experiment it has to be analysed in what extent the AZPPT is similar to or distinguishable from the LiLFA. A few issues are obvious. In contrast to the LiLFA thruster, which is operated under steady-state conditions, the AZPPT is a pulsed

device. This leads to a very unsteady geometry of the plume. Because of that it is not possible using the AZPPT to test the CMFP and the QCM under steady-state conditions. According to section 6.1.1 the strong z-pinch effect of the AZPPT leads to a plume which is concentrated axially, especially at short distances from the thruster. Due to that the largest mass deposition is expected to be on the axis and strong decreasing to the sides. The pinch effect of the LiLFA is much weaker compared with its primary electromagnetic acceleration force. Due to that the plume can be expected to be more uniform than the AZPPT plume.

Comparing characteristic performance parameters, the LiLFA has a much higher specific impulse which corresponds to a much higher speed and kinetic energy of the incoming particles hitting the QCM. In the test with the LiLFA the saturation time of the QCM is an issue. Unfortunately, the low mass bit of the AZPPT allows no determination of this saturation time because it would take an amount of shots on the order of one million to reach the maximum deposition. The lower  $I_{sp}$  and plume temperature of the AZPPT coupled with its lower total mass flow do not allow the simulation of the high temperature environment of the LiLFA. Due to that the cooling performance of the CMFP cannot be tested with this device. The water cooling of the QCM is sufficient for AZPPT testing and the use of a thermocouple is not necessary. The fact that the AZPPT uses Teflon as propellant does not allow the simulation of the high reactivity of the lithium plume. This reactivity may be an issue. The CMFP was designed to withstand this reactivity at least for the time of the LiLFA test by using stainless steel on its outside. It would be an advantage if this could be tested.

The only really corresponding feature between these two thrusters is the high ionization fraction in the plumes. Both thrusters have a much higher ionization grade than other types of electric propulsion devices like arc jets. Due to the fact that the QCM is an electrical device it would be an advantage to test this device in a charged plume to validate it for use in a highly charged environment.

## 6.2 Motivation of precursor tests with the QCM-probe and the AZPPT

Before the QCM probe was used in measurements with a thruster it was thought about ensuring the basic function of the QCM probe and its equipment with easier methods of mass deposition. A little deposition could be made by sticking, dripping, or spraying a small amount of material on the crystal in the QCM sensor head. The deposited mass displayed by the monitor of the QCM probe should be compared with the mass difference of the coated and uncoated crystal measured by a scale. This experiments failed altogether because they were made under atmosphere. Discussions with the vendor after these tests showed that the QCM probe is not made for deposition measurements under atmosphere. Due to that it was thought about ensuring the basic function of the QCM probe and its equipment with a deposition made by the AZPPT. A test with the AZPPT is made in vacuum. Apart from ensuring the basic function of the QCM a few other issues are important. During the experiment with the LiLFA the QCM probe is a part of the much larger Condensing Mass Flux Probe described in chapter 4. For a correct measurement of the mass flux in the plume it is important to know how and if the CMFP interacts with the plume. The AZPPT and its tank facility are convenient for such experiments in that measurements with both the QCM and the CMFP can be performed. A non-trivial problem is communication between the computer and the monitor of the QCM probe. During the

LiLFA test about 5 different parameters of the monitor have to be recorded and saved for a later analysis. To avoid a loss of data because of problems with the computer communication the correct function of hardware and software components have to be ensured in a precursor test. A better practical handling of the probe because of more experience and the possibility of discovering unanticipated problems are also good reasons for precursor tests with the AZPPT.

In addition to evaluating problems encounter with the LiLFA this test can stand alone. It yields useful information about the AZPPT. Mass flux measurements in the AZPPT plume could lead on one hand to a better understanding of the thruster operation of the AZPPT which is important for a future improvement of this concept and on the other hand to a validating and correcting of plume codes which are currently being developed.

## 6.3 Experimental setup

The experiments with the AZPPT took place in a large dielectric vacuum facility of about 25 feet in length with an inner diameter of 8 feet. The chamber is equipped with a high vacuum diffusion pump. At the backside of the chamber a liquid nitrogen baffle system reduces back streaming of oil from the diffusion pump. A pressure below  $p = 1.33 \times 10^{-3}$  Pa can be reached during the test. The AZPPT was mounted on a swinging-gate style microbalance thrust stand.

### 6.3.1 Positioning and supply of the probe

Basically the experiments had three goals. First of all the basic function of the QCM probe had to be validated. This included a validation of the statement that the measurements made with the QCM are still accurate if just a part of the crystal is covered by a material. Also it had to be shown that the CMFP in general has no significant influence on the measurement. The mentioned two issues required measurements performed with the CMFP and without the CMFP just using the QCM on the same position in the plume. The third goal was a rough scan of the plume at a fixed distance from the thruster. For that a measurement on different angles was necessary. Figure 6.2 shows the positioning of the CMFP and/or QCM for the required tests.

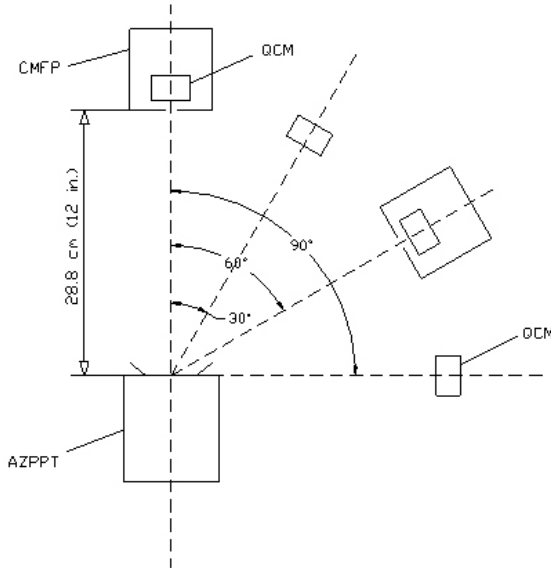


Figure 6.2: Positioning of CMFP and QCM.

The CMFP and/or QCM was always aligned in line with the center of the orifice of the AZPPT. This agrees with recommendations of the vendor of the QCM to be in line with the source of the mass flux. The probe was positioned much closer to the thruster than in the LiLFA tests. Because of the much lower total mass flux of the AZPPT compared with the LiLFA a smaller distance provides a mass flux to the crystal of about the same order as in the LiLFA tests at high distances from the thruster. On the other hand a small distance could cause a dangerous arc between the thruster and the sensor head. Due to that a distance of  $d_{AZPPT} = 28.8 \text{ cm (12 in.)}$  was seen as a good compromise. The arcing issue will be discussed in a deeper manner in section 6.3.2. Measurements with the CMFP and the integrated QCM were performed at angles of 0 deg. and 60 deg. The measurements will be compared with measurements performed using just the QCM for a determination of the influence of the CMFP at low and high angles relative to the thruster axis. A scan of the plume shall be performed by measurements on 0, 30, 60 and 90 degrees on the right side relative to the thruster axis. The plume is assumed to be symmetric. A measurement of different angles at the same distance helps to validate numerical plume codes developed for the AZPPT that are usually written in polar coordinates. Because of the expected very low mass flux at 90 deg. and the small aperture of the CMFP these measurements were performed just using the QCM.

For the mounting of the QCM in the tank a device consisting of a vertical bar welded on a compact base was positioned on the bottom of the tank. The CMFP was mounted without the stainless steel plates to ensure an easier mounting. Just the plate covering the front face of the CMFP was used. The CMFP or the QCM was clamped to the vertical bar by several clamps providing a save assembly. The aligning of the CMFP or QCM was performed with the help of a ruler, a protractor and a balance. Ensuring the correct distance and an aligning of the probes with the AZPPT. Unfortunately a positioner system for the AZPPT tank was not available. Due to that a measurement of different angles during one test was not possible.

The source for the necessary cooling water supply of the QCM was the tap of a sink located close to the tank. The water was pipelined to the QCM by a 0.45 mm inside

diameter water tube made of plastic outside the tank, the feedthrough of the tank and a water tube of the same type inside the tank. Swagelok connectors were attached to the water tubes of the QCM sensor head to connect them with the plastic tubes. The rewind of the cooling water was managed the same way as the supply and disposed in the sink. A water supply of the CMFP and the use of a thermocouple were not necessary because the temperature was not expected to increase.

The connection between the monitor unit outside the tank and the QCM sensor head is ensured outside the tank by a long coax cable and a diplexer which are part of the equipment of the monitor. An available BNC feedthrough is used in combination with a short coax cable inside the tank that is connected directly to the microdot BNC connector of the sensor head.

### 6.3.2 Avoiding an arc between the thruster and the sensor head

As mentioned in a former chapter the AZPPT (using Teflon as propellant) was operated at currents on the order of 10 kA and voltages between 800 and 1220 Volts. Because of contact between the plume and the thrust stand there could have been an arc between the stand/sensor and the thruster if all experimental components were grounded to a common potential. Such an arc could, in the worst case, destroy the sensor head or the monitor. Figure 6.3 shows the circuit schematic.

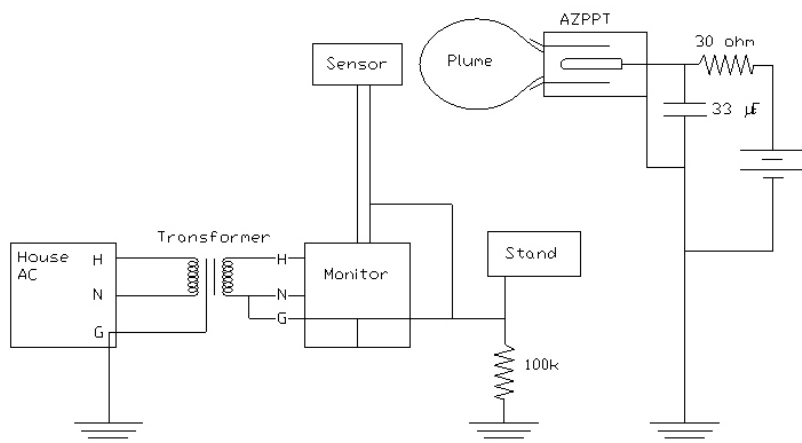


Figure 6.3: Circuit schematic of the AZPPT Experiments.

To avoid a discharge through the monitor, the equipment was floated by installing a resistor of  $100\text{ k}\Omega$  between the monitor and the ground. The  $100\text{ k}\Omega$  resistor allows for the removal of residual charges which may deposit on the sensor head or the monitor. Apart from that a large resistance is needed between the monitor and its power supply to avoid a discharge in that direction. However using a resistor between the monitor and the power supply is not possible because the monitor needs A/C-Power at 110 Volts and 60 Hz but placing a resistor in the circuit changes the A/C characteristics. Instead an isolation transformer is installed between the monitor and its power supply. An isolation transformer has nearly infinite electric resistance. In this setup the arc takes the easiest path to ground through the thruster instead of attaching to the floated equipment. This saves the QCM-equipment from unexpected and dangerous discharges.

### **6.3.3 Safety requirements**

Unfortunately the installing of the large resistor and the isolation transformer causes another serious problem:

Because of the limited lifetime of the crystal and a necessary saving of the data it is required to control a view figures by touching the buttons of the monitor during the firing of the thruster. One of theses figures is the percentage of the used lifetime. It is essential for estimating the remaining lifetime of the crystal until it fails and has to be controlled during the test. It can made visible only by pressing a button. Due to the high voltage on the monitor caused by the large resistors the touching of the monitor could cause a discharge through the person who is serving the equipment and lead to serious injury. To avoid personal injury the monitor has to be put in a non-metallic box and the functions of the monitor can be handled only by touching the buttons behind a Plexiglas foil. These circumstances make for a very uncomfortable operation of the QCM-device. The poor accessibility and the bad visibility of the display may lead to mistakes during the experiment.

Apart from that is has to be considered that the complete discharge of the capacitor is not guaranteed during the test. Because of that it is necessary that the remaining charge is removed with the help of discharge sticks. Only after that is done can the monitor or the attached equipment be touched or removed.

# Chapter 7

## Experiments with the LiLFA

After the experiments with the AZPPT, which showed the basic function of the QCM and the possibility of plume measurements with this device, the next step was the experimental setup for the LiLFA Experiment. It was clear that the tests with the LiLFA would be a larger challenge than the experiments with the AZPPT. The rough lithium environment requires the permanent use of the CMFP and much more accurateness concerning issues like cooling, shielding and temperature control. The much higher total mass flow requires the use of the shutter system to prevent the crystal from saturating and for a shielding of the crystal in case of an emergency. Due to the complicate firing procedure of the LiLFA, experiments can be performed just every few months. That confirms the importance of accurateness in the planning of the experimental setup.

At first the experimental setup is described concerning factors like mounting of the CMFP, water and gas supply, thermocouple and computer connections. It is shown that the length of the supplying coaxial cable of the QCM is an issue. After that, necessary precursor tests are explained and the results analysed. Finally, the methodology of the LiLFA contamination tests is described.

### 7.1 Experimental setup

The experiments with the LiLFA take place in a large vacuum tank of about 6 m in length with an inner diameter of 1.5 m. The chamber is equipped with a high vacuum diffusion pump. A pressure of  $p = 6.7 \times 10^{-3}$  Pa can be reached during the test. The LiLFA is mounted on an inverted pendulum-thrust stand centered horizontally in the tank. Its vertical position is 11.5 cm above the centerline of the tank. The experimental setup for the LiLFA test contains many components. Figure 7.1 shows the experimental setup apart from the mounting of the LiLFA. The drawing highlights the most important issues for a better understanding. The figure is not to scale.

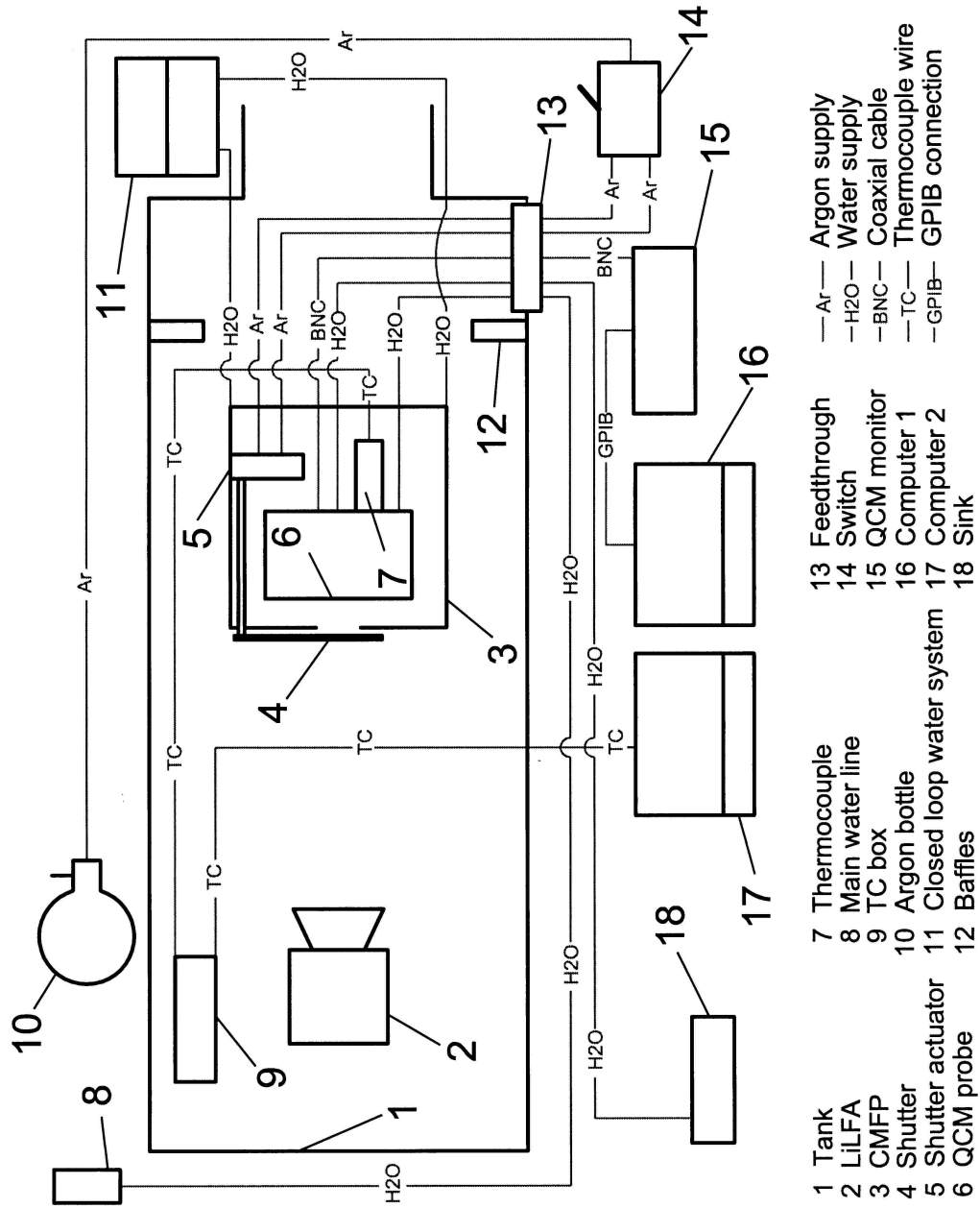


Figure 7.1: Experimental setup of the LiLFA experiments.

### 7.1.1 Mounting of the CMFP and feedthroughs

The goal of the program of surface contamination studies is a characterization of the plume of the LiLFA. For this the positioner system explained in chapter 5 is required. Unfortunately, the fabrication of this system was not finished in time. Because of that the measurements were limited to one position. An advantage of this fact is that moving parts, a shifting of the supplying connections to the CMFP, and the influence of the system on the plume needed not to be considered.

For the first test the maximum possible distance  $d=148$  cm to the thruster was chosen to reduce the heat flux to the CMFP and the QCM to a minimum. The maximum distance  $d$  to the thruster is limited by baffles which are situated at the end of the tank. The CMFP was mounted on the axis of the thruster to reduce the negative influences of the CMFP on high angles. These negative influences were discovered during the tests with the AZPPT and will be explained in chapter 8. Figure 7.2 shows the mounting of the CMFP for the first test with the LiLFA. The CMFP is mounted with the center of the aperture aligned with the thruster axis.

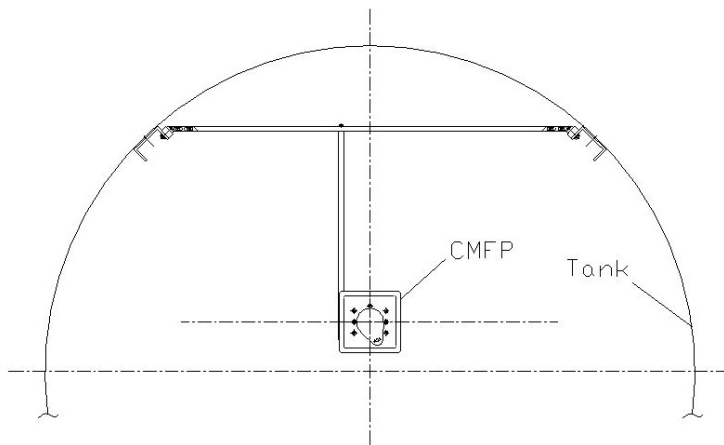


Figure 7.2: Mounting of the CMFP.

Fixed to the upper right and upper left inside of the tank are two U- shaped tracks which extend the length of the tank. A horizontal cross bar is fixed on the tracks with the help of an aluminum plate and an aluminum angle. A vertical bar is fixed on the cross bar by two bolts to hold the weight of the CMFP. The holes in the sides of the CMFP which were drilled to attach the copper plates to it are used to attach the CMFP to the vertical bar. The measures of the tracks surrounding the thruster were used for the design of the positioner system. Knowing this, the length of the parts and the position of the holes could be determined easily.

After the mounting of the CMFP, the setup of its supplying lines was done. First, it had to be determined how many and what kind of feedthroughs were needed. The connection between the QCM and the QCM monitor requires a feedthrough for a coaxial cable. Apart from that, the gas supply of the shutter actuator requires two feedthroughs. The water supply for the CMFP is a part of the closed water loop system and needs no additional feedthroughs. This will be explained later. The water supply for the QCM requires two feedthroughs similar to tests with the AZPPT. An aluminum window with swagelock connectors and a BNC connector provided the feedthrough. The mentioned

five feedthroughs are close together and located downstream behind the baffles to save them from the lithium environment.

### 7.1.2 Water and gas supply

The water lines are a very important part of the setup. They control the temperature and prevent measurement inaccuracies of the very temperature sensitive QCM. The water supply includes two independent systems, the water supply for the QCM and the water supply for the CMFP. The supply for the CMFP is provided by a closed loop water system that was made to provide cooling water for all systems in the tank. The water for the CMFP comes out of a reservoir. After cooling the CMFP, the water flows through a heat exchanger to cool it down again. The heat exchanger is in line with the university chilled water supply. After the heat exchanger the cooled water flows back into the reservoir for reuse. At first it was thought about connecting the water supply for the QCM also to the closed loop water system. But then it was discovered that the very thin water tubes of the QCM (3.2 mm inside diameter) would decrease the flow rate of the entire system significantly. Due to that, a separate external water supply for the QCM was installed. The source is the main water supply. The return water runs into a sink. For safety reasons the plastic tubes outside the tank are mounted close to the ceiling. Copper tubes were used inside the tank to survive the lithium plume. They provide enough flexibility for the use of a positioner system. This applies also for the tubes of the gas supply. A swagelok connector is used to hook the 0.64 mm copper tubes up to the 0.32 mm tubes of the QCM.

The gas supply of the shutter actuator provides other issues. At first it was determined which gas should be used for the task. In general, there are four sorts of gases which are used in the lab. Pressurized air, nitrogen (which was used for the leaking test of the shutter system), helium and argon. Finally argon was chosen. On one hand an argon bottle is located close to the tank anyway because it is used to prevent a reaction of the lithium during the refilling process of the feeding system. On the other hand because of this low reactivity with lithium argon will avoid a reaction in the case of leaks. As explained in section 4.3.2 one connection of the actuator has to release the gas if the other one is pressurized. This has to be ensured if the shutter shall work. For this a switching device is mounted between the argon bottle and the gas feedthroughs of the tank. The switching device has one incoming gas connector and two outgoing connectors for a supply of the actuator. If the switch is actuated it changes the pressurized tube and releases the gas of the other tube by two holes in its surfaces. With this the correct function of the shutter is ensured. Inside the tank copper tubes were used. They are connected to the gas connectors of the shutter actuator.

### 7.1.3 Critical cable length

Due to the damaging effects of the extreme thermal environment and the lithium itself it is necessary to run as much as possible of the coaxial cable of the QCM device along the walls of the tank. Just the part between the CMFP and the bottom of the tank will be in the plume and has to be shielded. As a result of this the required minimum cable length between the QCM and the feedthroughs on the wall of the tank is about 2.5 m if the minimum distance  $d = 40$  cm between the QCM and the thruster is assumed. This cable length is necessary to reach all positions which will be measured. This creates an unexpected problem. As explained in section 3.2.1 the varactor diode in the diplexer outside the tank has to compensate for the capacitance of the cable and has to store it as a

reference parameter. If there is too much capacitance between the QCM and the diplexer, due to a too long cable, the varactor diode will be unable to compensate for because of its limited tunable range. In that case the system cannot be used to measure depositions. Because of that the vendor limits the maximum cable length between the QCM and the feedthroughs to 1.8 m which is too short.

One possible solution is to add a capacitor in parallel with the varactor diode to augment to its tunable range. On one hand, this would lead to a lasting solution to the problem. On the other hand, it would require modifying a complex device, and this change could have unknown benefits and consequences. This approach was rejected. The solution settled on was to find a cable with lower capacitance per unit length than the cable suggested by the vendor. Calculations led to a maximum capacitance of about  $C = 171$  pF that can be attached to the diplexer and still allow it to operate. Anything larger than this may cause a "Crystal Failure" indication. Since 93 Ohm coax (RG-62) has half the capacitance of the RG-58 suggested by the vendor, it should be possible to double the maximum length to 3.6 m. When a length of 3.3 m was tested, there was no "Crystal Failure" indication, but flexing the cable caused the readings to jump over a wide range of values. It is presumed that the construction of this cable is the reason for this. Because a polyethylene "stringer" is wrapped around the center conductor (the rest of the volume is air), it is not possible to ensure that the center conductor remains centered when the cable is flexed. This causes changes in the value of the capacitance and these, combined with the extra length, may cause the control electronics to "think" the QCM has jumped modes, in this case unexpectedly. Longer cables caused a "Crystal Failure" to occur, and a length of 2.5 m was determined to be just about sufficient for the purpose and also stable when flexed. This is the length that is used for the tests.

#### 7.1.4 Other issues

Due to the mentioned extreme thermal environment the use of a thermocouple was necessary to monitor the temperature increasing during the test. For this a Type K thermocouple was attached to the QCM probe as showed in figure 7.3



Figure 7.3: QCM-probe with attached thermocouple.

The goal was to get the thermocouple as close as possible to the most critical parts in the inside of the sensor head. For this a screw was soldered to the tip of the thermocouple. The thermocouple was screwed in one of the tapped holes which were originally provided for a mounting of the probe. A high temperature resistant connector was attached to its cables to avoid a disturbance of the measurement by the extreme environment. Apart from the thermal environment there is another problem concerning the cables inside the

tank. The thruster and its applied magnetic field create a noisy environment, requiring that the cables were shielded. Due to that the two cables of the thermocouple were shielded separately from each other by a metallic coating like in a coaxial cable. Apart from that the shielded cables were put in a fiberglas coating to save them from the hot environment and the lithium. As much as possible of the distance to the thermocouple box the cables were run along the tank walls to save them from the plume. The shielded thermocouple box close to the thrust stand provides a connection to a computer for thermocouples that were used in former tests. Due to that the computer connections and the software interface for this device were already available. A completely new setup was not necessary.

The situation of the computer communication with the QCM monitor was different. The monitor comes with its own GPIB-connection (General Purpose Interface Bus). Unfortunately the computer which is hooked up to the thermocouple box does not have a GPIB-card and connector. Because of that a second computer was needed in the experimental setup to provide such a connection and a software interface for the communication with the monitor.

The connection between the monitor and the QCM inside the tank was provided like in the experiments with the AZPPT. Inside the tank, the coaxial cable was directly attached to one of the water tubes on the downstream side of the tube to cool the cable and to shield it from the plume. In addition, it was covered by aluminum foil.

## 7.2 Precursor tests

The explanation and summary of the basic specifications in section 3.3.2 showed the inaccuracies of the QCM probe. Not included are inaccuracies caused by the environment in the tank during the experiment and the performance of the experiment in general. Factors like temperature and pressure vary during the test. Also the influence of vibrations has to be determined as mentioned in section 3.2.2. Due to this the results and conclusions of a thermal calibration using different heat sources and a calibration of the QCM with pressure is presented. The influence of vibrations caused by the movement of the shutter was determined in a separate test. These results are also summarized.

### 7.2.1 Thermal calibration

The thermal calibration of the QCM is not a simple task. On one hand a heat source is needed which provides enough energy to increase the temperature of the QCM. On the other hand it has to be confirmed that the sensitive QCM will not be damaged due to a hot environment. That requires a monitoring of the temperature during the calibration. Due to that, the type K thermocouple that was introduced in section 7.1.4 and a computer connection is needed.

For the first test it was decided to run warm water through the water tubes of the QCM to increase the temperature and to determine the drift of the displayed total mass deposition caused by the temperature change. For this the QCM sensor head was hooked up to the water supply of a sink using the plastic tubes mentioned in section 7.1.2. The return water also ran into the sink. The experiment took place under atmosphere using the QCM without the CMFP because a mounting in the tank was not yet provided. At the beginning of the test a small amount of water was run through the tubes using slightly heated water. The monitor was zeroed when the temperature of the QCM asymptoted at the initial temperature of 24.15 deg. C. After that an increase of the temperature was

achieved by a repeated increase in the amount of hot water. Measurements were taken when the displayed temperature asymptoted. At the end a temperature of 62 deg. C could be achieved by just running hot water through the QCM sensor head. After that the QCM was cooled down very quickly to simulate an expected sharp decrease of the QCM temperature when the shutter is closed during the LiLFA experiment. Immediately after the cool down a second water thermal drift test was performed to determine if the results of the first warm up are repeatable after a sharp cool down by increasing the water temperature again. The monitor was not zeroed for the second warm up. Figure 7.4 shows the results of the mentioned test. The framed zero indicates the initial temperature on which the monitor was zeroed. The thermocouple has an accuracy of  $\Delta T = 2.2$  deg. C in the temperature range above 0 deg. C. The resolution of the QCM monitor is 1 ng according to section 3.3.2. The error of the monitor is very small compared with the inaccuracy of the thermocouple.

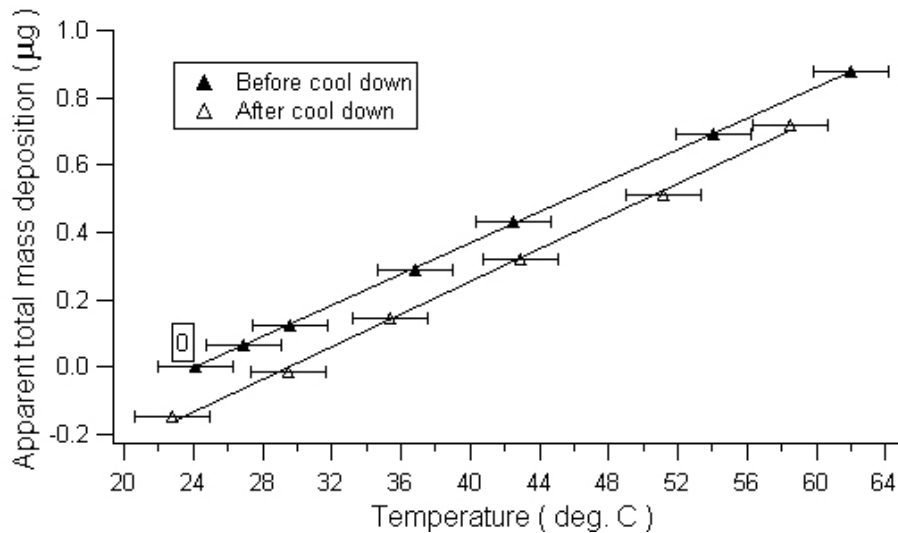


Figure 7.4: Results of the water-thermal drift test.

The very linear gradient is the first of two obvious characteristics of the displayed results. The second one is the shift in the linear characteristics after the fast cooling down of the crystal that is obviously not in the error bars. This shift appears to be a hysteresis. The very small amount of this shift may lead to the hypothesis that the crystal has slightly changed its position inside the sensor head due to tension forces that were introduced by the fast temperature change. This may lead to a slight changing of the piezoelectric properties of the crystal.

A line fit was calculated for the results of the initial warm up and for the results of the warm up after the cool down. With that a deposition gradient was found to  $\Delta M/\Delta T = 2.311 \times 10^{-2} \mu\text{g}/\text{deg. C}$  for the first warm up. The second warm up resulted in a gradient of  $\Delta M/\Delta T = 2.425 \times 10^{-2} \mu\text{g}/\text{deg. C}$ . The difference of the gradient is about 5 %. For the LiLFA test described in section 7.1 a mass flux in the order of  $0.1 \mu\text{g}/\text{s}$  is expected due to the large distance  $d$  and the small diameter of the aperture in the CMFP. That shows that the thermal drift of the QCM could be an issue if the temperature increases in the order of 1 deg. C per second during the test. The very linear gradient of the apparent total mass deposition also showed that the results of the thermal drift test could possibly be used as a correction factor for the deposited total mass in an analyzing of the results after the LiLFA test.

For a determination of the cooling performance of the CMFP and QCM and for a confirmation of the temperature gradient found in the first test a second thermal drift test was performed using another heat source. The test was performed under vacuum with the CMFP and the integrated QCM in the LiLFA tank. The CMFP and QCM were mounted and supplied as planned for the first firing experiment with the LiLFA. A 300 W radiation heater was positioned about 2.5 cm upstream of the CMFP front side in line with the aperture. It was planned to increase the temperature of the QCM by powering the heater. The water cooling of the QCM and the CMFP should stay switched on during the test to determine their cooling performance. The initial temperature at which the monitor was zeroed was 18.73 deg. C corresponding to the temperature of the supplied water for the QCM.

The first result of the test was that even after powering the heater for more than one hour no increase of the temperature of the QCM could be detected. Just after a shut down of both water supplies an increasing of the temperature of more than 1 deg. C could be reached. After a few hours a maximum temperature of 40 deg. C was detected. A further increase was avoided to not damage the probe after hours of heating without water cooling. After reaching this maximum temperature the heater was switched off and just the water supply of the CMFP was switched on which cooled the QCM to 21.9 deg. C. After that the water supply for the QCM was switched on which cooled the QCM to 18.5 deg. C. That shows that the temperature of the water supply for the QCM does not correspond to the temperature of the water supply for the CMFP that comes from the closed water loop. Figure 7.5 shows the results of this test before and after the cool down. Due to the fact that a control of the temperature was not possible it is obvious that the measurements could not be taken under steady state conditions as in the test with heated water.

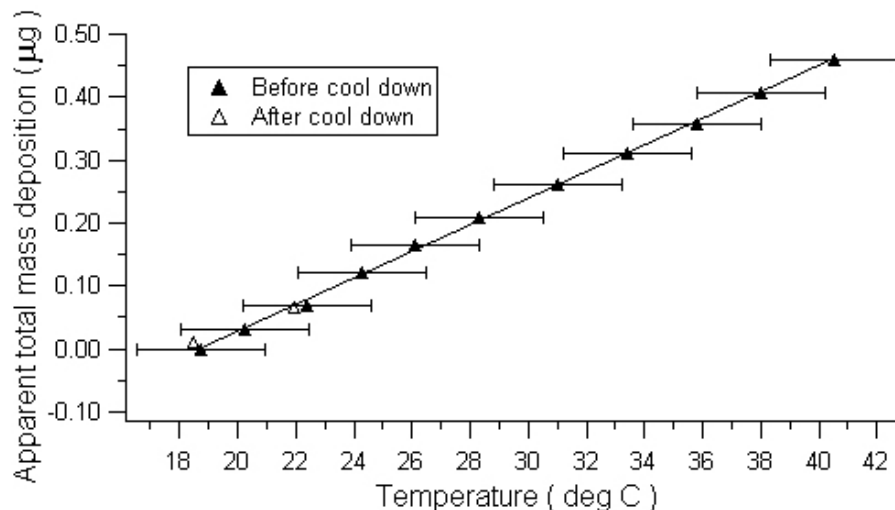


Figure 7.5: Results of the radiation-thermal drift test.

The results of this test confirm the very linear characteristics of the gradient discovered in the first test. A slight shift in the apparent total deposition as in the first test was not detected probably due to a much longer time for the cooling down than in the first test. The gradient of the calculated fit line is  $\Delta M / \Delta T = 2.215 \times 10^{-2} \mu\text{g}/\text{deg. C}$  which confirms the results of the first test.

In conclusion, it can be said that the thermal drift of the QCM may be an issue if the

temperature increases in the order of 1 deg. C per second during the LiLFA test. In a later analysis of the results of the LiLFA experiment the gradient of the total mass deposition determined in the thermal drift tests can be used for a correction of the results because its characteristic was found very linear concerning a change of the temperature.

### 7.2.2 Pressure calibration

Earlier experiments with the LiLFA showed that the desired tank pressure of  $p = 6.67 \times 10^{-3}$  Pa could be held during most of the experiment. A pressure increase was just discovered during the starting process when the anode and other parts of the thruster heat up due to heat flux from the developing arc. The heat is radiated to other parts in the tank including its walls. This leads to outgassing processes and to an increased pressure during the first minute of the firing. Although the pressure drops fast and an opening of the shutter is planned at the earliest thirty seconds after the appearance of an arc, the pressure could still be in the order of 0.1 Pa when the first measurements are taken. Due to that, it has to be determined if a changing pressure in the range between  $6.67 \times 10^{-3}$  Pa and 1 Pa has an influence on the measurements with the QCM.

There are two different processes available for such a task, the pump-down process and the venting process of the LiLFA tank. If the tank is vented the pressure rises very fast which means that the needed pressure range is crossed in a few seconds. To ensure a more accurate determination of a pressure drift of the QCM it was decided to determine this issue during the pump-down process.

The QCM and the CMFP were mounted in the tank and setup, as explained in section 7.1. The temperature measured by the mentioned thermocouple was also recorded. During the test a slight change of the temperature of the chilled water for the QCM could disturb the measurements and lead to wrong conclusions. The total mass deposition provided by the QCM monitor was recorded for the whole time of the pump-down process. The initial pressure was  $p_I = 10.06 \times 10^5$  Pa. During the entire test the pressure in the tank was measured with a vacuum gauge that was unfortunately not hooked up with a computer interface. The manual recording of the pressure and the limited accuracy of the vacuum gauge lowered the accuracy of the measurement. Also, the minimum pressure of 0.1 Pa of the vacuum gauge was an issue. After the monitor was zeroed and the software interfaces were started, the tank was pumped down, first with the roughing pump. During the first few seconds of the pumping process a sharp decrease of the total mass deposition to -0.17  $\mu\text{g}$  was detected. After that, the total mass deposition increased again and stabilized at about -0.02  $\mu\text{g}$  at a pressure of about  $9 \times 10^3$  Pa. After the stabilization, the total mass deposition stayed in a range between -0.04  $\mu\text{g}$  and -0.01  $\mu\text{g}$  until the minimum pressure of about  $p = 6.67 \times 10^{-3}$  Pa was reached. Even when the roots blower or the diffusion pump was switched on, which caused a fast pressure change, the QCM showed no significant reaction.

In conclusion, it can be said that a changing pressure is not an issue in the range between  $p = 6.67 \times 10^{-3}$  Pa and 1 Pa. Due to this it is very likely that a changing pressure does not influence the experiments with the LiLFA and the QCM. The outgassing process at the beginning of the process however could be an issue apart from the increasing pressure. The QCM is cooled by chilled water that could cause a condensation of the outgassed materials on its crystal and with that an increase in the total mass deposition that is not caused by lithium. This has to be considered in a later analysis of the results.

### 7.2.3 Influences of the shutter system

During the mounting of the QCM for the AZPPT experiments, it was discovered that the QCM is very sensitive to movements and vibrations. This could be an issue if a positioner system is used for a repositioning of the QCM or even if the shutter is moved at the beginning or the end of a measurement period. As explained in section 7.1.1, the use of a positioner system was not planned for the first experiment with the LiLFA. Due to that the movement of the shutter system remains as the only source for movements or vibrations during the experiment. For this it was planned to determine the influence of the opening and closing of the shutter on the total mass deposition measured by the QCM.

The circumstances are basically the same as described in section 7.2.2 with the difference that the tank is under vacuum at a pressure of  $p = 6.67 \times 10^{-3}$  Pa that is not changed during the experiment. The shutter was opened and closed five times at each case leaving a time period of at least 5 minutes between the movements of the shutter. The total mass deposition was recorded during and after each movement of the shutter. It was discovered that the opening of the shutter caused a jump in the total mass deposition between  $+0.004 \mu\text{g}$  and  $+0.006 \mu\text{g}$ . The total mass deposition did not return to zero. The monitor has a resolution of  $0.001 \mu\text{g}$ . The closing of the shutter induced no measurable change in the total mass deposition.

In conclusion, it can be said that an opening of the shutter has a slight influence on the measurement. Compared with the expected mass flux of  $0.1 \mu\text{g}/\text{s}$  the influence of vibrations caused by a movement of the shutter are negligible in all likelihood.

## 7.3 Methodology

Experiments with the LiLFA and the QCM come with their own requirements and issues. Five different parameters have to be synchronized with time to ensure the comparability of the results:

Table 7.1: Parameters to synchronize

|  |
|--|
| Total mass deposition                    |
| Rate of the total mass deposition        |
| Used crystal lifetime in percent         |
| Status of shutter (open/closed)          |
| Temperature measured by the thermocouple |

The time provided by the monitor is used as a reference. Due to that the synchronization of the first three parameters is not an issue because they are reported by the monitor and are in time with the provided time of the monitor. The synchronization of the remaining two parameters is an issue. The status of the shutter cannot be detected by any of the used computers. The temperature measured by the thermocouple is recorded by another computer than the computer used for a recording of the parameters provided by the monitor. Due to that the preparation of a methodology for the measurements in the LiLFA Experiment is necessary to avoid an inaccurate synchronization of the parameters with time.

In earlier tests it was discovered that the zeroing of the monitor is slow. Usually it takes more than one second between a pressing of the button and a zeroing of the device.

That leads to synchronization problems if this is seen as a reference for other parameters. Due to that a planned zeroing of the monitor every time the shutter is moved was rejected. It was decided that moving the shutter at a specific time displayed by the monitor would probably lead to less inaccuracies in the synchronization. The eastern standard time displayed by the software interface that drives the recording of the thermocouple data should be inscribed at a specific time displayed by the QCM monitor to synchronize these two times for a later analysis of the results. Also there is another problem that comes with the monitor. When the device is switched on it shows a negative drift probably because it takes time to heat up the parts of the very sensitive monitor. Earlier tests showed that this drift lasts at least for one hour. Due to that the monitor should be switched on at least two hours before the LiLFA experiment. At the same time the water supply of the QCM and the CMFP should be switched on to ensure a steady temperature of these devices before the firing of the LiLFA.

There are also requirements that come with the plume and the desired data. In the summary of the reasons for a shutter system it was mentioned that at the beginning of the firing the plume consists also of liquid or solid particles that can damage the QCM when they hit it. Also the goal of the experiment is to determine the mass flux under steady state conditions. Earlier firings of the LiLFA showed that it takes about thirty seconds after the first appearance of an arc until there are no more liquid or solid particles in the plume and at least 5 minutes until the plume is steady state. Tests performed during the last firing of the LiLFA showed also that a shutter system could not be opened due to a blockage by lithium contamination that increases with time. Finally, it was chosen to open the shutter as soon as the plume contains no liquid or solid particles anymore due to the risk of a blocked shutter. In section 4.2.3 it was shown that saturation is not an issue at such a large distance  $d$  to the thruster. Also the thermal charge of the probe is negligible. As soon as a measurement is taken under steady state conditions the shutter should be closed and opened again after a few seconds to determine if the shutter works well under these conditions and if the closing of the shutter really leads to a complete interception of the mass flux. This should be repeated until the firing stops. The start and the stop of the firing are labeled as the appearance or the disappearance of an arc. This condition is very obvious.

In conclusion the requirements mentioned above lead to the following methodology:

Table 7.2: Methodology of the LiLFA experiment using the CMFP and the QCM

|    | Time                                       | Action  |
|----|--|---|
| 1  | 2 hours before firing                      | Switching on of the monitor.<br>Switching on of the water supply for the QCM and CMFP.  |
| 2  | 10 minutes before firing                   | Ensuring the function of the shutter system.  |
| 3  | 2 minutes before firing                    | Start of the software interfaces of computer 1 and computer 2.  |
| 4  | 1 minute before firing                     | Zeroing of the QCM monitor, (monitor time 0:00).  |
| 5  | Monitor time 0:10                          | Writing down of the eastern standard time EST displayed by the software interface of computer 2 (thermocouple).   |
| 6  | Monitor time 1:00                          | Ignition of the LiLFA.  |
| 7  | 30 seconds after appearance of an arc      | Opening of the shutter.<br>Writing down of the monitor time.  |
| 8  | After performing steady-state measurements | Closing of the shutter at a specific monitor time.<br>Writing down of the monitor time.<br>Saving of the obtained data to a file.<br>Restart of the software interface. |
| 9  | 30 seconds after closing of the shutter.   | Opening of the shutter.<br>Writing down of the monitor time.  |
| 10 | Until firing stops                         | Repeating of steps 8 and 9 thirty seconds after opening of the shutter.   |
| 11 | Stop firing                                | Writing down of the monitor time.   |
| 12 | After stop of the firing                   | Stopping of both software interfaces.<br>Saving of obtained data in file.   |

Unfortunately the firing of the LiLFA never reached steady-state conditions. This may lead to a changing of this schedule during the firing.

# Chapter 8

## Results and Analysis

As mentioned in chapter 6 the AZPPT is comparatively much easier to handle than the LiLFA. Technical problems and waiting for necessary parts that were manufactured externally delayed the experiments several times. Due to that many more experiments with the AZPPT could be performed than with the LiLFA.

In this chapter the results and the analysis of the experiments are presented starting with the AZPPT experiments. After that the results and the analysis of one performed experiment with the LiLFA are discussed.

### 8.1 AZPPT Experiments

The experiments with the AZPPT were performed mainly to ensure the basic function of the QCM and its equipment. The issues that come with the probe and the experiments in general were also determined. Apart from that the necessary experiments were used to perform a rough scan of the plume of the AZPPT.

#### 8.1.1 Results of the AZPPT experiments

First of all, it had to be ensured that the QCM that is put into the CMFP is working in general and is producing repeatable measurements. For this the CMFP with the QCM inside without the shutter was positioned  $d_{AZPPT}=28.8$  cm downstream of the thruster with the center of the aperture of the CMFP in line with the thruster axis. The experimental setup was described in section 6.3. After the pump-down of the tank the AZPPT fired 100 shots. After stopping the firing there were several minutes until the next firing took place. The firing procedure including the breaks was repeated 25 times until the total amount of shots reached 2500. The tank was vented and the CMFP and the QCM were removed from the tank. The same experiment was repeated three days later with the same experimental setup and the same firing procedure. Figure 8.1 shows the results of the two experiments. The mass deposition rate was divided by the area of the aperture in the CMFP to obtain the mass flux. The resolution of the QCM monitor is 1 ng. For the diameter of the aperture an error of  $\Delta d_A=\pm 0.04$  mm was assumed because of the tolerance of the drill that was used. Error bars are used just for the results of the first experiment to ensure a better clearness. The error bars of the second experiment are of the same order.

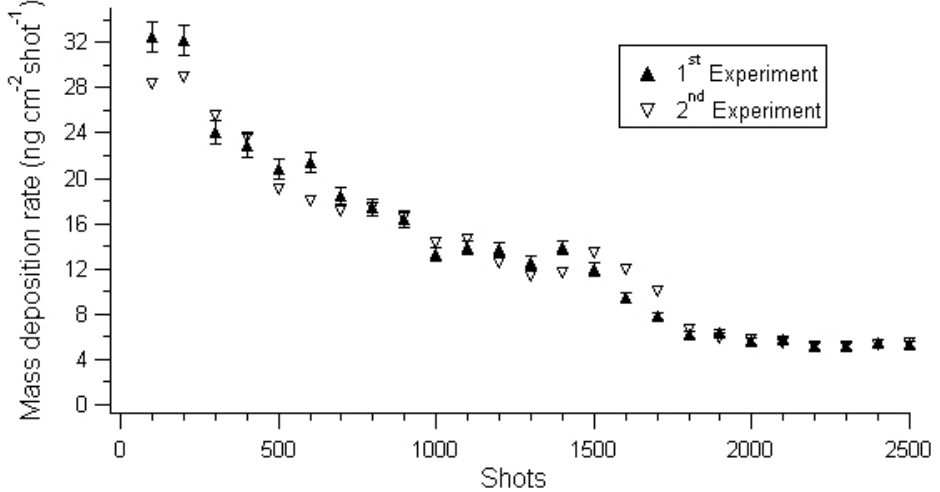


Figure 8.1: Results of the first two experiments using the QCM in the CMFP.

Figure 8.1 shows that in general this measurement is very repeatable. Apart from five measurement points all measurements from each experiment are within the error bars. Very obvious is the decrease in the mass deposition rate between the initial and the last measurement point. The mass deposition rate drops from the initial  $32.5 \text{ ng}/(\text{cm}^2 \text{ shot})$  to  $5.6 \text{ ng}/(\text{cm}^2 \text{ shot})$  after 2000 shots. After 2000 shots the mass deposition rate seemed to reach steady-state conditions. The measurements following 2000 shots remain in the error bar of the measurement at 2000 shots.

A positive drift remained for 4 to 5 minutes after the end of each firing sequence. The apparent amount of added mass during the drift period was between  $180$  and  $250 \text{ ng}/\text{cm}^2$ . The end of the drifting was defined when the change in the total mass deposition-reading was less than  $1 \text{ ng}$  in one minute. After that the next 100 shorts were fired.

After ensuring the repeatability of the results with the QCM in the CMFP, it had to be determined if the results for the mass flux obtained with the QCM in the CMFP were repeatable if just the QCM without the CMFP was used under the same conditions. For this just the QCM was mounted with the center of its crystal exactly at the same position as the center of the aperture of the CMFP in the first two experiments. The tank was pumped down and the thruster ran the same firing procedure as in the first two experiments. After 2500 shots were fired the experiments stopped for 3 hours without venting the tank. The experiments were repeated one time after 3 hours to see if the cool down of the thruster influences the measurements or if the measured mass flux remains on the low steady-state level of  $5.7 \text{ ng}/(\text{cm}^2 \text{ shot})$ . Unfortunately a cool down under vacuum over night was not possible because of the lack of liquid nitrogen. Liquid nitrogen is needed for the baffles at the end of the tank to avoid a flow of diffusion pump oil into the tank. Due to that just a few hundred shots could be fired after the break of 3 hours. Figure 8.2 shows the results of this experiment. The measured mass deposition rate of the QCM was divided by the exposed area of the crystal to ensure comparability with the results of the experiments using the QCM in the CMFP.

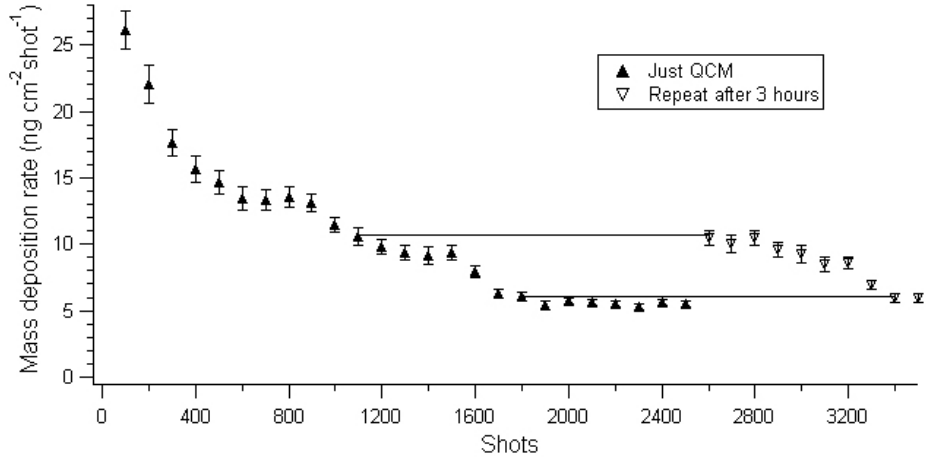


Figure 8.2: Results of the experiments using just the QCM without the CMFP.

It is obvious that a decrease in the mass flux also takes place if the CMFP is not used. The mass flux drops from its initial  $26.1 \text{ ng}/(\text{cm}^2 \text{ shot})$  to  $5.7 \text{ ng}/(\text{cm}^2 \text{ shot})$  after 2000 shots. The measured initial mass flux is  $6.4 \text{ ng}/(\text{cm}^2 \text{ shot})$  lower than the initial mass flux of the experiments using the CMFP. That is not in the error bars. A steady-state condition is reached after 2000 shots with a mass flux of  $5.7 \text{ ng}/(\text{cm}^2 \text{ shot})$ . This amount is in the error bars of the steady-state value of the experiments with the CMFP. The time and value of the drift was about in the same order than in the experiments with the CMFP. The results of the experiment accomplished 3 hours after the earlier one showed that the mass flux does not start at the low level of  $5.7 \text{ ng}/(\text{cm}^2 \text{ shot})$  that was reached at the end of the first experiment. Its initial value is  $10.5 \text{ ng}/(\text{cm}^2 \text{ shot})$ , which is nearly double the amount than at the end of the earlier test. In figure 8.2 it is obvious that the gradients of the two experiments have the same characteristics. Unfortunately a steady-state value could not be reached in the later test due to the necessary shut down of the diffusion pump.

Other experiments were set up to determine the influence of the CMFP on the measurements. In section 4.2.2 it was shown for the LiLFA experiments that the size and the shape of the CMFP have little gasdynamic influence on the measurement because the flow can be seen as molecular. That applies also to the experiments with the AZPPT where the total mass flow is even lower than in the LiLFA test. But the influence of sputtering, reflecting or other phenomena that could be caused by the CMFP could possibly have a non-negligible influence. For this measurements with and without the CMFP were performed at an angle of 0 deg. and 60 deg. relative to the thruster axis in the horizontal plane at a distance of  $d_{AZPPT}=28.8 \text{ cm}$  (12 in.) to the thruster. The crystal or the aperture of the CMFP was pointed to the center of the orifice of the AZPPT according to section 6.3.1. The measurements at 60 deg. were performed to determine a possible influence of the CMFP on higher angles. In contrast to previous experiments the AZPPT was fired for 2500 shots (or 2000 shots on 60 deg.) nonstop without a break to obtain a more steady condition and to avoid the drift during the experiment. Figure 8.3 shows the results of the experiments accomplished at an angle of 0 degrees. Figure 8.4 shows the obtained results of the performed experiments at 60 degrees. The diameter of the exposed area of the QCM was measured with a micrometer that has an accuracy of  $\pm 0.024 \text{ mm}$  ( $\pm 0.001 \text{ in.}$ ). In the experiments using just the QCM the error bars are smaller than the markers. Due to that a use of error bars was avoided.

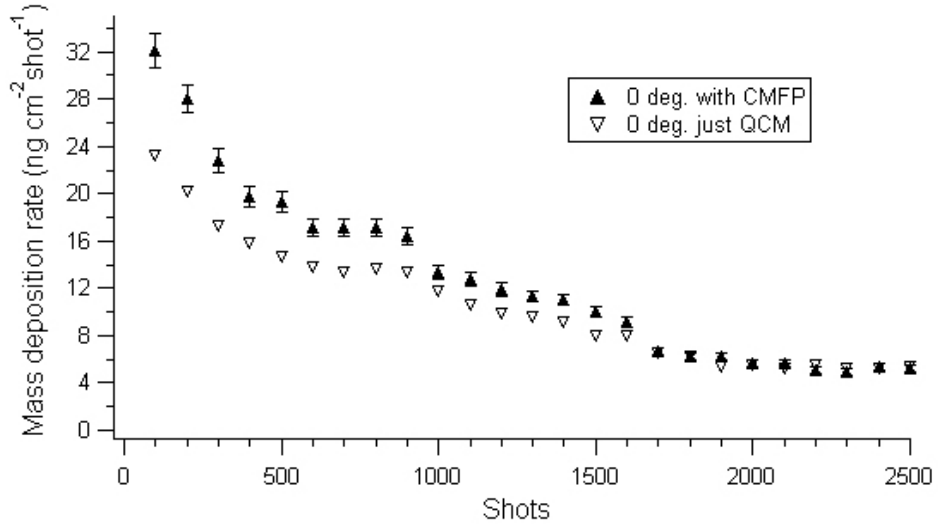


Figure 8.3: Results of the measurements at 0 degrees.

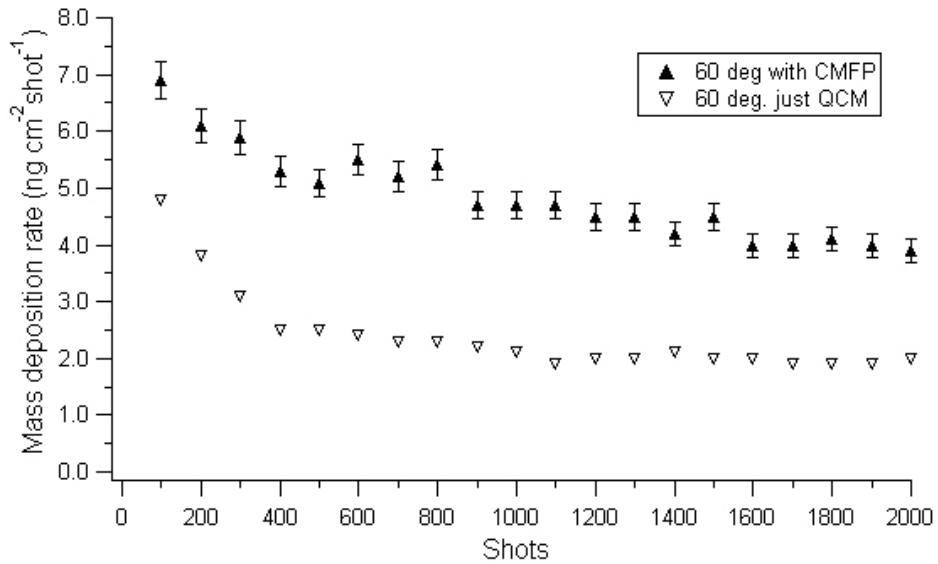


Figure 8.4: Results of the measurements at 60 degrees.

Figure 8.3 shows that the characteristic is quite the same if the thruster is fired without the break. At 0 degrees and with the CMFP the initial value is  $31.9 \text{ ng}/(\text{cm}^2 \text{ shot})$  dropping to a steady state value of  $5.5 \text{ ng}/(\text{cm}^2 \text{ shot})$  after 2000 shots. If we compare these results with the results of the measurements just using the QCM it is obvious that the initial value using just the QCM is much lower. It starts with  $23.3 \text{ ng}/(\text{cm}^2 \text{ shot})$ . The measured mass flux of the experiment just using the QCM remains lower and not in the error bars of the results of the experiment with the CMFP. Just shortly before reaching steady-state conditions both gradients remain in the error bars of each other and reach the same steady-state value.

The results of the experiments at 60 degrees are different. The measured mass fluxes are much lower than the mass fluxes measured at 0 degrees. The initial value of the mass flux of the experiment using the CMFP is  $6.9 \text{ ng}/(\text{cm}^2 \text{ shot})$ . Steady-state conditions are

reached earlier than at 0 degrees after 1600 shots at a value of  $4.0 \text{ ng}/(\text{cm}^2 \text{ shot})$ . The ratio between the initial value and the steady state value is 1.725 at 60 degrees, which is much lower than the ratio of 5.84 at 0 degrees. If we look at the results of the experiment at 60 degrees just using the QCM a few differences are obvious. All measured mass fluxes are much below the values of the experiment with the CMFP and are not in the error bars. It is difficult to determine after how many shots steady-state conditions are reached due to the very small error bars. The results after 1500 shots can be seen as steady state if we use a very liberal approximation. It is obvious that the characteristic of the mass flux using just the QCM is smoother than the characteristic of the mass flux using the CMFP.

If we look at the ratio between the tests with and without the CMFP shown in figure 8.5 some facts are getting clearer. Due to their small value the use of error bars was avoided.

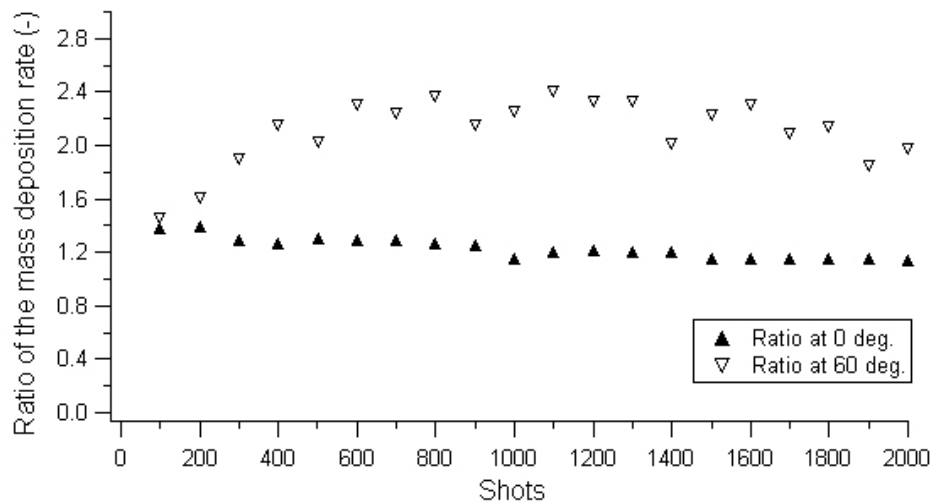


Figure 8.5: Ratio of the deposition rates (CMFP/just QCM) at 0 and 60 degrees.

At 0 degrees the initial ratio is 1.377 dropping to 1.136 after 2000 shots. At 60 degrees the initial value is 1.45, which is of the same order as the initial ratio at 0 degrees. In the next 500 shots the ratio is increasing until its maximum at 2.41. It remains between 2 and 2.5, which means that the results of the mass flux measured with the CMFP are more than two times higher than the mass flux measured with just using the QCM.

Apart from the experiments performed to determine issues that come with the CMFP and the QCM itself, it was planned to obtain a rough scan of the AZPPT plume by measuring the mass flux at different angles at the same distance of 28.8 cm (12 in.) from the thruster. Experiments were performed just using the QCM without the CMFP. The experimental setup and the angles measured can be seen in section 6.3.1. At every angle the thruster was fired for 2000 shots without a break. For a repositioning of the probe the tank was vented and the thruster cooled down for at least one day to ensure that thermal effects have no influence on the results. Figure 8.6 shows the measured mass flux of every experiment. The plume was assumed to be symmetric to the thruster axis. The error bars are smaller than the markers.

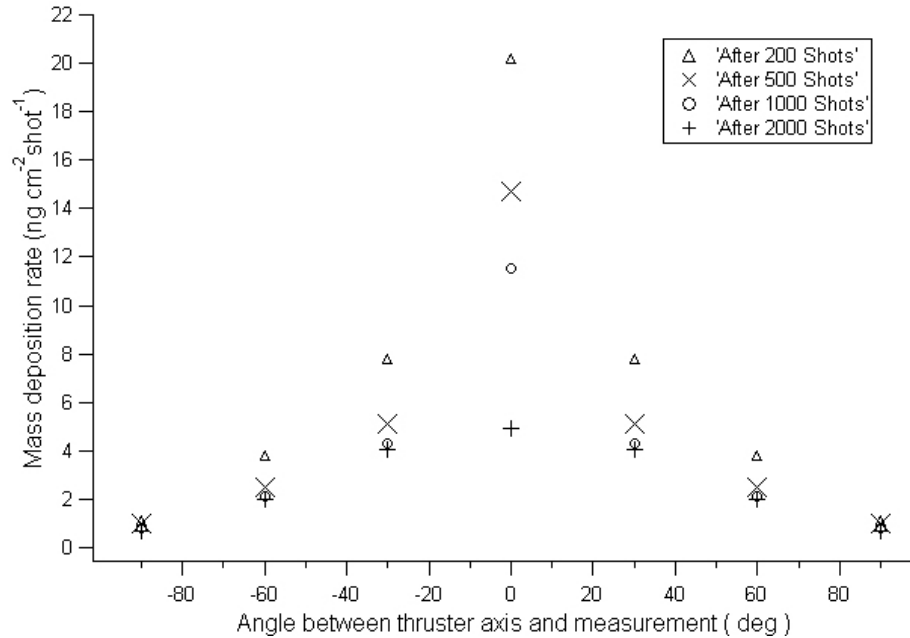


Figure 8.6: Rough characterization of the mass flux in the AZPPT plume.

It is obvious that the mass flux decreases with an increasing angle to the thruster axis. Especially close to the axis the mass flux drops very fast with an increasing angle. The distribution is reminiscent of a Gaussian distribution. It is also obvious that the mass flux decreases with the number of shots at every measured angle. Even at 90 degrees the measured mass flux after a different number of shots does not stay within the error bars. If we calculate the ratio between the measurement results at 0 degrees and at 90 degrees we can see that the ratio drops from 18.36 after 200 shots to 7.1 after 2000 shots.

The ratio between the initial value and the steady-state value for the mass flux decreases with an increasing angle to the thruster axis. This can be seen in figure 8.7. The error bars are smaller than the markers.

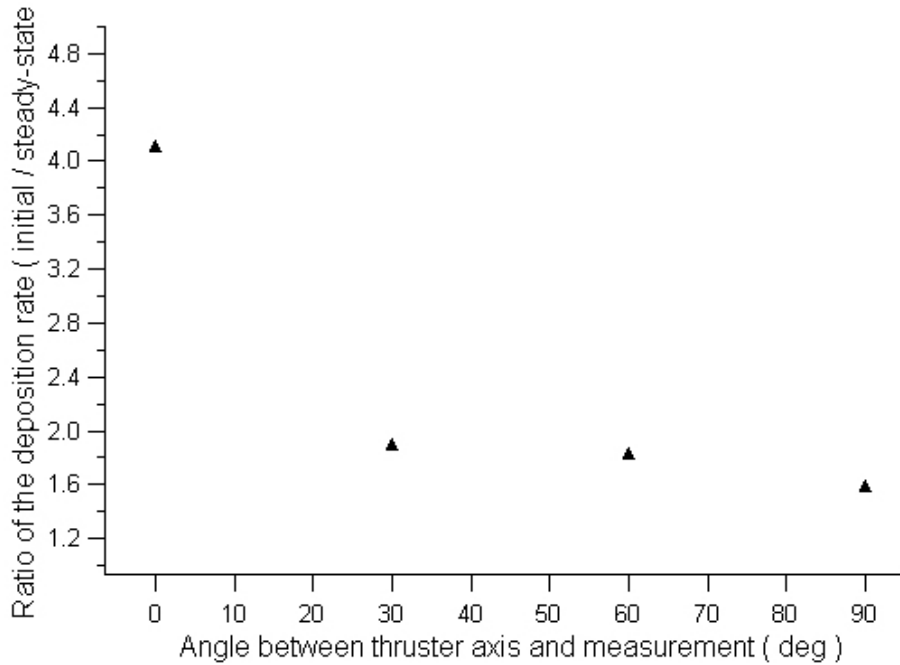


Figure 8.7: Ratio of the deposition rate between the initial and the steady-state value.

It is obvious that the largest decrease takes place between 0 and 30 degrees. It was also discovered that steady-state conditions are reached earlier with increasing angle. At 0 degrees steady state conditions were reached after 2000 shots, at 30 degrees after 1800 shots, at 60 degrees after 1500 shots and at 90 degrees even after 900 shots.

More results of these tests are given in appendix A.

### 8.1.2 Analysis of the AZPPT experiments

The goal of the first two experiments was basically to determine if the QCM in combination with the CMFP is working and is producing repeatable results. It can be said that in general this setup produces very repeatable measurements. An unexpected fact however is the strong decrease in the mass flux with increasing number of shots. If we assume that the flow speed stays nearly constant, that implies that the impulse bit is decreasing about 80% during the experiment. In Markusic et. al. [15] it was found that the impulse bit of the first 100 shots was about 25% higher than the steady state value, most likely due to surface contamination. After about 100 shots the impulse bit asymptoted at a level never lower than 25% of the initial value. In our case, that implies that the exhaust velocity is increasing about 50% from its initial value to its value after 2000 Shots. This is very unlikely. To determine the effects of outgassing or temperature change an experiment was performed that repeats the firing after 3 hours without venting the tank. The results can be seen in figure 8.2. If the decrease in the mass flux is caused by surface contamination of the propellant, the measured initial mass flux after 3 hours without venting should correspond to the steady-state value of the measured mass flux of the earlier experiment. This is obviously not the case. Due to that it is unlikely that the decreasing mass flux in our case is caused by surface contamination. Much more likely is the hypothesis that temperature changes in general are responsible for the decreasing measured mass flux. That would also explain the reaching of a steady-state value that could be caused by reaching the maximum temperature of the AZPPT. Basically there are three hypothesis that can

be determined. First, the thruster heats up during the experiment, which could cause a change of the acceleration process and with that a change of the shape of the plume. If the plume spreads out more with time that could cause a decrease in the mass flux at 0 degrees where our measurements took place even if the total mass bit and the impulse bit are not changing. Second, the vaporized propellant coming out of the thruster possibly gets hotter with time due to the thruster heating up. It is possible that less material is able to transfer its entire energy at the surface of the crystal that is necessary to stick on it. Due to that less mass flux is measured with time. Another hypothesis comes with the thermal properties of the materials. The crystal is covered by a thin layer of gold which has a high thermal conductivity. The high thermal conductivity makes it easier for the incoming Teflon propellant to lose its energy on the surface of the crystal. Once the crystal starts to get covered by the Teflon the situation gets worse due to the low thermal conductivity of Teflon. It is possible that the mass flux asymptotes when the exposed area of the crystal is completely covered by the Teflon. Also a combination of the three mentioned issues is possible. Experiments at different angles were necessary to determine these three hypothesis. If we take a look at figure 8.6 we can see that the mass flux is decreasing with an increase of the number of shots on every measured angle. If the hypothesis that the plume is spreading out with time was true an increase of the mass flux at higher angles could be detected. That is obviously not the case. Due to that this hypothesis can be ruled out. The hypothesis that the detected effect is caused by the Teflon covering the crystal is also unlikely. During the experiments at higher angles it was discovered that the number of shots that is needed to reach steady-state conditions is decreasing with increasing angle. If the decrease in the mass flux would be caused by the worse thermal conductivity of the Teflon, the mass flux should asymptote faster on smaller angles because the mass flux at smaller angles is higher in general. That would cause a faster coverage of the crystal and with that a faster asymptoting. The hypothesis that less material sticks on the crystal due to its higher energy caused by a heating up of the thruster seems to be the most likely one. Apart from the mentioned indications there is another fact that supports this theory. In Markusic et. al. [15] it was found that at similar conditions (Voltage 1220 Volts,  $E = 25$  Joule) the total mass bit was about  $m_{bit} = 250 \mu\text{g}/\text{shot}$ . The mass bit was obtained by measuring the weight of the propellant bar with a scale before and after the firing of several thousand shots. If we calculate the total mass bit based on our measurement results at different angles we obtain a total mass bit after 200 shots of approximately  $m_{bit} = 27 \mu\text{g}/\text{shot}$ . This is just about 10% of the mass bit that was measured with the scale. At steady-state conditions the mass bit of about  $m_{bit} = 13 \mu\text{g}/\text{shot}$  is even just about 5% of the value measured with the scale. Due to these results it is very likely that not the entire incoming Teflon deposits on the crystal, probably because the Teflon is not able to transfer its entire energy to the crystal. This hypothesis is supported by one of the experiments introduced in section 3.2.2. This experiment was performed with a Teflon PPT [9]. In the paper it was mentioned explicitly that the QCM's were cooled down to liquid nitrogen temperature to ensure that the Teflon which impinges on the QCM's is actually deposited on its surface. Our QCM is just water cooled. In the LiLFA experiment such effects are probably a even more significant issue because the melting temperature of lithium is much lower. This effect has to be considered in a later analysis of the LiLFA results.

Apart from the significant decrease of the mass flux during the experiments the discovered positive drift after each firing procedure was also a not expected fact. There are basically two hypotheses for an explanation of this effect. First, it is possible that the very temperature sensitive crystal of the QCM heats up due to energy flux caused by the plume. According to the thermal drift tests explained in section 7.2.1 an increasing

temperature leads to an increasing total mass deposition displayed by the QCM. Second, vaporized Teflon remaining in the tank could deposit on the cooled crystal even after the firing stopped. If we take into account the temperature gradient of about  $2.5 \times 10^{-2} \mu\text{g}/\text{C}$  found in the thermal drift test it is clear that the temperature had to increase more than 1000 deg. C to cause a drift in the order of the measured amounts. Due to that the second hypothesis is much more likely. However, this effect was not determined in a deeper matter because it was showed that a continuous firing procedure leads to the same results than a firing procedure that interrupts the firing until the total mass deposition is asymptoted.

The experiments that were accomplished to detect issues that could be caused by the CMFP showed that the decreasing mass deposition is not caused by the CMFP. The mass deposition decreased in the same order also if just the QCM without the CMFP was used. If we take a look at figure 8.3 it is obvious that at 0 degrees the mass flux reached steady-state conditions at the same value if the CMFP is used or just the QCM. That supports the statement given by the vendor of the QCM that said that the QCM measures exact also if just a part of the crystal is covered by the material if this part is circular and in the center of the crystal. Before reaching steady-state conditions the mass flux of the experiment that includes a use of the CMFP was slightly higher than the mass flux if just the QCM was used. This difference is obviously not in the error bars. Possibly the mass flux in the thruster axis can not be seen as uniform even over such a small area as the crystals area. Due to the pinch effect the mass flux on the thruster axis is higher than slightly beside the axis. Figure 8.6 shows that the sharp peak of the mass flux at the thruster axis is flattening out with increasing number of shots. This could explain why the difference between the two experiments vanishes with time. The experiments accomplished at an angle of 60 degrees show a different characteristic. The difference between the mass flux obtained with the CMFP is significantly higher than the obtained mass flux if just the QCM is used. Figure 8.4 shows that the results of the two experiments are not within the error bars. We considered the possibility that the direction of the incoming mass flow is not normal to the aperture in the case of a measurement at 60 degrees. In this case the mass flux should be slightly lower if the CMFP is used, however the opposite is the case. The only hypothesis that could be made is that due to a closer distance to the parts of the thrust stand the interaction between CMFP and thrust stand could cause more reflected particles that flow through the aperture. However, more measurements of the mass flux with and without CMFP at different angles are necessary for a determination of this effect.

The characterization of the plume of the AZPPT shown in figure 8.6 shows that the plume is not just changing quantitatively but also qualitatively with increasing number of shots. As mentioned before the sharp peak of the mass flux at the thruster axis is flattening out with time. This means that the ratio between the mass flux at 0 degrees and at higher angles is decreasing during the experiment. One reason for that could be that the pressure in the thruster apart from the axis is going up due to an increasing temperature of the pinched gas. With this the pressure gradient between the thruster axis and the remaining space inside the thruster is not so large anymore. This could possibly lead to a more uniform distribution of the mass flux in the plume.

## 8.2 LiLFA Experiments

Mass flux measurements in the plume of the LiLFA were performed at a distance of  $d=148$  cm from the cathode tip on the thrust axis. Five firings were performed at a discharge current of  $I=300$  A a total mass flow of  $\dot{M}=10$  mg/s and an applied field strength of

$B=0.07$  T. The water-cooled CMFP utilizing the water-cooled QCM was used to ensure a correct measurement. The recording of the obtained data was ensured by a software interface which was connected to the QCM monitor.

### 8.2.1 Results of the LiLFA experiments

According to the methodology introduced in section 7.3 the shutter of the CMFP was closed during the starting sequence of the LiLFA to avoid a damaging of the QCM by solid or liquid parts of lithium. The time is referred to the start of the software interface because the appearance of an arc was not always very clear. The sampling rate was 4 Hz. The shutter was opened about 1 minute after the firing started. Figure 8.8 shows the results of the third firing which took about 4 minutes. The measurements were probably not yet performed under steady-state conditions due to the short period.

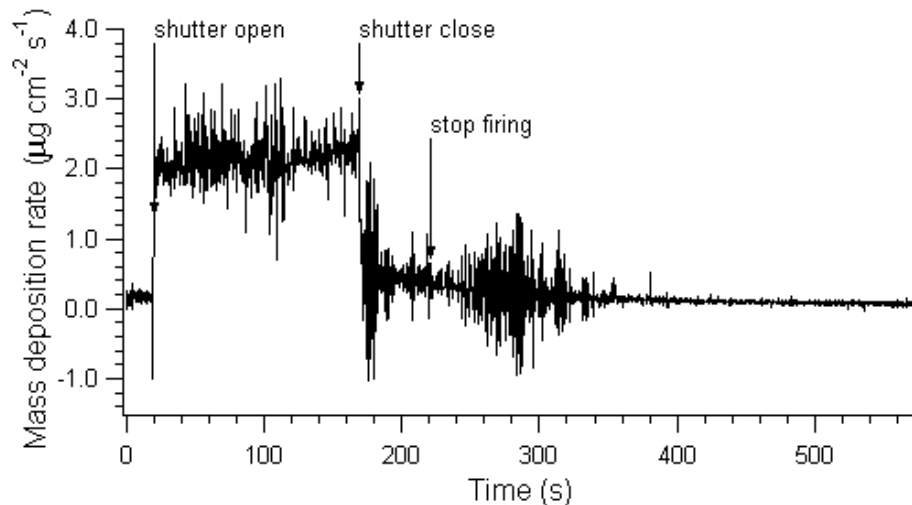


Figure 8.8: Mass flux measurements performed during the 3rd firing.

It is obvious that the errors caused by the tolerance of the aperture and by the resolution of the monitor are negligible if compared with the apparent introduced noise. The measurement in general seemed to be very noisy. Nevertheless the opening of the shutter at 23 s and the closing of the shutter at 165 s after the start of the software interface are recognizable. During the firing period prior to the opening of the shutter the measured mass flux remained below  $\dot{m}=0.3 \mu\text{g cm}^{-2}\text{s}^{-1}$ . After the shutter was opened the signal became more noisy. The measured mass flux during the period with opened shutter was  $\dot{m}=2.0 \pm 1.25 \mu\text{g cm}^{-2}\text{s}^{-1}$ . It seemed to stay in this order. The shutter was closed before the stop of the firing to avoid negative influences caused by changing parameters. After the close of the shutter the data remains noisy for a period of time. A similar phenomenon can be recognized after the shut down of the thruster which took place 225 s after the start of the software interface. About 150 s after the shut down the signal becomes less noisy. For a better view on the data that was obtained after the closing of the shutter the measured mass flux was smoothed by collecting and averaging the data of the last 10 s. The results can be seen in figure 8.9.

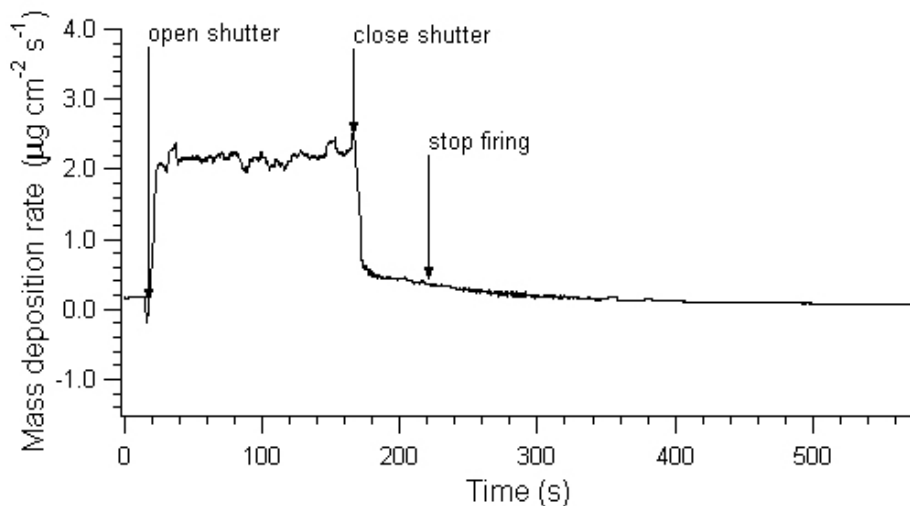


Figure 8.9: Smoothed mass flux results of the 3rd firing.

Prior to the opening of the shutter the average mass flux is about  $0.2 \mu\text{g cm}^{-2}\text{s}^{-1}$ . During the opened shutter period the average mass flux seems to increase slightly with time. After closing the shutter it decreases quickly to about  $0.7 \mu\text{g cm}^{-2}\text{s}^{-1}$ . In the following 300 s the average mass flux decreases slowly on to the initial value of about  $0.2 \mu\text{g cm}^{-2}\text{s}^{-1}$  which was obtained prior to the opening of the shutter.

During a later firing the shutter was opened later due to the goal to obtain data under steady-state conditions without saturating the QCM. Figure 8.10 shows the results of the measurements during this firing which lasted for about 12 minutes. The shutter was opened about 4 minutes after the appearance of an arc.

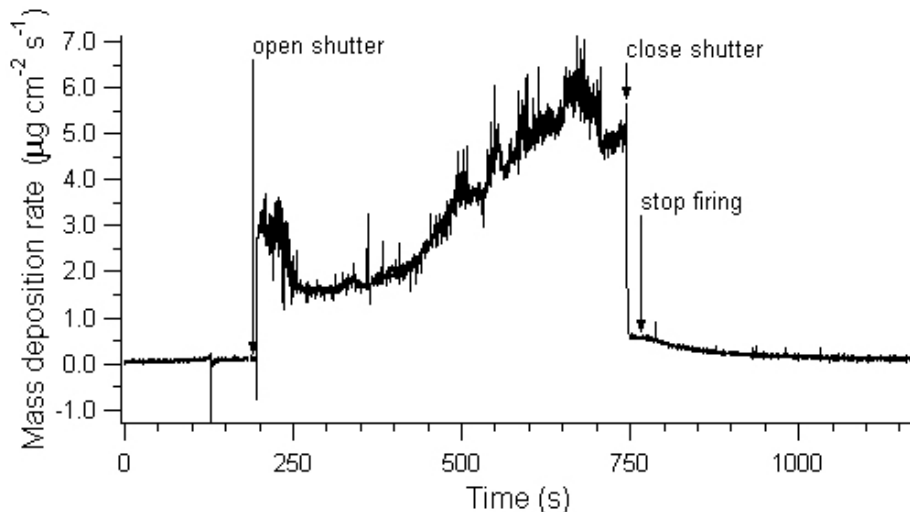


Figure 8.10: Mass flux measurements performed during the 4rd firing.

The signal seems to be less noisy when compared with the signal of the earlier firing. The opening of the shutter which took place 185 s after the start of the software interface and the closing of the shutter at 738 s are recognizable. Prior to the opening of the shutter the obtained mass flux stayed below  $\dot{m}=0.1 \mu\text{g cm}^{-2}\text{s}^{-1}$  which is a lower value than in the earlier test. As in the earlier firing an increasing noise could be observed after the shutter was opened. After the opening a measured mass flux of  $\dot{m}=3.0 \pm 1.0 \mu\text{g cm}^{-2}\text{s}^{-1}$

was obtained. Unlike the earlier test the mass flux did not seem to be steady. In the first 50 s after the opening of the shutter the mass flux seems to decrease to about  $\dot{m}=1.7\pm0.5 \mu\text{g cm}^{-2}\text{s}^{-1}$ . After that the mass flux was increasing for about 400 s until a maximum of about  $\dot{m}=6.0\pm1.0 \mu\text{g cm}^{-2}\text{s}^{-1}$  was reached. Following it was decreasing again to about  $\dot{m}=5.0\pm1.0 \mu\text{g cm}^{-2}\text{s}^{-1}$ . Unfortunately a further recording of the mass flux was not possible due to an emergency shut down of the LiLFA. After the closing of the shutter the mass flux decreased rapidly to about  $0.7 \mu\text{g cm}^{-2}\text{s}^{-1}$  followed by a slow decrease until the initial value was reached. This corresponds to the results of the earlier firing.

The measured mass flux during the other three firings was much more noisy. The measured mass fluxes during the periods with opened shutter stayed between 2 and  $6 \mu\text{g cm}^{-2}\text{s}^{-1}$ . The opening and closing of the shutter was recognizable in all these tests.

The temperature of the QCM measured by the attached thermocouple stayed constant during all three firings. Even during the longest firing sequence which took 12 minutes no increasing temperature could be detected. The apparent total mass deposition after all of the tests were finished was about  $593 \mu\text{g}$ . The QCM monitor showed a percentage of the used lifetime of the crystal of 9%.

### 8.2.2 Analysis of the LiLFA experiments

Due to the fact that no increasing temperature of the QCM was detected and no crystal failure appeared it can be said that the method of using the CMFP utilizing a QCM succeeded in providing a permanent mass flux measurement in the plume of the LiLFA without damaging the probe or a drift caused by temperature changes. The fact that the shutter system worked reliable and without leaking during all these firings validated this system for a permanent use in the high temperature, corrosive lithium environment of the plume of the LiLFA. The very low mass flux prior to the opening of the shutter showed that the closed shutter is shielding the crystal sufficiently.

The introduced noise is an issue. It is probably introduced by the discharge current and the applied magnetic field of the LiLFA. Due to the noise the error is between 20% and 80% of the measured mass flux. The noise which appears after closing of the shutter in figure 8.8 shows that even with the closed shutter the CMFP is not able to shield the QCM from such influences.

The mass flux shows a different characteristic when compared with the results obtained during the experiments with the AZPPT. In the short third firing the mass flux stays nearly constant during the open period of the shutter. In the long forth period the mass flux also showed a constant mass flux of about  $0.7 \mu\text{g cm}^{-2}\text{s}^{-1}$  during a short period of time. It even increases most of rest of the time while we saw a strong decreasing mass flux with time when using the AZPPT. One hypothesis for the decreasing characteristic of the mass flux in the experiments with the AZPPT was, that the ablated Teflon propellant in the plume heats more up with time due to an increasing temperature of the thruster. Due to the entirely different acceleration process of the LiLFA it could be that the temperature of the lithium that escapes from the thruster is not increasing with time. The amount of material that is loosing its entire energy and is sticking on the crystal is possibly not decreasing with time.

As mentioned in section 2.2.2 the LiLFA is probably not steady-state during the first 6-10 minutes after the appearance of an arc. When the cathode heats up during the start of the firing, caused mainly by added heat of the arc, the vaporization rate increases

and the vaporization point moves upstream inside the cathode until it stabilizes. It is very likely that this fact is responsible for the increasing mass flux during the long firing four that can be seen in figure 8.10. A responsibility of the temperature of the QCM for this phenomenon can be ruled out because no change in the temperature could be detected during every firing. The reaching of a maximum mass flux after about 700 s and the apparent stabilizing at a slightly lower level can possibly be seen as the reaching of steady-state conditions if we use liberal approximation. Further, longer firings are required to determine that.

As in the test with the AZPPT a positive drift was discovered after the mass flow to the crystal stopped in this case caused by the closing of the shutter. This drift decreases but remains for a few minutes and could be an issue if the time period between the firings is short. Too much material could be detected. The decrease of the positive drift leads to the hypothesis that it is caused by vaporized lithium in the CMFP which is depositing on the crystal even after the closing of the shutter.

If we use the very liberal modelling of the plume introduced in section 4.1 we obtain a mass flux at the distance  $d=148$  cm from the cathode tip of about  $\dot{m}=1.3 \mu\text{g cm}^{-2}\text{s}^{-1}$ . If we compare the estimation with the measured mass flux of between  $2.0 \pm 1.25 \mu\text{g}/(\text{cm}^2 \text{s})$  and  $6.0 \pm 1.25 \mu\text{g}/(\text{cm}^2 \text{s})$  we can say that the model of the plume of section 4.1 can be used for rough estimations of the mass flux in the plume.

The apparent used crystal lifetime at the end of all experiments was 9% at an apparent total mass deposition of about  $593 \mu\text{g}$ . If we assume that the crystal saturates if the apparent used crystal lifetime is 100% we obtain a maximum possible mass deposition of  $\Delta M_{max} = 6.59 \text{ mg}$ . This is very likely because it lays between the amount which was obtained by the vendor with similar materials of about  $\Delta M_{max} = 5.0 \text{ mg}$  and the theoretical amount of  $\Delta M_{max} = 7.1 \text{ mg}$  which was calculated in section 3.3.2. The obtained amount of  $\Delta M_{max} = 6.59 \text{ mg}$  can be used for an estimation of the saturation time of the crystal in future tests with the LiLFA.

# Chapter 9

## Conclusions

This chapter comprises the conclusions based on the work presented in Chapters 2-8 including a summarize of the important findings from each chapter. Finally recommendations and suggestions for further research work are made.

In chapter 2 it was found that performing experiments with the LiLFA is challenging and dangerous due to the alkali metal propellant. It was explained why mass flux measurements are necessary. Not much data of earlier experiments with the LiLFA can be made useful for the planned experiments. The Quartz Crystal Microbalance Method (QCM) was found to be the most promising method for mass flux measurements in the LiLFA plume. Its basics and the surrounding technique were explained in chapter 3 including a summary of the possibilities and limits that come with this technique. In a literature search it was found that QCMs have been used before in thruster contamination experiments. The results of these tests and the discovered issues were considered for a later design and the setup of the LiLFA experiments. In chapter 4 the mentioned issues were determined in a deeper manner. It was found that the high temperature in the LiLFA plume and the saturation of the QCM may be an issue if the distance to the thruster is small. It was also found that the size and shape of a bluff body in the LiLFA plume are most likely negligible. A design that considered the mentioned issues lead to the development and fabrication of a Condensing Mass Flux Probe (CMFP) that surrounds and protects the QCM. This design included the design and fabrication of a necessary shutter system. To ensure the ability to scan the LiLFA plume without stopping the test a conceptual design for a positioner system for the CMFP was made. In chapter 5 this positioner system is introduced including kinematic aspects and the limits of the system. To ensure the basic function of the QCM and the CMFP and due to the fact that the LiLFA was not available for a long period of time, precursor tests were performed using the more reliable Ablative Z-Pinch Pulsed Plasma Thruster (AZPPT) in combination with the CMFP and QCM. In chapter 6 this thruster and the experimental setup for tests with it were introduced including the issues that come with the experimental setup. These issues include the possibility of an arc between the thruster and the QCM and human safety problems. The experimental setup for the test with the LiLFA was explained in chapter 7. It was shown that the CMFP has to be supplied with argon gas for the shutter system and with chilled water for a cooling of the QCM and CMFP. Also the attachment of a necessary thermocouple to the QCM probe was explained. In precursor tests, including a thermal calibration of the QCM, a calibration with pressure and the determination of influences of vibration on the measurement, it was found that the temperature might be an issue if it rises quickly during the experiment due to a discovered temperature dependant drift of the QCM. Changes in pressure and the influence of vibrations caused by a movement

of the shutter were found to be negligible. A methodology was introduced that ensures a synchronization of different kinds of data during the experiment and for a later analysis. In chapter 8 the results and the analysis of the AZPPT experiment were introduced. It was shown that the QCM integrated in the CMFP produces repeatable measurements and that the area of the exposed crystal can be reduced to save the probe from the environment without significantly disturbing the measurements. The mass deposition rate measured with the QCM was found to decrease with the number of shots during the test to about 15% of its initial value and asymptote at this low level. It was determined that this phenomenon is not due to the use of the CMFP. In a later analysis it was found that the phenomenon is most likely due to thermal effects. The assumption that the plume gets hotter with time and not all of the hot Teflon transmits its energy to the QCM and sticks on it was made. This probably caused the decrease in the mass deposition rate. This theory was supported by the disagreement with results of earlier tests with the AZPPT. Other tests were performed which showed that the CMFP has an influence on the measurements if these measurements were taken far off the thruster axis. A reason for that could not be found due to the lack of sufficient data. A rough scan of the AZPPT plume was performed that showed that the mass flux is decreasing quickly with an increasing angle to the thruster axis. This was expected because of the pinch effect. It was found that the peak of the mass flux in the thruster axis flattens out with time, most likely due to thermal effects in the thruster which influences the acceleration process. The results and the analysis of the LiLFA experiment were introduced. It was shown that the CMFP utilizing the QCM succeeded in keeping the temperature of the probe constant which allowed the probe to function without problems during the experiment. The opening and closing of the shutter was performed without a leaking of the air cylinder and was recognizable in the results of the measurements. The signal in general provided by the QCM was found to be very noisy. The mass flux was found to increase with time during the firing sequence. This is probably due to the fact that the vaporization rate in the cathode increase with time and the plume is not steady-state in the first minutes of the firing sequence.

In conclusion it can be said that it is very likely that the QCM probe in the form used in the experiments is not proper for a quantitatively measurement of the mass flux in the plume of a electric propulsion device. The water cooling is probably insufficient because not the entire impinging mass is able to transfer its entire energy to the crystal due to a too warm environment. Probably most of the material is reflected and not measured. This might be even worse in the experiments with the LiLFA due to the much lower melting temperature of lithium compared with Teflon. However, a qualitative measurement of the mass flux in a plume should be possible.

It future studies it should be determined how the QCM can be cooled to a much lower temperature without damaging it. The use of liquid nitrogen could be a solution. The performed measurements need to be repeated with the better cooled QCM to determine if the mass flux is increasing due to the lower temperature. Another issue discovered in the performed tests is the fact that the CMFP has an significant influence on the measurements if measurements were taken far off the thruster axis. More measurements using the AZPPT at different angles using a combination of CMFP and QCM and just QCM need to be performed to provide enough data for an analysis of this phenomenon. Before performing more measurements in the plume of the LiLFA it has to be determined how the QCM and its equipment can be shielded from the introduced noise. More measurements in the plume of the LiLFA need to be performed at the same distance at different angles to the thruster axis to determine if the total mass flow obtained by these measurements corresponds with the total mass flow provided by the feed system. Details of the positioner

system still need to be addressed including the shielding and cooling of critical parts. If the positioner system is used in a future experiment, it has to be determined (without firing the thruster) if a repositioning of the QCM has an influence on the measurements—for instance due to a drift caused by its movement.

## Appendix A

### Complete AZPPT Results

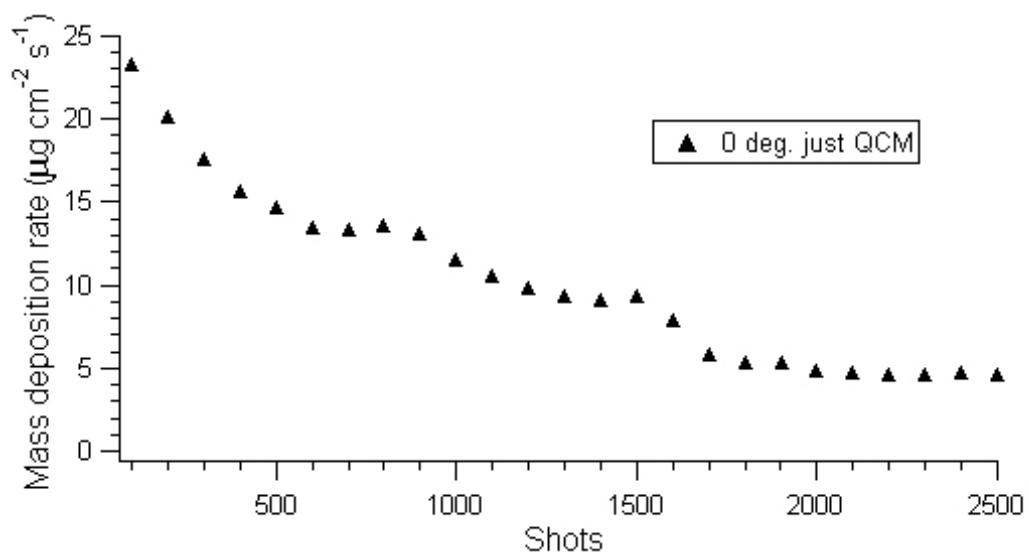


Figure A.1: Mass deposition rate at 0 deg. using just the QCM without the CMFP.

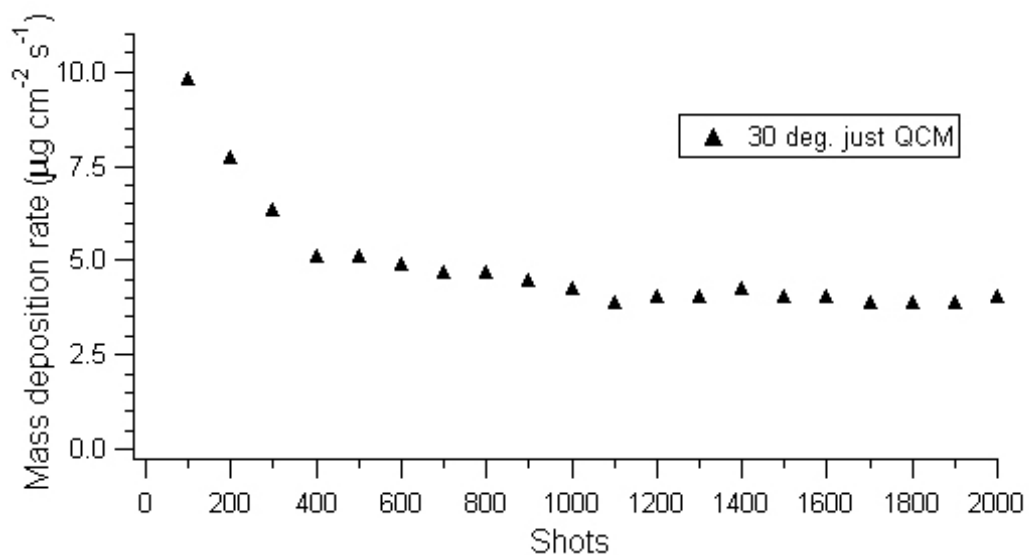


Figure A.2: Mass deposition rate at 30 deg. using just the QCM without the CMFP.

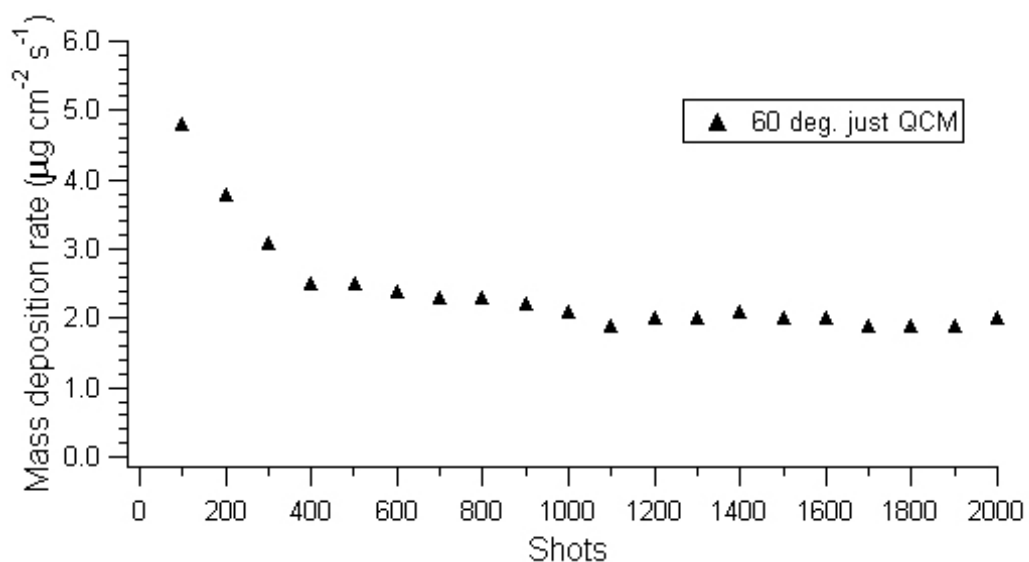


Figure A.3: Mass deposition rate at 60 deg. using just the QCM without the CMFP.

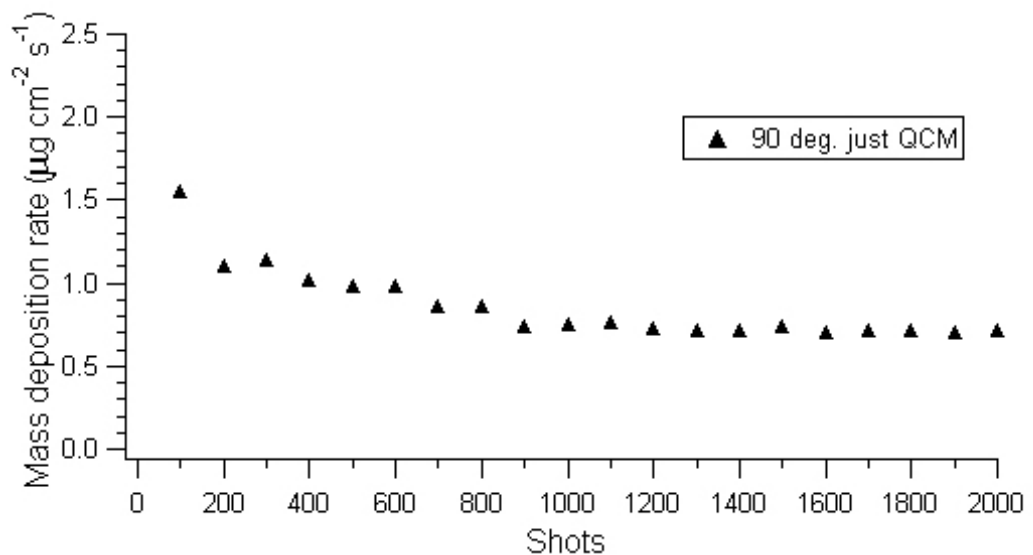


Figure A.4: Mass deposition rate at 90 deg. using just the QCM without the CMFP.

# Appendix B

## CMFP Detailed Photos

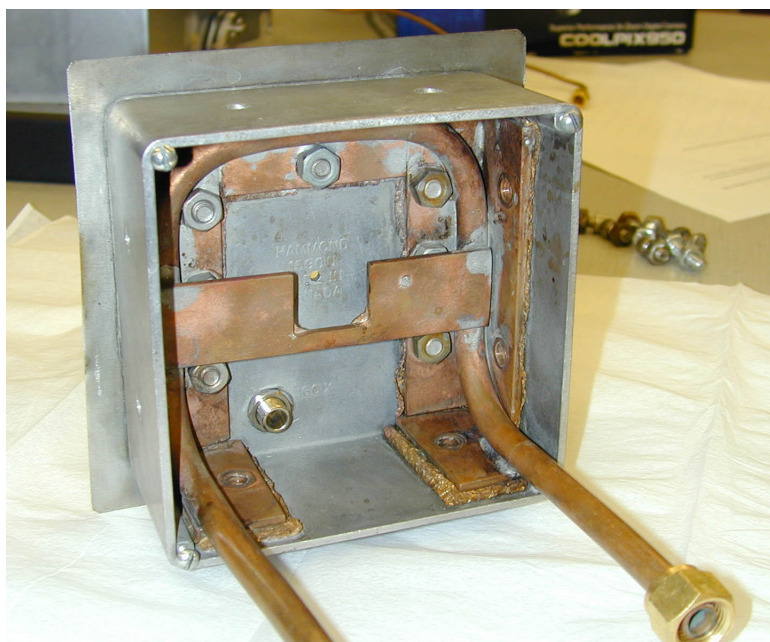


Figure B.1: Rear-view of the CMFP without QCM and without aluminum back plate.

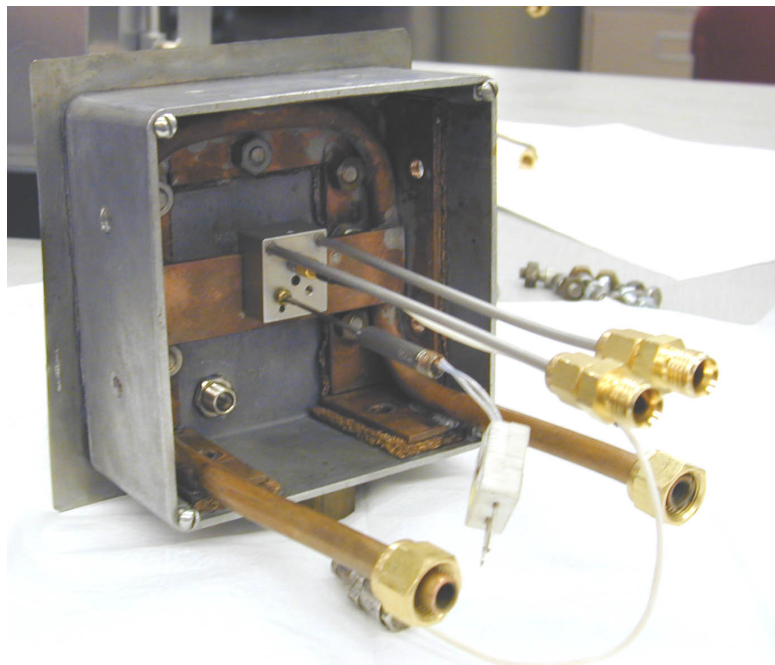


Figure B.2: Rear-view of the CMFP with integrated QCM, without aluminum back plate.

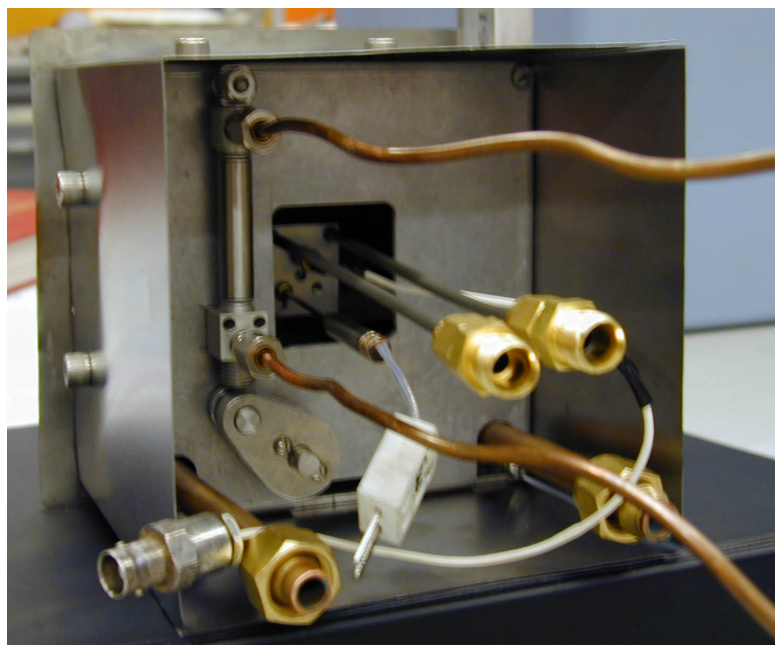


Figure B.3: Rear-view of the CMFP with QCM, with aluminum back plate and shutter system.

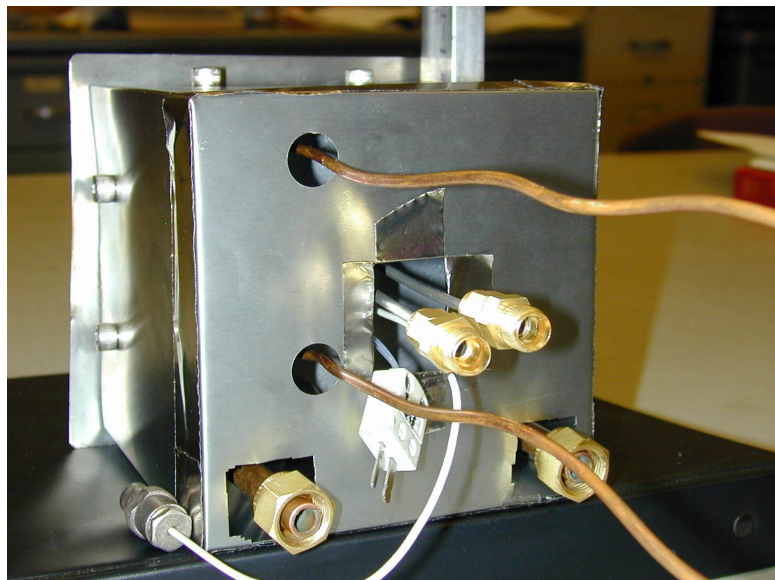


Figure B.4: Rear-view of the entirely mounted CMFP with all included systems.

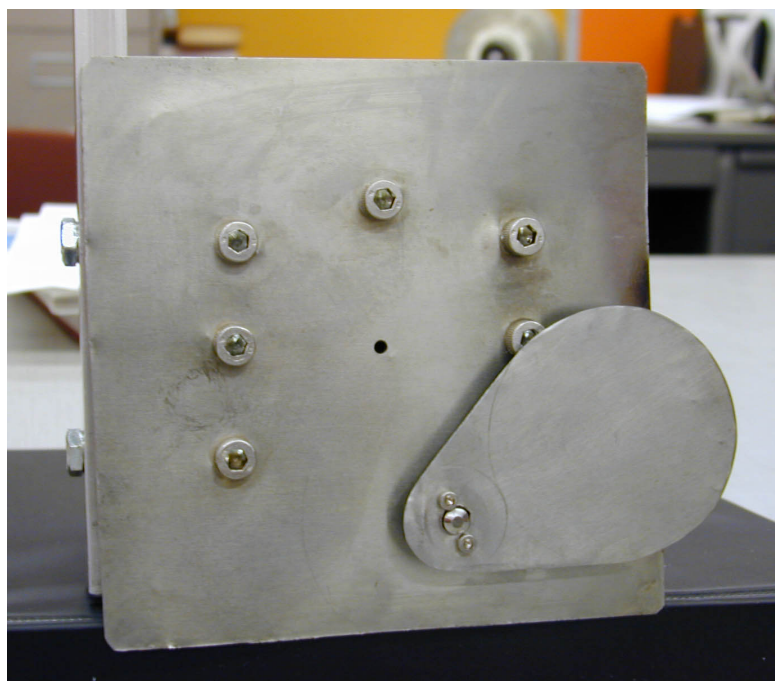


Figure B.5: Front-view of the CMFP with opened shutter.

# Bibliography

- [1] J.E. Polk and T.J. Pivrotto. “Alkali metal propellants for MPD thrusters”. In *AIAA/NASA/OAI Conference on advanced SEI technologies*, Cleveland, OH, USA, 4-6 September 1991. AIAA 91-3572.
- [2] L.D. Cassady, A.D. Kodys, and E.Y. Choueiri. “A thrust stand for high-power steady-state plasma thrusters”. In *38<sup>th</sup> AIAA/ASME/SAE/ASEE Joint Propulsion Conference*, Indianapolis, IN, USA, 7-10 July 2002. AIAA 2002-4118.
- [3] “Material safety data sheet about lithium hydroxide and lithium carbonate”. Technical report, June 2002.
- [4] V. Kim, V. Tikhonov, and S. Semenikhin. “The fourth quarterly (Final) report on the stages no 3 C, D of the contract on the research studies between RIAME MAI and NASA”. Final Report NASW-4851, Research Institute of Applied Mechanics and Electrodynamics of Moscow Aviation Institute, April 1997.
- [5] “Personal communication with Rick Mueller, Inficon Inc., E.Syracuse, NY, USA”. Technical report, August 2002.
- [6] E.Y. Choueiri. “Lithium Lorentz Force Accelerator Research”. Statement of Work for NASA-JPL, Electric Propulsion and Plasma Dynamics Lab (EPPDyL) MAE Dept., Princeton University, October 1999.
- [7] “XTM/2 Deposition Monitor”. Operating Manual IPN 074-186K, Inficon Inc., E.Syracuse, NY, USA, 2001.
- [8] C. Hurd. “United States Patent 5,117,192”. Patent, Inficon Inc., E.Syracuse, NY, USA, May 1992.
- [9] L.K. Rudolph, L.C. Pless, and K.G. Harstad. “Pulsed Plasma Thruster Backflow Characteristics”. In *15<sup>th</sup> AIAA/ASME/SAE Joint Propulsion Conference*, Las Vegas, Nevada, USA, 18-20 June 1979. AIAA 79-1293.
- [10] L.N. Ahmed and M.W. Crofton. “Surface Modification Measurements in the T5 Ion Thruster Plume”. *Journal of Propulsion and Power*, **14**(3):336–347, May-June 1998.
- [11] G.G. Spanjers, J.H. Schilling, S.F. Engelman, D.R. Bromaghim, and L.K. Johnson. “Mass Deposition Measurements from 26-Kilowatt Electric Propulsion Space Experiment Flight”. *Journal of Propulsion and Power*, **18**(4):772–776, July-August 2002.
- [12] L.C. Thomas. *Fundamentals of heat transfer*. Prentice-Hall, 1980.
- [13] D.R. Lide. *Handbook of Chemistry and Physics*. CRC Press. Inc., 1996.

- [14] W.G. Vincenti and C.H. Kruger. *Introduction to Physical Gas Dynamics*. Krieger Publishing Company, 1965.
- [15] T.E. Markusic, K. Polzin, J.Z. Levine, C.A. McLeavey, and E.Y. Choueiri. “Ablative Z-Pinch Pulsed Plasma Thruster”. In *36<sup>th</sup> AIAA/ASME/SAE Joint Propulsion Conference*, Huntsville, Alabama, USA, 16-19 July 2000. AIAA 2000-3257.